Toyohashi University of Technology

Doctoral Thesis

Design and Control of a Redundant Wheeled Drive System for Fail Safe Motion and Energy Saving

---

Author:

Shuaiby Mohamed Shuaiby Ragab

Supervisor:

Prof. Naoki Uchiyama

*A thesis submitted in fulfillment of the requirements
for the degree of Doctor of Engineering*

in the

Systems Engineering Laboratory
Department of Mechanical Engineering

豊橋技術科学大学
Toyohashi University of Technology

July 2017

Declaration of Authorship

I, Shuaiby Mohamed Shuaiby Ragab, declare that this thesis entitled "Design and Control of a Redundant Wheeled Drive System for Fail Safe Motion and Energy Saving" and the work presented therein are my own. I confirm that:

- This work was done wholly or mainly while in candidature for a research degree at this University.

- Where any part of this thesis has previously been submitted for a degree or any other qualification at this University or any other institution, this has been clearly stated.

- Where I have consulted the published work of others, this is always clearly attributed.

- Where I have quoted from the work of others, the source is always given. With the exception of such quotations, this thesis is entirely my own work.

- I have acknowledged all main sources of help.

- Where the thesis is based on work done by myself jointly with others, I have made clear exactly what was done by others and what I have contributed myself.

Signed:

_____

Date:

_____

TOYOHASHI UNIVERSITY OF TECHNOLOGY

Design and Control of a Redundant Wheeled Drive System for

Fail Safe Motion and Energy Saving

Doctor of Engineering Thesis

of

Shuaiby Mohamed Shuaiby Ragab

Committee Members: *Signature:*

Prof. Zhong Zhang   —————————————

Prof. Kaiji Sato   —————————————

Prof. Naoki Uchiyama   —————————————

Systems Engineering Laboratory

Department of Mechanical Engineering

Toyohashi University of Technology

July 2017

Toyohashi University of Technology

Abstract

Toyohashi University of Technology

Department of Mechanical Engineering

Doctor of Engineering

Design and Control of a Redundant Wheeled Drive System for Fail Safe Motion and Energy Saving

by Shuaiby Mohamed Shuaiby Ragab

Mobile robots are widely used in many different applications and areas, such as transportation, the military domain, medicine, search and rescue, guidance, hazard detection, and carpet cleaning. Because of their relatively low mechanical complexity, simple controllers, and energy consumption, wheeled robots are the most widely used class of mobile robots. Robots usually carry limited power sources, such as rechargeable batteries. In addition, because it is generally impossible to add more power while working, the battery capacity determines the operating time of mobile robots. Energy saving is important topic in mobile robots for increasing the operating time under limited capacity.

With ever more people who are elderly or have disabilities, there is growing demand for mobility support devices and care equipment to improve their quality of life. Nowadays, Japan's declining birthrate and aging population are having a profound impact on society, the economy, and culture. Hence, an essential task for Japanese

society is to improve the quality of life for people who are elderly or have disabilities and to support their self-movement.

A differential wheeled mobile robot (WMR) involves two independently driven wheels on a common axis. The robot moves forward or backward in a straight line when the wheels rotate at the same speed, but follows a curved path along the arc of an instantaneous circle around the instantaneous center of rotation (ICR) when one wheel rotates faster than the other. The robot turns about the midpoint of the two driving wheels when both wheels rotate at the same velocity in opposite directions. If one of the motors was to break down or become damage for some reason, the robot would roll around the wheel connected to the damaged motor. Eventually, there could be a risk to the passenger's life because he or she could no longer continue moving. According to existing surveys incidents with wheelchairs were in 33% of the collected cases caused by component failure such as control system and drive train.

This work presents the design of a new system that consists of a redundant drive system that allows motion to continue safely should one of the motors break down, and that is also able to operate for longer because of lower energy consumption. This provides the use of each motor at its efficient operating condition. The system has two drive wheels with three motors and two planetary gears. Motors 1 and 2 are connected to the left and right wheels, respectively, through each planetary gear. Motor 3 is connected to both the right and left planetary gears and supplies power to both wheels. The planetary gears consist of an internal gear, a planetary carrier, and an a planet gear that revolves around a sun gear. In this system, the sun gear connects to Motor 3, the internal gear connects to Motors 1 and 2, and the planetary carrier connects to each wheel.

This dissertation consists of three main parts. The first part considers the dynamic modeling of a redundant wheeled drive system with nonholonomic constraints. In addition, it is assumed that, as for a personal mobility vehicle such as an electric wheelchair, the desired linear and angular velocities of the vehicle are given by its operator. These velocities are typically transformed into desired velocities of the left and right wheels. Next, these wheel velocities are transformed into angular velocities

of three motors by using a distribution controller. In addition, a fixed ratio d of angular velocities of a wheels to the velocity of Motor 3 is introduced. The optimum value of d depends on the actuator specifications and is found by simulation/experiment.

The second part of this thesis describes the possibility of the proposed new drive system for energy saving and fail safety by applying two controllers, namely a distribution controller and a state-feedback controller. The distribution controller creates a reference angular velocity of the motors. In addition, by assuming that the commercial motor controllers are based on proportional-derivative (PD) control, a state-feedback controller is applied to the proposed WMR as the feedback controller. The feedback gains of that controller are obtained by the pole placement method. Experiments are conducted to verify the effectiveness of the proposed method; for the linear and circular motion, a distribution ratio of $d = 2$ provides reduction of 20.45% and 13.05%, respectively, in the consumed energy compared to the case in which only two motors operate.

The third part of this thesis considers robust tracking and energy-saving control for a redundant wheeled drive system using sliding-mode control (SMC). A comparative study is conducted between a linear quadratic regulator (LQR) and pole placement control (PPC). Computer simulations are performed to verify the effectiveness of the proposed method, and there are no significant differences among the SMC, LQR, and PPC approaches. The effectiveness and reliability of the proposed method are evaluated in a real environment with disturbances by performing multiple experiments. For linear motion, the minimum mean energy required is 50.08 J for SMC ($d = 1.5$), 38 J for SMC with sat(.) ($d = 2$), 59.89 J for LQR ($d = 2$), and 63.43 J for PPC ($d = 2$). For circular motion, the minimum mean energy required is 50.92 J for SMC ($d = 1.5$), 41.32 J for SMC with sat(.) ($d = 2$), 57.3 J for LQR ($d = 1.5$), and 59.37 J for PPC ($d = 2$). The experimental results show that SMC with sat(.) provides robust tracking performance with less energy.

Finally, the dissertation is concluded and future work is described.

Acknowledgements

Contents

List of Figures

List of Tables

List of Abbreviations

WMR	Wheeled Mobile Robot
DWMR	Differential Wheeled Mobile Robot
ICR	Instantaneous Center of Rotation
DA	Digital-to-Analog
PWM	Pulse-Width Modulation
PPC	Pole Placement Control
SMC	Sliding Mode Control
PD	Proportional-Derivative
LQR	Linear Quadratic Regulator

To my parents, my wife, and my children, with all of my love . . .

Chapter 1

Introduction

1.1   Background

Mobile robots are expected to be applied not only to transportation work in factories but also to living support in an aging society. WMRs are very popular in applications requiring relatively low mechanical complexity and energy consumption. An electric wheelchair is one of the most commonly used assistive devices for enhancing the personal mobility of people with disabilities, being the only mode of independent travel that affords the possibility of moving freely both indoor and outdoor.

Nowadays, Japan's declining birthrate and aging population are having a profound impact on society, the economy, and culture. So, an essential task for Japanese society is to improve of the quality of life for people who are elderly or have disabilities, and to support their self-movement. With ever more people being elderly or having disabilities, there is growing demand for mobility support devices and care equipment to improve their quality of life [1–9]. Alex Mihailidis *et al.* developed an intelligent powered wheelchair to support safe and productive mobility of the disabled and the aged [1]. The system uses an infrared sensor to avoid collisions. Prassler *et al.* used a commercial wheelchair that has been equipped with an intelligent control and navigation system to support elderly people and people with disabilities, and to provide them with a certain amount of mobility and independence [2]. David E Miller *et al.* described two low-cost robotic wheelchairs that assist the operator of the wheelchairs in avoiding obstacles and going to pre-designated places [3]. In addition,

wheelchairs take the human user to the destination in a variety of forms ranging from direct control to specification of the desired final position. Babel *et al.* discussed a navigation assistance system for power wheelchairs with obstacle detection and avoidance to support people with limited motion skills such as elderly and disabled people, and to provide them with the possibility to travel indoor and outdoor independently [4]. A smart electric wheelchair equipped with a stereo omni-directional camera system has been developed to support safe self-movement of the people with impaired mobility in [5]. This electrical wheelchair can realize the functions of detecting potential hazards in a moving environment and the postures and gestures of a user.

Autonomous wheelchairs based on commercially available motorized wheelchairs have been proposed to support people with certain types and degrees of handicap in [6]. In addition, a brief survey of research on intelligent wheelchairs has been conducted and is still ongoing at some institutions. In [7] an intelligent wheelchair has been developed in order to support safe mobility for people who are elderly or have disabilities with various impairments . The authors used in this work two different control schemes, namely joystick control and system control. In addition, this system offers obstacle detection and avoidance. Holly Yanco *et al.* developed a low-cost assistive robotic wheelchair system for people who have disabilities [8]. The assistive robotic wheelchair offers obstacle avoidance and automatic driving to target places specified by a user. The authors of [9] performed clinical evaluation of the drive-safe system for people with disabilities. The drive-safe system performs in avoiding collisions for independent and safe mobility for visually impaired wheelchair users. However, the safe motion control of a powered wheelchair requires a significant level of skill, attention, judgment, and appropriate behavior.

A differential wheeled mobile robot (DWMR) involves two independently driven wheels on a common axis [10]. The robot moves forward or backward in a straight line when the wheels rotate at the same speed, but follows a curved path along an arc of the instantaneous circle, around the ICR when one wheel rotates faster than the other [10]. The robot turns about the midpoint of the two driving wheels when both wheels rotates at the same velocity in opposite directions.

If one of the motors was to break down or become damage for some reason, the robot would roll around the wheel connected to the damaged motor. Eventually, there could be a risk to the passenger's life because he or she could no longer continue to move. Unfortunately, powered wheelchairs can pose a risk to users when failures occur. According to existing survey incidents with wheelchairs were in 33 % of the collected cases caused by component failure such as control system and drive train [11]. Xiang *et al.* reports 20 % of adult injuries were associated with component failure [12, 13]. Wheelchair breakdown can result in a lack of mobility, which has been linked with reduced quality of life [13].

1.1.1 Energy saving in mobile robots

Mobile robots are usually powered by rechargeable batteries. However, these generally take time to charge, it is not possible to supply additional energy while the robot is working, and extending the duration of movement is a major issue. The batteries are a limited source of power, which hence constrains the operating time of the mobile robot. Therefore, saving energy is important in order to increase the robot's operating time [14–18]. A genetic algorithm has been used to generate optimal solutions of the coverage path planning problem for autonomous mobile robots on natural terrain with respect to energy consumption [14]. In addition, the authors have taken into account the electrical losses provided by the model of an electrical motor driven robot. Barili *et al.* [15] proposed a method to control the traveling speed of an autonomous mobile robot working in environments cluttered with unpredictable obstacles such as civil buildings. The authors of [16] proposed an energy-optimal control for differential-driven wheeled mobile robot to minimize the total energy drawn from the batteries. However, they considered only the translational motion of the WMR. An innovative scout design has been proposed in [17]. The scout combines jumping locomotion and rolling capabilities. A case study of a mobile robot has been presented in [18]. In addition, they introduced two energy-conservation techniques, namely dynamic power management and real-time scheduling to reduce the power consumption and extend the operation time of mobile robots.

WMRs usually have many components, such as sensors, batteries, motors, controllers, and motor drivers. There are several ways to save energy, such as improving the power efficiency of the motor power supply and using energy-efficient motors and an energy-minimizing control [19–22]. An energy-optimal control strategy for incremental motion of dc drives has been developed, and its microprocessor-based implementation is proposed in [19]. An efficient iterative search algorithm for battery-powered wheeled mobile robots has been proposed in [20] to generate an energy-efficient velocity profile which extends the operating time of WMRs . In addition, they have been developed a new objective function related to motor dynamics, control input, and velocity profile. A new approach has been proposed to find energy-efficient motion plans for mobile robots in [21]. The authors used manipulator Jacobian for computing the energy consumption of different plans. An optimal motion planning has been proposed for wheeled mobile robot [22]. In addition, the authors have been formulated the motion planning problem as two stage planning. First, the path is planned using geometric methods under kinematic constraints. Then a optimal trajectory is generated considering dynamic properties.

In the past few decades, much research has been conducted into energy saving in mobile robots [21, 23–34]. An optimal motion planning method has been proposed for a mobile robot with minimum energy consumption [23]. However, only a straight line motion was considered. Makimoto *et al.* [24] suggested that the mobile robot would be provide a tremendous challenges for future low power design. A robot deployment approach has been proposed to reduce the deployment overhead [25]. In addition, the deployment method considers both energy and timing constraints and it is applied to covering areas with obstacles. A class of nonlinear optimal control problems including energy minimization combined with time minimization and obstacle avoidance has been developed in [26]. Ueno *et al.* proposed a differential-drive steering system for the caster drive wheel of an omni-directional mobile robot [27]. However, that system is complex because it uses two motors for each wheel. Furthermore, the improvement in energy consumption was not analyzed theoretically or experimentally.

Deshmukh *et al.* discussed the significance of power management for long-term operation of mobile robots [29]. Duleba and Sasiadejk discussed a modification of the Newton algorithm applied to nonholonomic motion planning for energy optimization [30]. However, the amount of consumed energy could not be estimated. Francisco *et al.* proposed a trajectory-tracking controller for a unicycle-like mobile robot, including a neural adaptive compensator [31]. A nonlinear adaptive trajectory tracking has been proposed for autonomous mobile robot [32]. A simple neuron-based adaptive controller for trajectory tracking has been proposed for nonholonomic mobile robots [33]. An adaptive controller has been proposed for a nonholonomic mobile robot by using a nonlinear proportional-integral-derivative (PID) based analog neural network [34]. However, none of those studies considered the issue of energy saving in the control.

1.2 Motivation and Research Objectives

Mobile robots are expected to be applied not only to transportation work in factories but also to living support in an aging society. With ever more people who are elderly or have disabilities, there is growing demand for mobility support devices and care equipment to improve their quality of life. Although many drive mechanisms have been proposed for mobile robots so far, from the viewpoint of practicality, two-wheeled differential robots such as electric wheelchairs are still widely used. With a two-wheeled differential robot, by controlling the speeds of both wheels independently, translation and turning of the body can be realized. However, if one wheel fails, this movement cannot continue and there could be a risk to the passenger's life. For this reason, it is important to increase the number of drive wheels and add redundancy.

In addition, mobile robots are powered mainly by rechargeable batteries, but these generally take time to charge. Therefore, saving energy is studied to increase the operating time. To this end, this thesis proposes a new system consisting of a redundant drive system, that has two driven wheels with three motors and two planetary gears.

This system allows to continue the motion safely should one of the motors break down for some reason, and that is also able to operate for longer by saving energy.

1.3   Thesis Contributions

The main contributions of this thesis are as follows:

(1) Design of a new redundant drive system, that has two driven wheels with three motors and two planetary gears. This system maintains the motion to continue safely should one of the motors break down for some reason, and that is also able to operate for longer by saving energy.

(2) Modeling of the dynamics of the proposed system.

(3) Design of a distribution controller and introduction of a fixed ratio d of angular velocities of a wheels to the velocity of Motor 3. The optimum value of d depends on the actuator specifications, with the optimum value being found by simulation/experiment for different WMR systems.

(4) Investigation of energy saving and fail-safe motion of the proposed new drive system.

(5) Enhancement of the tracking performance with less energy by applying SMC.

1.4   Thesis Outline

This thesis is divided into five chapters. The rest of this thesis is organized as follows:

- Chapter 2: In this chapter, design of a new redundant drive system, that has two driven wheels with three motors and two planetary gears. The redundant wheeled drive system was driven is modeled dynamically. The derived models are used in the controller design. This chapter also details the experimental testbed and its parameters.

- Chapter 3: This chapter investigates the possibility of the proposed new drive system for energy saving and fail safety by applying two controllers, namely a distribution controller and state-feedback controller. In addition, it is assumed that, like a personal mobility vehicle such as an electric wheelchair, the desired linear and angular velocities of the vehicle are given by its operator. Thus, these velocities are typically transformed into desired velocities of the left and right wheels. Next, these wheel velocities are transformed into motor velocities of three motors by using a distribution controller. In addition, by introducing a fixed ratio d of the angular velocities of a wheels to the velocity of Motor 3. The optimum value of d depends on the actuator specifications and the driving situation, it being found by simulation/experiment for different WMR systems. In addition, it is assumed that the commercial motor controllers are based on proportional-derivative(PD) control, and the state-feedback controller was applied to the proposed WMR as the feedback controller. Multiple experiments are conducted to assess the effectiveness of the proposed method.

- Chapter 4: In this chapter, robust tracking and energy-saving control is considered for a redundant wheeled drive system using SMC. For the distribution controller presented in chapter 3, a comparative study is conducted between using a LQR and PPC . Computer simulations are performed to verify the effectiveness of the proposed method, and there are no significant differences among the SMC, LQR, and PPC approaches. the effectiveness and reliability of the proposed method are evaluated in a real environment with disturbances by performing several experiments. The experimental results show that SMC with sat(.) provides robust tracking performance with less energy.

- Chapter 5: This chapter presents conclusions and suggestions for future work.

Chapter 2

Design and Modeling of a Redundant Wheeled Drive System

2.1 Introduction

Mobile robots are mechanical devices capable of moving in an environment with a certain degree of autonomy. The difference between mobile robots and most industrial robots is that the former move freely within predefined workspaces, whereas the latter are confined to their assigned workspaces. This mobility capability enables such robots to be deployed in a wide range of structured and unstructured environments.

WMRs can be used in many different fields, from civil applications to military ones. These applications include search and exploration, guidance, rescue, hazard detection, surveillance, transportation, and many other tasks [10, 35]. WMRs are very popular in applications requiring relatively low mechanical complexity and energy consumption. The maneuverability of a WMR depends on the wheels and drives used: three degrees of freedom (DOFs) enable the maximal maneuverability needed for planar motion, such as movement through hospitals and museums and on warehouse floors and roads [10, 36, 37]. Non-holonomic WMRs have fewer than three planar DOFs but are simpler and cheaper to construct because they require fewer than three motors. The main problems in WMR design are control, stability, maneuverability, and traction.

WMRs are typically equipped with differential drives that consist of two fixed powered wheels mounted on the left and right sides of the robot platform. The two wheels are driven independently. Balance and stability are provided by one or two passive castor wheels. A differential drive is the simplest mechanical drive because it requires no rotation around the driven axis. If the wheels rotate at the same speed, the robot moves forward or backward in a straight line; if one wheel rotates faster than the other, the robot follows a curved path along an arc of the instantaneous circle. If both wheels rotate at the same speed in opposite directions, the robot turns about the midpoint of the two driving wheels.

With a two-wheeled differential robot, by controlling the speeds of both wheels independently, translation and turning of the body can be realized. However, if one of the motors should break down or become damaged for some reason, the robot would roll around the wheel that is connected to the damaged motor. Eventually, there could be a risk to the passenger's life because he or she could not continue moving. For this reason, it is important to increase the number of drive wheels and add redundancy. The research group of which the author was a member design a redundant drive system using three motors and two planetary gears and it is possible to drive two wheels by three motors. This system allows the motion to continue safely should one of the motors break down, and that is also able to operate for longer because of lower energy saving consumption.

In this chapter, the dynamics of the proposed system and the derived models were used in the controller design in this study are discussed. This chapter also details the experimental testbed and its parameters.

2.2 Design of a Redundant Wheeled Drive System

2.2.1 System structure

In general, a DWMR has two driving wheels which are attached to both sides of the device, and each wheel is driven by one motor independently. The system proposed

in this study is a two-wheeled differential-drive mobile robot, and considers a redundant wheeled drive system as shown in Figs. 2.1 and 2.2. The proposed system has two drive wheels with three motors and two planetary gears. The gears have high transmission efficiency and durability for high power. In addition, there are two front caster wheels that are used for balance and stability. As shown in Fig. 2.1, Motors 1
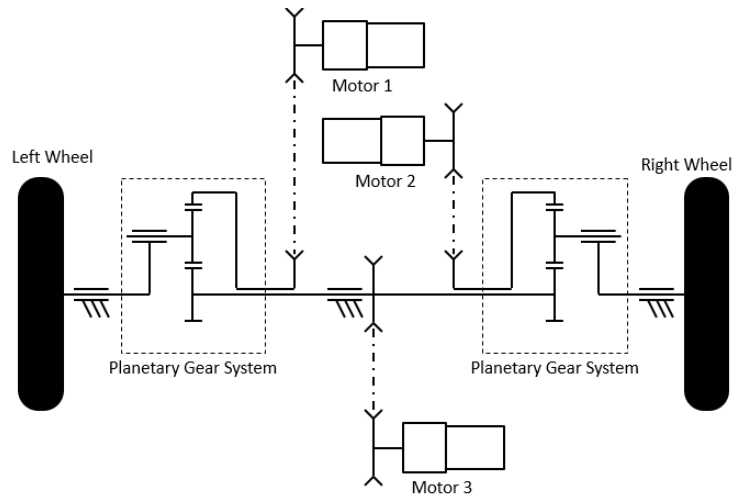
FIGURE 2.1: Redundant wheeled drive system
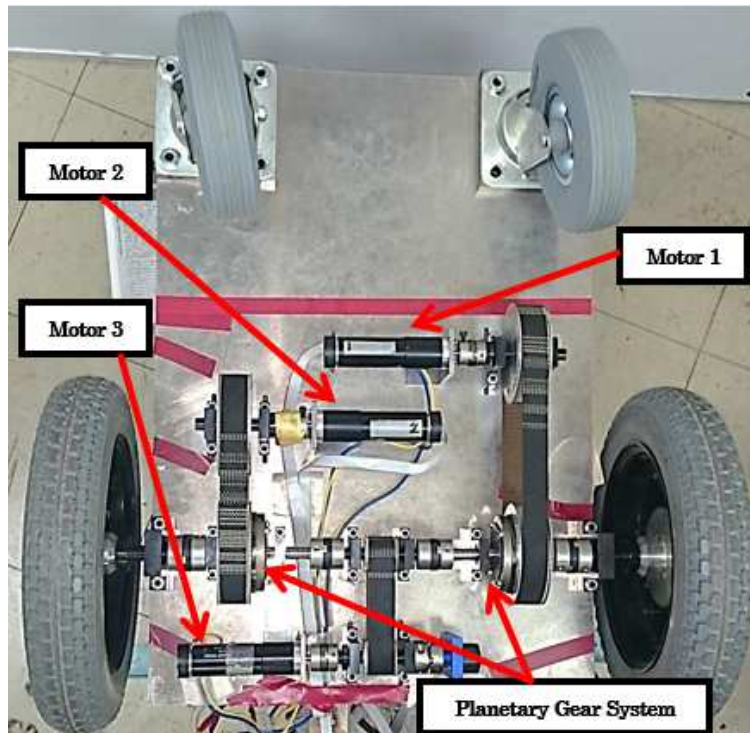
FIGURE 2.2: Experimental device (Back Side)

and 2 are connected to the left and right wheels, respectively, through each planetary

gear. Motor 3 is connected to both right and left planetary gears and supplies power for both wheels. The planetary gears consist of four main part, namely an internal gear, a planetary carrier, and an a planet gear that revolves around a sun gear. The sun gear connects to Motor 3, the internal gear connects to Motors 1 and 2, and the planetary carrier connects to each wheel.

2.2.2 Experimental setup

For this work, as shown in Fig. 2.3, an experimental testbed of a redundant wheeled drive system was used as designed by the research group of which the author was a member.
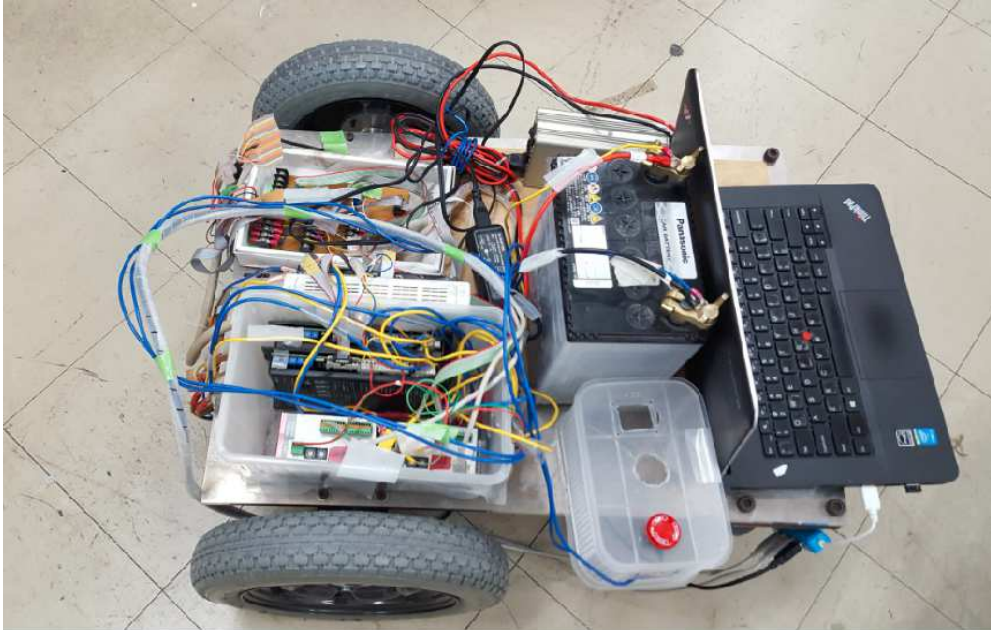
FIGURE 2.3: Experimental redundant wheeled drive system testbed

As shown in Fig 2.4, the WMR was connected to a personal computer (PC) installed with a pulse-counter board with two channels of 24-bit up/down counters and a digital-to-analog (DA) board with 16-bit resolution. Figures 2.5-2.7 show the DA board, the counter board, and the motor driver, respectively. The laptop PC acted as a controller to these boards, generating the input and output signals. In addition, to measure the angular speeds of the motors, two optical encoders of resolution 0.352 °/count are attached to Motors 1 and 2, and an optical encoder of resolution 0.18

$^\circ$/count is attached to motor 3. The motor drivers shown in Fig 2.7 are also used in a current-control mode by which an electric current is supplied that is proportional to the voltage commanded from the laptop PC to each motor. The experimental components of a redundant wheeled drive system testbed that is utilized in the study are given in Table 2.1.

Tables 2.2-2.9 list the parameters of the experimental system.
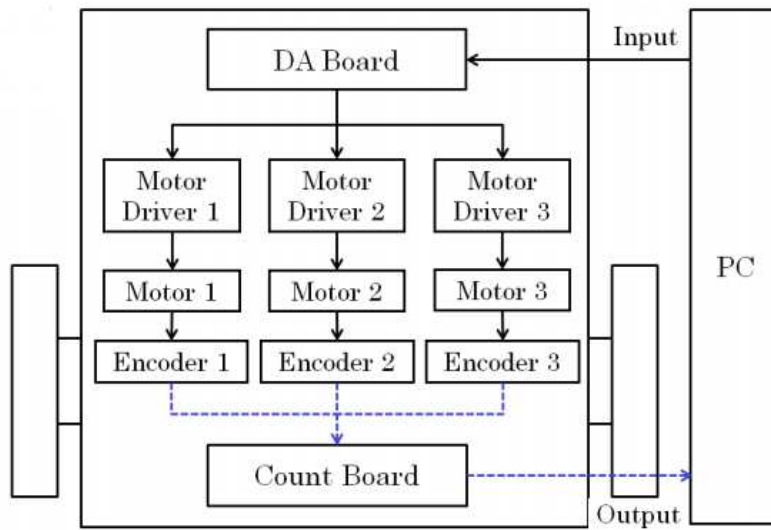
FIGURE 2.4: Overview of the control system

FIGURE 2.5: DA board

FIGURE 2.6: Counter board

FIGURE 2.7: Motor driver

TABLE 2.1: Components of experimental testbed

Components	Type	Manufacturer
DC motor	RE30, 60 Watt	Maxon motor
Motor driver	ADS 50/5	Maxon motor
Encoder of Motor 3	HEDL 5540	Maxon sensor
Encoders of Motors 1 and 2	MR Type L	Maxon sensor
Counter board	CNT24-2(USB)GY	Contec
Planetary-gear system	LGU75-M-4MDD	Matex
DA converter board	AO-1604LX-USB	Contec
PC	Intel(R) Core(TM) i7-4712MQ CPU G630 @ 2.30GHz 2.29GHz Windows 8.1 64 bits	Microsoft

TABLE 2.2: Parameters of the WMR

Symbol	Parameter	Value[unit]
M_w	Mass	46.0[kg]
I	Moment of inertia	0.625[kgm^2]
R_w	Radius of wheels	0.165[m]
L	Distance from WMR's center point to either driving wheel	0.275 [m]

TABLE 2.3: Specifications of the three Motors

Parameter	Value	Unit
Nominal voltage	12	[V]
No-load speed	8,170	[rpm]
No-load current	301	[mA]
Nominal speed	6,730	[rpm]
Nominal torque (max. continuous torque)	51.6	[mNm]
Nominal current (max. continuous current)	4	[A]
Rotor inertia	$33.7x10^{-7}$	[kgm^2]]
Torque constant	13.9	[(mNm)/A]
Max. efficiency	85	[%]

TABLE 2.4: Specifications of motor driver

Parameter	Value	Unit
Power supply voltage V_{cc}	12-50	[V]
Maximum output voltage	0.9 V_{cc}	[V]
Maximum output current	10	[A]
Continuous output current	5	[A]
PWM frequency	50	[kHz]
Setting (command) value	$-10 \cdots +10$	[V]

TABLE 2.5: Specifications of encoders of Motors 1 and 2

Item	Specification
Counts per turn	256
Number of channels	3
Max. operating frequency	80 [kHz]
Maximum speed	18,750[rpm]
Output signal	TTL compatible
Phase shift ϕ	90 e° $\pm$ 45 e°
Moment of inertia of code wheel	$\leq 1.7 x 10^{-7}$ [kgm^2]

TABLE 2.6: Specifications of encoder of Motor 3

Item	Specification
Counts per turn	500
Number of channels	3
Max. operating frequency	80 [kHz]
Maximum speed	1,200[rpm]
Output signal	EIA RS 442
Phase shift ϕ	90 e° $\pm$ 45 e°
Moment of inertia of code wheel	$\leq 0.6 x 10^{-7}$ [kgm^2]

TABLE 2.7: Specifications of DA board

Item	Specification
Isolated specification	Non-isolated
Number of output channels	4 channels
Output range	Bipolar $\pm$ 10 [V]
Absolute max. output current	$\pm$ 3[mA]
Resolution	16 [bit]
Output impedance	1Ω or less
Conversion speed	10 [s]

TABLE 2.8: Specifications of counter board

Item	Specification
Channels count	2 channels
Counting system	Up/down counting
Max. count	FFFFFFH (binary data)
Input resistance	220Ω and above
Input ON current	15-25[mA]
Conversion speed	10 [μs]

TABLE 2.9: Specifications of planetary-gear system

Item	Specification
Nominal speed reduction ratio	4
Maximum torque	$785x10^{-2}$[Nm]

2.3 Modeling a Redundant Drive System

2.3.1 Dynamical model

The motion of the WMR is shown schematically in Fig. 2.8. The proposed model includes a planetary gear property. The WMR has a plate body that has two identical driving rear wheels that are controlled by three independent actuators, and two front caster wheels that are used for motion stability. In this study, it is assumed that any slipping of the wheels can be ignored. Dynamic modeling is based on the laws of mechanics and involves three physical elements that exist in any real mechanical system, namely inertia, elasticity, and friction, [10, 37, 38]. The dynamics of the present mobile robot shown in Fig. 2.8 in is given by

$$M_w \dot{v} = D_R + D_L, \tag{2.1}$$

$$I_w \ddot{\phi} = (D_R - D_L)L, \tag{2.2}$$

where M_w, I_w, $\dot{v}$, and $\ddot{\phi}$ are the mass, moment of inertia, translational acceleration, and angular acceleration of the robot, respectively, and D_R, D_L, and L represent the driving forces applied to the right and left wheels, and the distance from the WMR's center point to either driving wheel, respectively. The relationship between the linear
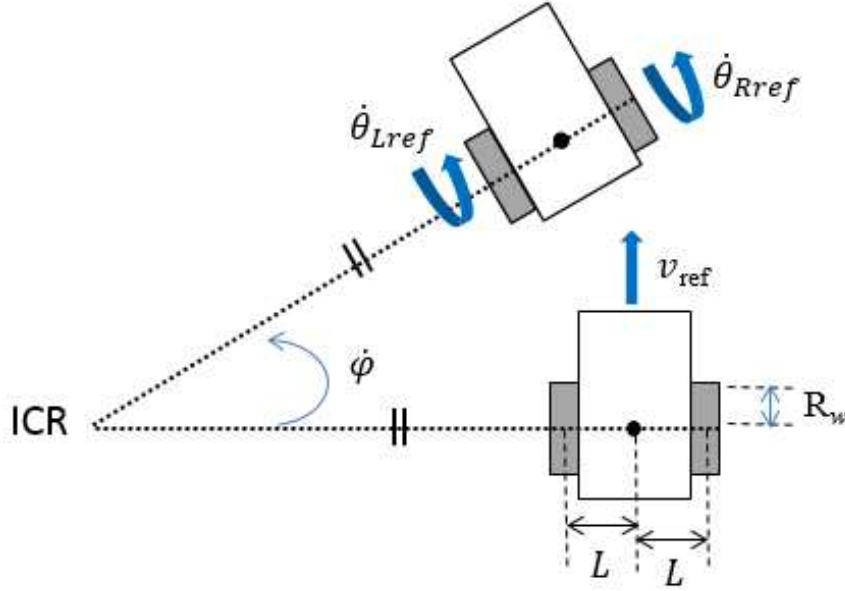
FIGURE 2.8: Two-wheeled mobile robot

velocity v of the WMR, its angular velocity $\dot{\phi}$, and the angular velocity of the two driving wheels is given by

$$\begin{bmatrix} v \\ \dot{\phi} \end{bmatrix} = \begin{bmatrix} R_w/2 & R_w/2 \\ -R_w/2L & R_w/2L \end{bmatrix} \begin{bmatrix} \dot{\theta}_L \\ \dot{\theta}_R \end{bmatrix}, \tag{2.3}$$

where $\dot{\theta}_R$ and $\dot{\theta}_L$ represent the angular velocity of the right and left wheels, respectively, and R_w is the wheels radius. The linear acceleration $\dot{v}$ of the WMR and its angular acceleration $\ddot{\phi}$ in Eqs (2.1) and (2.2) are given by the following equations:

$$\dot{v} = \frac{R_w}{2}(\ddot{\theta}_L + \ddot{\theta}_R) \tag{2.4}$$

$$\ddot{\phi} = \frac{R_w}{2L}(\ddot{\theta}_R - \ddot{\theta}_L) \tag{2.5}$$

where $\ddot{\theta}_R$ and $\ddot{\theta}_L$ represent the angular accelerations of the right and left wheels, respectively.

From Eqs. (2.1)-(2.5), the driving forces D_L and D_R, are obtained as follows:

$$D_L = \frac{R_w}{4}(M_w + \frac{I_w}{L^2})\ddot{\theta}_L + \frac{R_w}{4}(M_w - \frac{I_w}{L^2})\ddot{\theta}_R \qquad (2.6)$$

$$D_R = \frac{R_w}{4}(M_w - \frac{I_w}{L^2})\ddot{\theta}_L + \frac{R_w}{4}(M_w + \frac{I_w}{L^2})\ddot{\theta}_R \qquad (2.7)$$

2.3.2 Planetary-gear mechanism

The planetary-gear set, also known as the epicyclic gear train, is one of the most important and interesting inventions in engineering. It is a great mechanisms for varying speed, and is often used in automobiles as a vital part of an automatic transmission [39, 40]. A planetary-gear mechanism has two DOFs and four main parts, namely a sun gear, a planetary gear, an internal (ring) gear, and a planetary carrier, as shown in Fig. 2.9 [41].
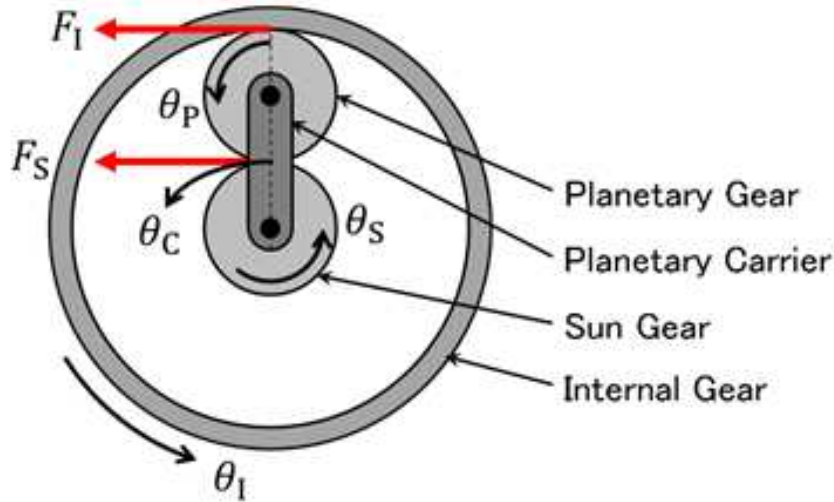
FIGURE 2.9: Planetary-gear system

In this study, a planetary-gear mechanism is used as a power combining mechanism with the sun gear and the internal gear as the input shaft, and Motors 1 and 2 are connected to the left and right planetary gears, respectively. The shaft of Motor 3 is connected to the sun gears of the left and right planetary-gear mechanisms and supplies power for both wheels. The left and right driving wheels are connected to the planetary carrier, which is the output shaft of the left and right planetary-gear

mechanisms.

When the internal gear is fixed, the relationship between the rotation speeds of the sun, carrier, and planetary gears is given by

$$R_s\dot{\theta}_C = R_s\dot{\theta}_s + R_p\dot{\theta}_p \tag{2.8}$$

where R_s and R_p represent the radii of the sun and planetary gears, respectively. Additionally $\dot{\theta}_s$, $\dot{\theta}_C$, and $\dot{\theta}_p$ represent the angular speed speeds of the sun, carrier, and planetary gears, respectively.

When the sun gear is fixed, the relationship between the rotation speeds of the internal, carrier, and planetary gears is given by

$$R_I\dot{\theta}_I = R_I\dot{\theta}_C + R_P\dot{\theta}_p \tag{2.9}$$

where R_I and $\dot{\theta}_I$ represent the radius and angular speed, respectively, of the internal gear.

From Eqs. (2.8) and (2.9), the relationship between the angular speeds of the sun and internal gears as the input shaft and the angular speed of the planetary carrier as the output shaft is obtained as follows:

$$\dot{\theta}_C = \frac{R}{R+1}\dot{\theta}_I + \frac{1}{R+1}\dot{\theta}_s, \qquad R = \frac{R_I}{R_s} \tag{2.10}$$

where R is the ratio of the internal gear radius to the sun gear.

The equation of motion of each element in the planetary-gear mechanism is as follows:

$$J_s\ddot{\theta}_s + C_s\dot{\theta}_s = \tau_s - R_sF_s \tag{2.11}$$

$$J_I\ddot{\theta}_I + C_I\dot{\theta}_I = \tau_I - RR_sF_I \tag{2.12}$$

$$J_P\ddot{\theta}_P + C_P\dot{\theta}_P = R_PF_I - R_PF_s \tag{2.13}$$

$$J_C\ddot{\theta}_P + C_C\dot{\theta}_C = R_IF_I - R_sF_s - T_C \tag{2.14}$$

where J_{ii}, τ_{ii}, and C_{ii} ($ii = s, I, P$, or C) represent the moment of inertia, the torque,

and the viscous friction coefficient, respectively, of each element in the planetary-gear mechanism shown in Fig. 2.9. The subscript *ii* is distinguished by substituting s, I, P, or C represent the sun gear, internal gear, planetary gear, or planetary carrier, respectively. The term F_s represents the force acting between the sun and planetary gears, F_I represents the force acting between the planetary and internal gears, and T_C represents the external torque acting on the planetary carrier.

In addition, there is no external device attached to the planetary gear. Therefore, the values of J_P and C_P are sufficiently small and to be neglected. Therefore, by assuming $J_P = C_P = 0$, Eq. (2.13) will be as follows:

$$F_I = F_s = F \tag{2.15}$$

By substituting Eq. (2.15) into Eqs. (2.11), (2.13), and (2.14), then

$$J_s \ddot{\theta}_s + C_s \dot{\theta}_s = \tau_s - R_s F \tag{2.16}$$

$$J_I \ddot{\theta}_I + C_I \dot{\theta}_I = \tau_I - R R_s F \tag{2.17}$$

$$J_C \ddot{\theta}_P + C_C \dot{\theta}_C = (R+1) R_s F - T_C \tag{2.18}$$

2.3.3 Redundant drive system

In this study, Motors 1 and 2 are connected to the internal gears of the left and right planetary-gear sets, respectively, and Motor 3 is connected to the sun gears of both planetary-gear sets as shown in Fig. 2.10. The left and right drive wheels are connected to the planetary carriers of both planetary-gear sets. Therefore, the relationship between the angular velocity $\dot{\theta}_R$, of the right wheel, the angular velocity $\dot{\theta}_L$ of the left wheel, and the velocities of the three motors can be obtained similarity to Eq. (2.10).

$$\dot{\theta}_L = \frac{R}{R+1} \dot{\theta}_1 + \frac{1}{R+1} \dot{\theta}_3 \tag{2.19}$$
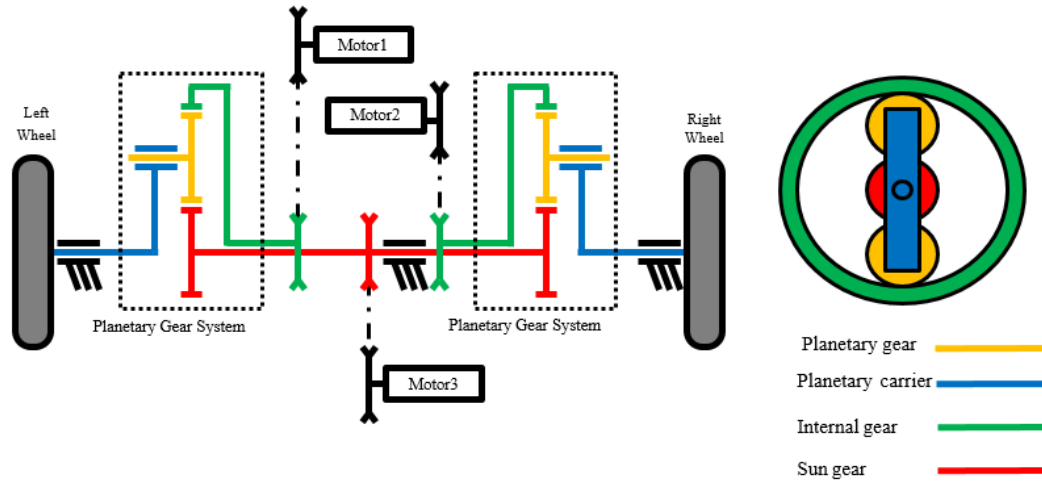
FIGURE 2.10: Drive mechanism

$$\dot{\theta}_R = \frac{R}{R+1}\dot{\theta}_2 + \frac{1}{R+1}\dot{\theta}_3 \tag{2.20}$$

where $\dot{\theta}_1$, $\dot{\theta}_2$, and $\dot{\theta}_3$ represent the angular velocities of motors 1, 2 and 3, respectively.

The dynamical equations of the motors are given by

$$J_1\ddot{\theta}_1 + C_1\dot{\theta}_1 = \tau_1 - RR_sF_L \tag{2.21}$$

$$J_2\ddot{\theta}_2 + C_2\dot{\theta}_2 = \tau_2 - RR_sF_R \tag{2.22}$$

$$J_3\ddot{\theta}_3 + C_3\dot{\theta}_3 = \tau_3 - R_sF_L - R_sF_R, \tag{2.23}$$

where J_i and τ_i ($i = 1,2,3$), represent the moment of inertia and the torque, respectively, of motor i in Figs. 2.1 and 2.2. Here C_i is the viscous friction coefficient and R_s is the radius of the sun gear.

The equations of motion of the left and right wheels can be obtained from Eq. (2.18) as follows:

$$J_L\ddot{\theta}_L + C_L\dot{\theta}_L = (R+1)R_sF_L - R_wD_L \tag{2.24}$$

$$J_R\ddot{\theta}_R + C_R\dot{\theta}_R = (R+1)R_sF_R - R_wD_R \tag{2.25}$$

where J_R and J_L represent the moments of inertia for the right and left wheels, respectively; C_R and C_L are the viscous friction coefficients for the right and left wheels, respectively.

By substituting Eqs. (2.19) and (2.20) into Eqs. (2.6) and (2.7), the driving forces D_L and D_R, are obtained as follows:

$$D_L = \frac{RR_w}{4(R+1)}\left(M_w + \frac{I_w}{L^2}\right)\ddot{\theta}_1 + \frac{RR_w}{4(R+1)}\left(M_w - \frac{I_w}{L^2}\right)\ddot{\theta}_2 + \frac{M_wR_w}{2(R+1)}\ddot{\theta}_3 \quad (2.26)$$

$$D_R = \frac{RR_w}{4(R+1)}\left(M_w - \frac{I_w}{L^2}\right)\ddot{\theta}_1 + \frac{RR_w}{4(R+1)}\left(M_w + \frac{I_w}{L^2}\right)\ddot{\theta}_2 + \frac{M_wR_w}{2(R+1)}\ddot{\theta}_3 \quad (2.27)$$

By substituting Eqs. (2.19), (2.20), and (2.26) into Eqs. (2.24), then

$$\begin{aligned}
R_sF_L = \frac{R}{(R+1)^2}&\left\{J_L + \frac{R_w}{4}\left(M_w + \frac{I_w}{L^2}\right)\right\}\ddot{\theta}_1 + \frac{RR_w^2}{4(R+1)^2}\left(M_w - \frac{I_w}{L^2}\right)\ddot{\theta}_2 \\
&+ \frac{1}{(R+1)^2}\left(J_L + \frac{M_wR_w}{2}\right)\ddot{\theta}_3 + \frac{R}{(R+1)^2}C_L\dot{\theta}_1 + \frac{1}{(R+1)^2}C_L\dot{\theta}_3
\end{aligned} \quad (2.28)$$

By substituting Eq. (2.28) into Eq. (2.21) and multiplying by $\frac{R+1}{R}$, then

$$\begin{aligned}
(\frac{R+1}{R})\tau_1 = &\left\{\frac{R+1}{R}J_1 + \frac{R}{R+1}\left\{J_L\frac{R_w}{4}\left(M_w + \frac{I_w}{L^2}\right)\right\}\right\}\ddot{\theta}_1 \\
&+ \frac{RR_w^2}{4(R+1)}\left(M_w - \frac{I_w}{L^2}\right)\ddot{\theta}_2 + \frac{1}{R+1}\left(J_L + \frac{M_wR_w}{2}\right)\ddot{\theta}_3 \\
&+ \left(\frac{R+1}{R}C_1 + \frac{R}{R+1}C_L\right)\dot{\theta}_1 + \frac{1}{R+1}C_L\dot{\theta}_3
\end{aligned} \quad (2.29)$$

By substituting Eqs. (2.19), (2.20), and (2.27) into Eq. (2.25), then

$$\begin{aligned}
R_sF_R = &\frac{RR_w^2}{4(R+1)^2}\left(M_w - \frac{I_w}{L^2}\right)\ddot{\theta}_1 + \frac{R}{(R+1)^2}\left\{J_R + \frac{R_w}{4}\left(M_w + \frac{I_w}{L^2}\right)\right\}\ddot{\theta}_2 \\
&+ \frac{1}{(R+1)^2}\left(J_R + \frac{M_wR_w}{2}\right)\ddot{\theta}_3 + \frac{R}{(R+1)^2}C_R\dot{\theta}_2 + \frac{1}{(R+1)^2}C_R\dot{\theta}_3
\end{aligned} \quad (2.30)$$

By substituting Eq. (2.30) into Eq. (2.22) and multiplying by $\frac{R+1}{R}$, then

$$\begin{aligned}
(\frac{R+1}{R})\tau_2 = &\frac{RR_w^2}{4(R+1)}\left(M_w - \frac{I_w}{L^2}\right)\ddot{\theta}_1 + \left\{\frac{R+1}{R}J_2 + \frac{R}{R+1}\left\{J_R + \frac{R_w}{4}\left(M_w + \frac{I_w}{L^2}\right)\right\}\right\}\ddot{\theta}_2 \\
&+ \frac{1}{R+1}\left(J_R + \frac{M_wR_w}{2}\right)\ddot{\theta}_3 \\
&+ \left(\frac{R+1}{R}C_2 + \frac{R}{R+1}C_R\right)\dot{\theta}_2 + \frac{1}{R+1}C_R\dot{\theta}_3
\end{aligned}$$

$$(2.31)$$

By substituting Eqs. (2.28) and (2.30) into Eq. (2.23), then

$$
\begin{aligned}
(R+1)\tau_3 = {} & \frac{R}{R+1}\left(J_L + \frac{M_w R_w^2}{2}\right)\ddot{\theta}_1 + \frac{R}{R+1}\left(J_R + \frac{M_w R_w^2}{2}\right)\ddot{\theta}_2 \\
& + \left((R+1)J_3 + \frac{1}{R+1}\left(J_L + J_R + M_w R_w^2\right)\right)\ddot{\theta}_3 + \frac{R}{R+1}C_L\dot{\theta}_1 \quad (2.32) \\
& + \frac{R}{R+1}C_R\dot{\theta}_2 + \left((R+1)C_3 + \frac{1}{R+1}(C_L + C_R)\right)\dot{\theta}_3
\end{aligned}
$$

From Eqs. (2.29), (2.31), and (2.32), the equation of motion of the redundant wheeled mobile robot is obtained as follows:

$$
M\ddot{\theta} + C\dot{\theta} = G\tau, \tag{2.33}
$$

where M is the 3x3 inertia matrix, C is the 3x3 viscous friction matrix, and G is the 3x3 control input matrix, as follows:

$$
M = \begin{bmatrix} m_{11} & m_{12} & m_{13} \\ m_{21} & m_{22} & m_{23} \\ m_{31} & m_{32} & m_{33} \end{bmatrix}, \tag{2.34}
$$

$$
\dot{\theta} = \begin{bmatrix} \dot{\theta}_1 \\ \dot{\theta}_2 \\ \dot{\theta}_3 \end{bmatrix}, \quad \ddot{\theta} = \begin{bmatrix} \ddot{\theta}_1 \\ \ddot{\theta}_2 \\ \ddot{\theta}_3 \end{bmatrix}, \quad \tau = \begin{bmatrix} \tau_1 \\ \tau_2 \\ \tau_3 \end{bmatrix}, \tag{2.35}
$$

$$m_{11} = \frac{J_1}{R_R} + \frac{R_R R_w^2}{4} \left\{ M_w + \frac{I}{L^2} \right\} + J_L R_R,$$

$$m_{12} = \frac{R_R R_w^2}{4} \left\{ M_w - \frac{I}{L^2} \right\},$$

$$m_{13} = \frac{M_w R_1 R_w^2}{2} + J_L R,$$

$$m_{21} = \frac{R_R R_w^2}{4} \left\{ M_w - \frac{I}{L^2} \right\},$$

$$m_{22} = \frac{J_2}{R_R} + \frac{R_R R_w^2}{4} \left\{ M_w + \frac{I}{L^2} \right\} + J_R R_R, \qquad (2.36)$$

$$m_{23} = \frac{M_w R_1 R_w^2}{2} + J_R R_1,$$

$$m_{31} = \frac{M_w R_R R_w^2}{2} + J_L R_R,$$

$$m_{32} = \frac{M_w R_R R_w^2}{2} + J_R R_R,$$

$$m_{33} = M_w R_1 R_w^2 + J_L R_1 + J_R R_1 + \frac{J_3}{R_1},$$

$$G = \begin{bmatrix} 1/R_R & 0 & 0 \\ 0 & 1/R_R & 0 \\ 0 & 0 & 1/R_1 \end{bmatrix}, \qquad (2.37)$$

$$R_1 = \frac{1}{1+R}, \quad R_R = \frac{R}{1+R}, \qquad (2.38)$$

$$C = \begin{bmatrix} \frac{C_1}{R_R} + C_L R_R & 0 & C_L R_1 \\ 0 & \frac{C_2}{R_R} + C_R R_R & C_R R_1 \\ C_L R_R & C_R R_R & \frac{C_3}{R_1} + C_L R_1 + C_L R_1 \end{bmatrix}, \qquad (2.39)$$

Chapter 3

Velocity Distribution for Energy Saving with a Redundant Wheeled Drive System

3.1   Introduction

Mobile robots are widely used in many different applications, such as transportation, the military, search and rescue, guidance, hazard detection, and domestic cleaning [10, 42–44]. Robots usually carry limited power sources, and it is generally impossible to supply additional energy while working, so energy conservation is an important concern for mobile robots [14–18].

A differential wheeled mobile robot (DWMR) involves two independently driven wheels on a common axis [10]. The robot moves forward or backward in a straight line when the wheels rotate at the same speed, but follows a curved path along an arc of the instantaneous circle around the ICR when one wheel rotates faster than the other [10]. The robot turns about the midpoint of the two driving wheels when both wheels rotate at the same speed in opposite directions. If one of the motors should break down or become damaged for some reason, the robot would roll around the wheel that is connected to the damaged motor. Eventually, there could be a risk to the passenger's life because he or she could not continue moving.

Energy saving is also an important topic in relation to mobile robots for increasing the operating time using the same battery capacity. Duleba and Sasiadejk [30] discussed a modification of the Newton algorithm applied to nonholonomic motion planning for energy optimization. However, the amount of energy consumed was not estimated. Ueno *et al.* [27] proposed a differential-drive steering system for the caster drive wheel of an omni-directional mobile robot. However, the system is complex because it uses two motors for each wheel. Because mobility demands limit the ability to use independent power sources, energy management is the key factor when it comes to completing tasks. To overcome this, the research group of which the author was a member designed a wheeled system consisting of a redundant drive system to continue its motion safely should one of the motors break down for some reason [45, 46]. In addition, the redundancy allows each motor to be operated at its most efficient. The system uses three motors and two planetary-gear systems that have high transmission efficiency and durability for high power.

This chapter deals with a new design of WMRs to guarantee secure motion even if one drive system does not work. In addition, its effectiveness for energy saving is analyzed to increase the operating time using the limited battery capacity. Furthermore, simulation and experimental results demonstrate that the proposed method is effective practically .The experimental results in this chapter show that the method in saving energy by 20.45% for linear motion and 13.05% for circular motion compared to a conventional drive system.

This chapter relates to the work presented in Refs. [46] and [47].

3.2 Controller Design

3.2.1 Distribution controller

The control inputs of a WMR in are usually considered to be its linear and angular velocities. Figure 3.1 shows the block diagram of the control system. By assuming that, as with a personal mobility vehicle such as an electric wheelchair, the reference

linear velocity v_{ref} and angular velocity $\dot{\phi}_{ref}$ of the vehicle are given by its operator. These velocities are then typically transformed into desired velocities of the left and right wheels by using Eq. (3.2). Firstly, by introducing a fixed ratio d of angular
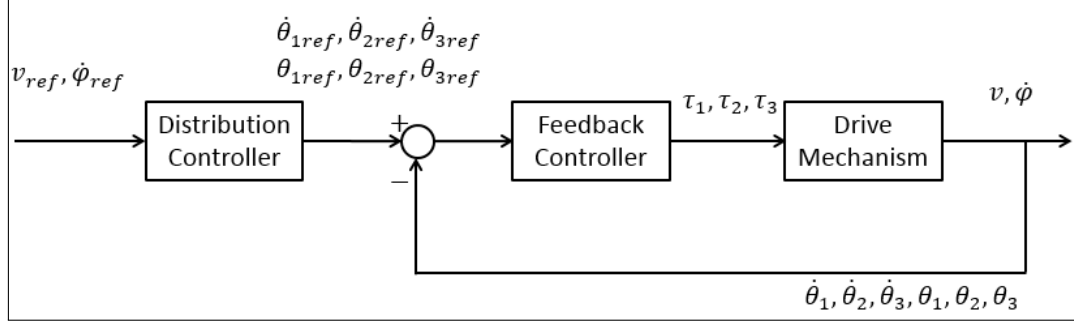

FIGURE 3.1: Block diagram of the control system

velocities of a wheels to the velocity of Motor 3 as follows:

$$R_1\dot{\theta}_{3ref} = \frac{v_{ref}}{R_w}\cdot\frac{1}{d} \tag{3.1}$$

By rewriting Eq. (2.3), the relationship between the desired linear velocity v_{ref} of the WMR, its desired angular velocity $\dot{\phi}_{ref}$, and the desired angular velocity of the two driving wheels are obtained as follows:

$$\begin{bmatrix} v_{ref} \\ \dot{\phi}_{ref} \end{bmatrix} = \begin{bmatrix} R_w/2 & R_w/2 \\ -R_w/2L & R_w/2L \end{bmatrix}\begin{bmatrix} \dot{\theta}_{Lref} \\ \dot{\theta}_{Rref} \end{bmatrix}, \tag{3.2}$$

From Eq. (3.2), the desired linear velocity v_{ref} is obtained as follows:

$$v_{ref} = \frac{R_w}{2}(\dot{\theta}_{Lref} + \dot{\theta}_{Rref}) \tag{3.3}$$

By substituting Eq. (3.3) into Eq. (3.1), the desired angular velocity $\dot{\theta}_{3ref}$ of Motor 3 is obtained as follows:

$$\dot{\theta}_{3ref} = \begin{bmatrix} 1/(2dR_1) & 1/(2dR_1) \end{bmatrix}\begin{bmatrix} \dot{\theta}_{Lref} \\ \dot{\theta}_{Rref} \end{bmatrix}, \tag{3.4}$$

By rewriting Eqs. (2.19) and (2.20), the desired angular velocity $\dot{\theta}_{Rref}$ of the right wheel and the desired angular velocity $\dot{\theta}_{Lref}$ of the left wheel are represented by the

desired velocities of three motors as follows:

$$
\begin{bmatrix} \dot{\theta}_{Lref} \\ \dot{\theta}_{Rref} \end{bmatrix} = \begin{bmatrix} R_R & 0 \\ 0 & R_R \end{bmatrix} \begin{bmatrix} \dot{\theta}_{1ref} \\ \dot{\theta}_{2ref} \end{bmatrix} + \begin{bmatrix} R_1 \\ R_1 \end{bmatrix} \dot{\theta}_{3ref},
\tag{3.5}
$$

By substituting Eq. (3.4) into Eqs. (3.5), the following equation is obtained

$$
\begin{bmatrix} \dot{\theta}_{Lref} \\ \dot{\theta}_{Rref} \end{bmatrix} = \begin{bmatrix} R_R & 0 \\ 0 & R_R \end{bmatrix} \begin{bmatrix} \dot{\theta}_{1ref} \\ \dot{\theta}_{2ref} \end{bmatrix} + \begin{bmatrix} 1/(2d) & 1/(2d) \\ 1/(2d) & 1/(2d) \end{bmatrix} \begin{bmatrix} \dot{\theta}_{Lref} \\ \dot{\theta}_{Rref} \end{bmatrix},
\tag{3.6}
$$

Rearranging (3.6), the desired angular velocities $\dot{\theta}_{1ref}$ and $\dot{\theta}_{2ref}$ of Motors 1 and 2 are obtained as follows:

$$
\begin{bmatrix} \dot{\theta}_{1ref} \\ \dot{\theta}_{2ref} \end{bmatrix} = \frac{1}{R_R} \begin{bmatrix} 1 - 1/(2d) & -1/(2d) \\ -1/(2d) & 1 - 1/(2d) \end{bmatrix} \begin{bmatrix} \dot{\theta}_{Lref} \\ \dot{\theta}_{Rref} \end{bmatrix},
\tag{3.7}
$$

By substituting Eq. (3.5) into Eq. (3.3), the desired linear velocity of the WMR is represented by the desired velocities of the three motors as follows:

$$
v_{ref} = \frac{R_w}{2}(R_R \dot{\theta}_{1ref} + R_R \dot{\theta}_{2ref} + 2R_1 \dot{\theta}_{3ref})
\tag{3.8}
$$

In this study, the following three cases of d are considered.

1. By substituting $d = 1$ into Eqs. (3.4) and (3.7), only Motor 3 is used for the motion.

$$
v_{ref} = R_1 R_w \dot{\theta}_{3ref}
\tag{3.9}
$$

2. By substituting $d = \infty$ into Eqs. (3.4) and (3.7), only Motors 1 and 2 are used for the motion.

$$
v_{ref} = \frac{R_w R_R}{2}(\dot{\theta}_{1ref} + \dot{\theta}_{2ref})
\tag{3.10}
$$

3. By substituting d such that $\infty > d > 1$ into Eqs. (3.4) and (3.7), all the three motors are used for the motion.

$$v_{ref} = \frac{R_w}{2}(R_R\dot{\theta}_{1ref} + R_R\dot{\theta}_{2ref} + 2R_1\dot{\theta}_{3ref}) \tag{3.11}$$

3.2.2 State-feedback controller

The dynamics of a redundant wheeled drive system in Eq. (2.33) can be represented in the following state-space form:

$$\dot{x}_e = Ax_e + Bu \tag{3.12}$$

By rearranging Eq. (2.33), the following equation is obtained :

$$\begin{aligned}\ddot{\theta} &= -M^{-1}C\dot{\theta} + M^{-1}G\tau, \\ &= A_1\dot{\theta} + B_1\tau,\end{aligned} \tag{3.13}$$

where the state variable $x_e = [\theta_i \quad \dot{\theta}_i]^T$ and the control input $u_i = \tau_i$, $(i = 1,2,3)$. The state equation of the redundant wheeled drive system is obtained by setting the coefficient matrix of Eq. (3.12) as follows:

$$A = \begin{bmatrix} O_3 & I_3 \\ O_3 & A_1 \end{bmatrix}, \quad B = \begin{bmatrix} O_3 \\ B_1 \end{bmatrix}, \tag{3.14}$$

where O_3 is the 3x3 zero matrix and I_3 is the 3x3 identity matrix. In this study, by assuming that the commercial motor controllers are based on PD control, and the state-feedback controller is applied to the proposed WMR as the feedback controller. The feedback gains are obtained by the pole placement method. Consider the following controller:

$$\tau = Kx_e, \tag{3.15}$$

where τ is the control input and K is the 3x6 feedback gain matrix as follows:

$$
K = \begin{bmatrix}
k_{p11} & k_{p12} & k_{p13} & k_{d11} & k_{d12} & k_{d13} \\
k_{p21} & k_{p22} & k_{p23} & k_{d21} & k_{d22} & k_{d23} \\
k_{p31} & k_{p32} & k_{p33} & k_{d31} & k_{d32} & k_{d33}
\end{bmatrix}, \tag{3.16}
$$

where k_{pij} and k_{dij}, $(i = j = 1,2,3)$, are the motor angle and velocity feedback gains, respectively, and x_e is the difference between the reference and actual value of each state variable.

$$
x_e = \begin{bmatrix}
\theta_{1ref} - \theta_1 \\
\theta_{2ref} - \theta_2 \\
\theta_{3ref} - \theta_3 \\
\dot{\theta}_{1ref} - \dot{\theta}_1 \\
\dot{\theta}_{2ref} - \dot{\theta}_2 \\
\dot{\theta}_{3ref} - \dot{\theta}_3
\end{bmatrix} \tag{3.17}
$$

3.3   Simulation and Experimental Results

In this work, should one motor break down, the operator would stop the system immediately and switch the drive mode of the vehicle into two-motor control mode. Thus, issues of singularity or instability during transition of the drive mode are not considered in this study and are left for future work and any sliding of the wheels is negligible. To verify the effectiveness and possibility of the proposed new drive system for energy saving and fail-safe motion, a computer simulation is conducted. A sample-decoupled PD controller is applied for each motor i, where the proportional and derivative gains are 10 Nm/rad and 1 Nms/rad, respectively.

Figure 3.2 shows the S-shaped velocity profile used as a reference translation velocity of the WMR. The velocity $v(t)$ and acceleration $a(t)$ of each period are described by the following equations:
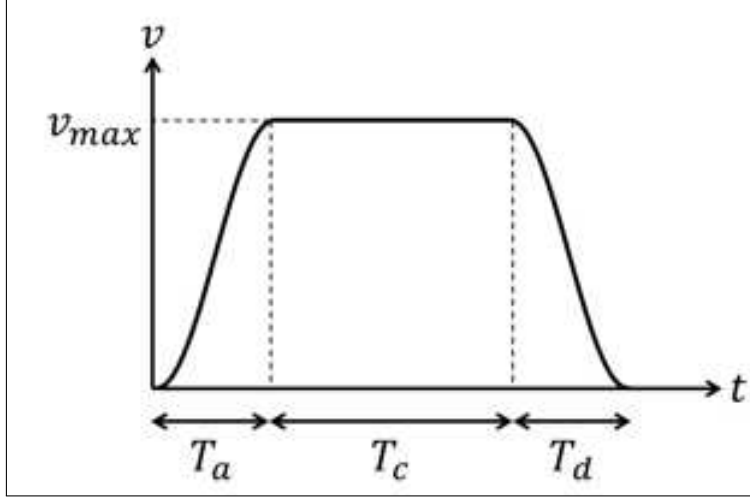
FIGURE 3.2: S-shaped velocity profile

$$
v(t) = \begin{cases} \frac{v_{max}}{2}\left(1 - \cos\left(\frac{\pi}{T_a}t\right)\right) & t \in [0, T_a) \\ v_{max} & t \in [T_a, T_a + T_c) \\ \frac{v_{max}}{2}\left(1 + \cos\left(\frac{\pi}{T_d}(t - T + T_a)\right)\right) & t \in [T_a + T_c, T] \end{cases} \quad (3.18)
$$

$$
a(t) = \begin{cases} \frac{v_{max}}{2}\left(\frac{\pi}{T_a}\sin\left(\frac{\pi}{T_a}t\right)\right) & t \in [0, T_a) \\ 0.0 & t \in [T_a, T_a + T_c) \\ \frac{v_{max}}{2}\left(\frac{\pi}{T_d}\sin\left(\frac{\pi}{T_d}(t - T + T_a)\right)\right) & t \in [T_a + T_c, T] \end{cases} \quad (3.19)
$$
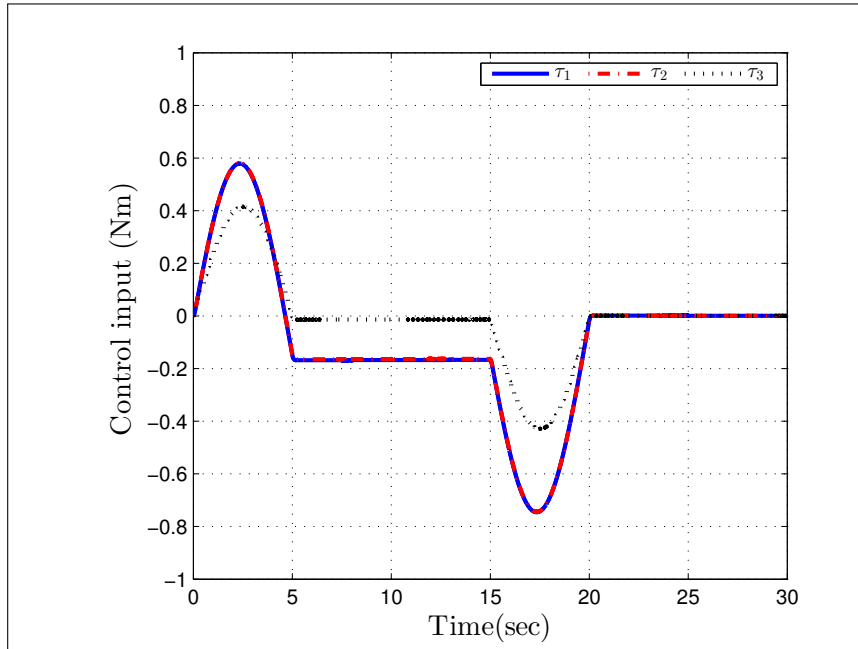
$$
v_{max} = \frac{L}{T - T_a}, \quad (3.20)
$$

where T_a is the acceleration period, T_c is the constant velocity period, T_d is the deceleration period, T is the total motion time, L is the total motion distance, and v_{max} is the constant velocity.

This study considers only smooth trajectories. If a non-smooth trajectory is required, the robot must stop once to avoid infinite acceleration. The dynamic parameters are listed in Table 3.1. In straight-line motion, the rotational velocity is set as $\dot{\phi} = 0.0$ rad/s. The maximum velocity is set as $v_{refmax} = 0.668$ m/s, with $T_a = 5$ s, $T_c = 10$ s, and $T_d = 5$ s. This simulation applies various values of d. Figures 3.3, 3.4, and 3.5 show the simulation results for the control input of each motor. Figures 3.6, 3.7, and 3.8 show the simulation results for the translational speed and linear velocity of

31

each motor. In Fig. 3.6, for $d = \infty$, only Motors 1 and 2 operate, as expected. In Fig. 3.7, for $d = 1$, only Motor 3 operates, as expected. For any other value of d, all three motors work, as shown in Fig. 3.8. Circular motion is obtained by setting the rotational velocity $\dot{\phi} = 0.5$ rad/s, as shown in Fig. 3.9, whereupon the path has the velocity profile shown in Fig 3.10. Figures 3.11 and 3.12 show the tracking performance from off-trajectory initial conditions, showing the effectiveness of the feedback controller.

TABLE 3.1: Dynamical parameters values

Parameter	Value	Unit
M_w	46.0	[kg]
I	6.25 x 10^{-1}	[kgm^2]
R_w	1.65 x 10^{-1}	[m]
L	2.75 x 10^{-1}	[m]
J_1, J_2	1.49 x 10^{-2}	[kgm^2]
J_3	1.81 x 10^{-3}	[kgm^2]
J_L, J_R	3.4 x 10^{-2}	[kgm^2]
C_1, C_2	2.68 x 10^{-2}	[Nms/rad]
C_3	1.02 x 10^{-2}	[Nms/rad]
C_L	7.13 x 10^{-3}	[Nms/rad]
C_R	5.84 x 10^{-3}	[Nms/rad]
R	3	-

FIGURE 3.3: Control input of all three motors ($d=\infty$), the same profile is obtained for τ_1 and τ_2
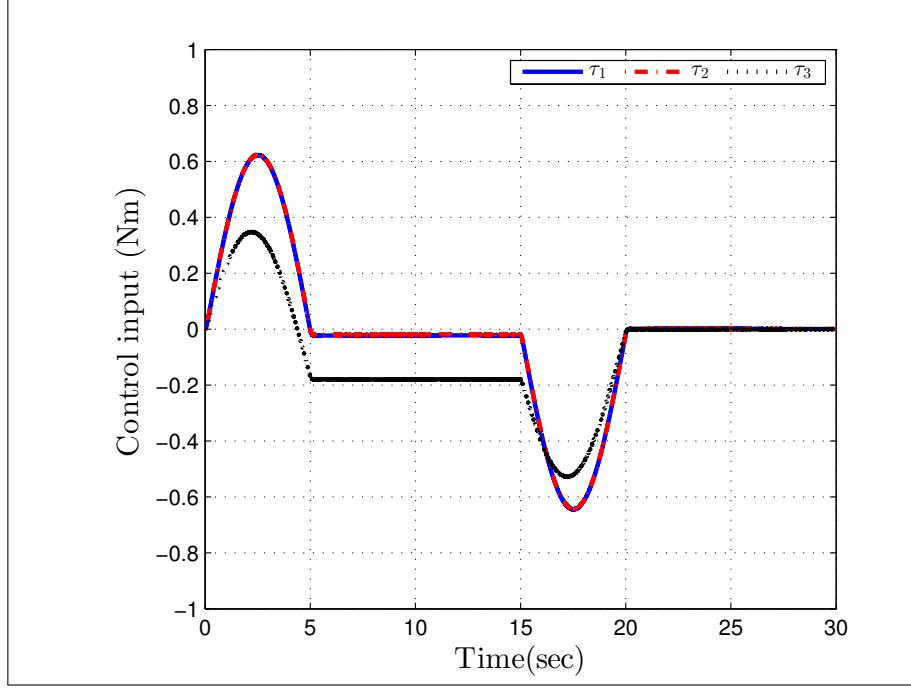
FIGURE 3.4: Control input of all three motors (*d=1*), the same profile is obtained for τ_1 and τ_2
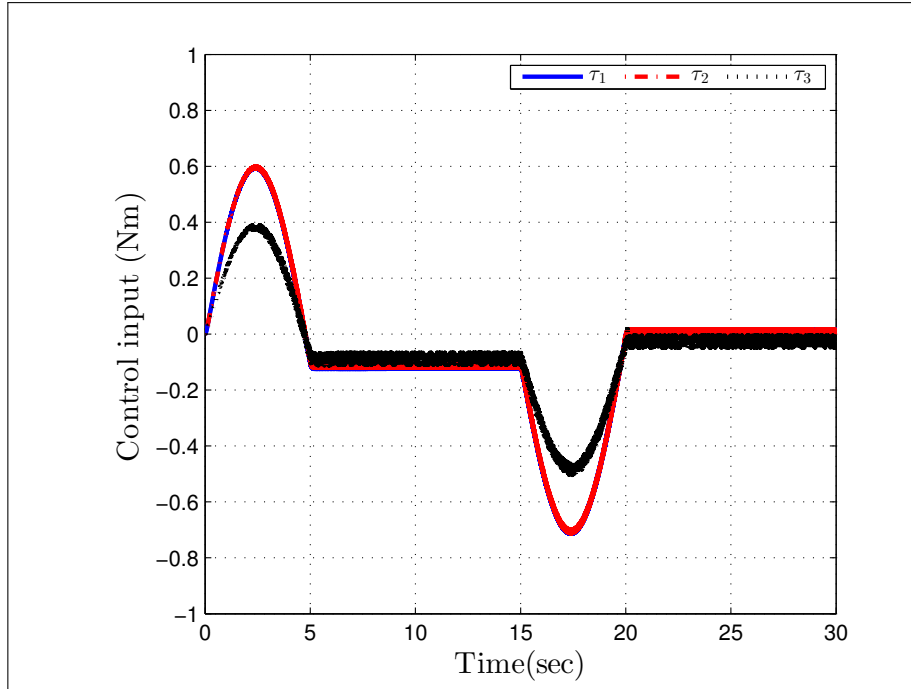

FIGURE 3.5: Control input of all three motors (*d=3.5*), the same profile is obtained for τ_1 and τ_2

Different robot speeds are assessed in the simulation by setting a maximum velocity of $v_{refmax} = 1$ m/s in the S-shaped velocity profile by as shown in Figs. 3.13-3.15. Simulations and experiments are conducted with the same parameters to verify the effectiveness of the proposed method. The feedback gains as given in Table 3.2 are
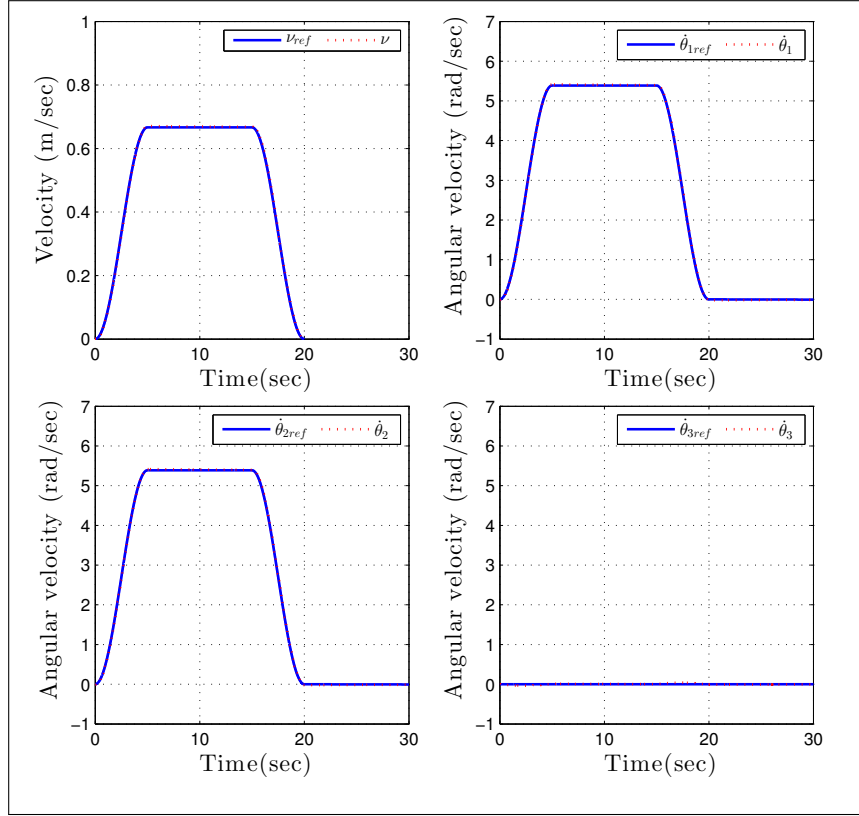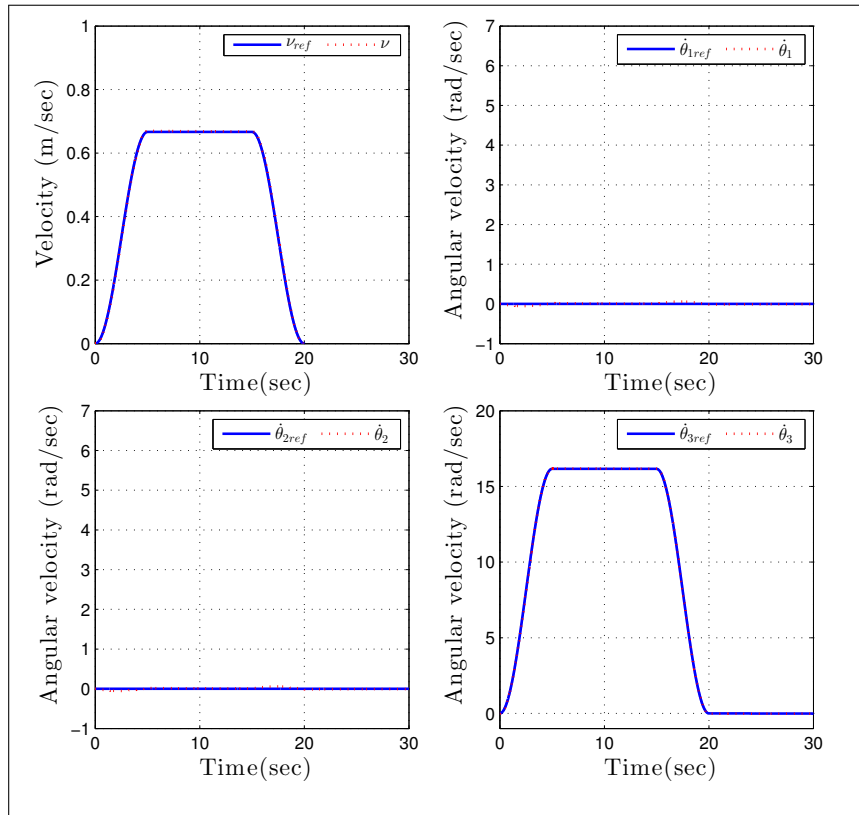
FIGURE 3.6: Simulation result ($d=\infty$)
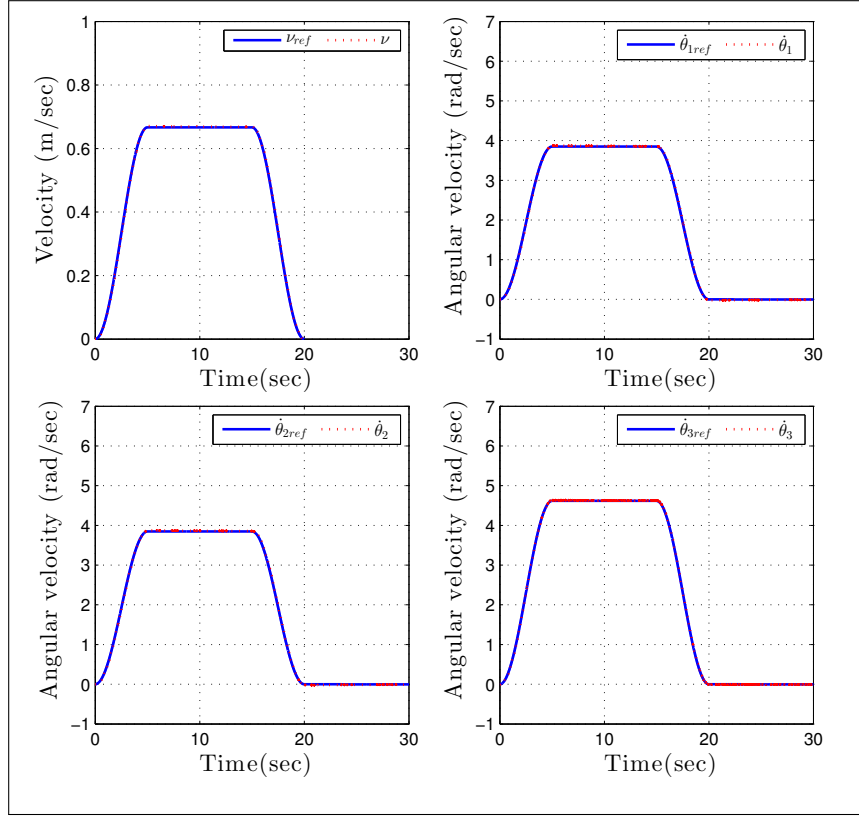

FIGURE 3.7: Simulation result ($d=1$)

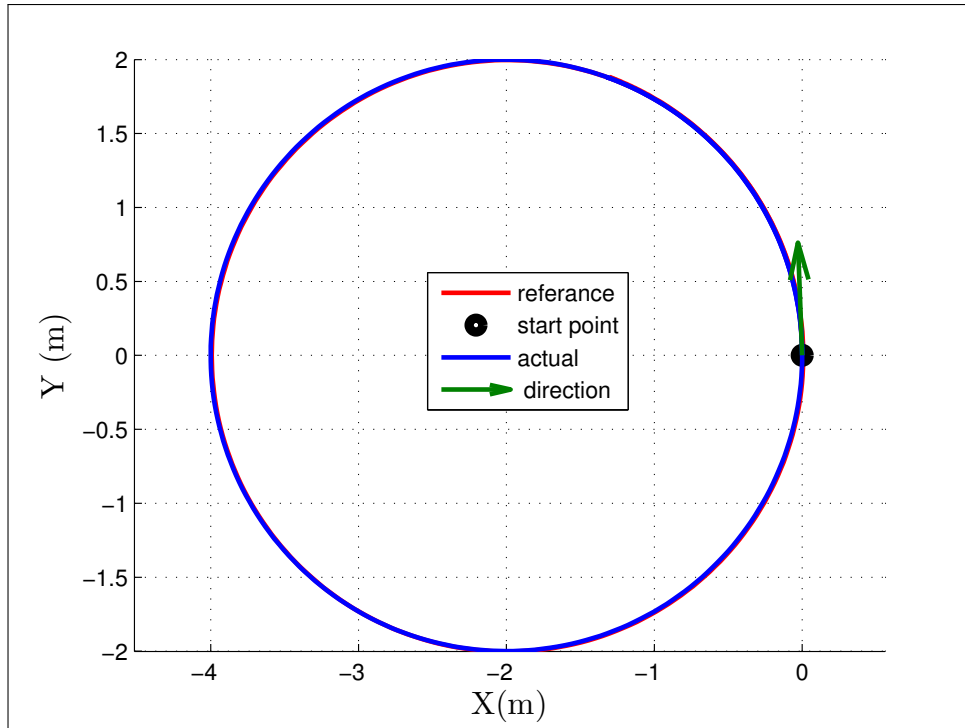FIGURE 3.8: Simulation result (*d=3.5*)

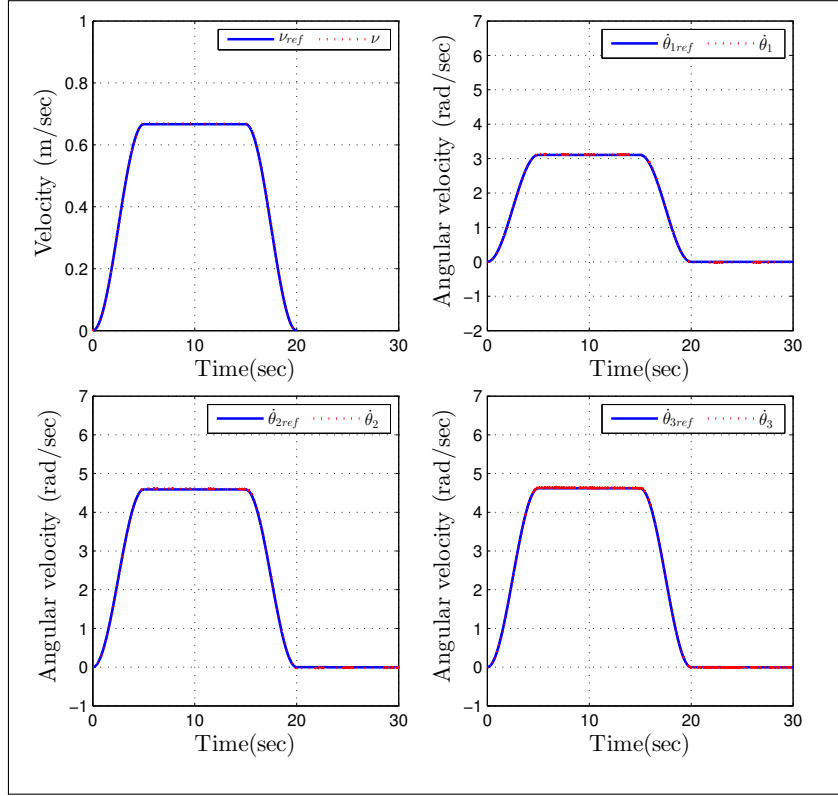FIGURE 3.9: Simulation result for circular motion (*d=3.5*)

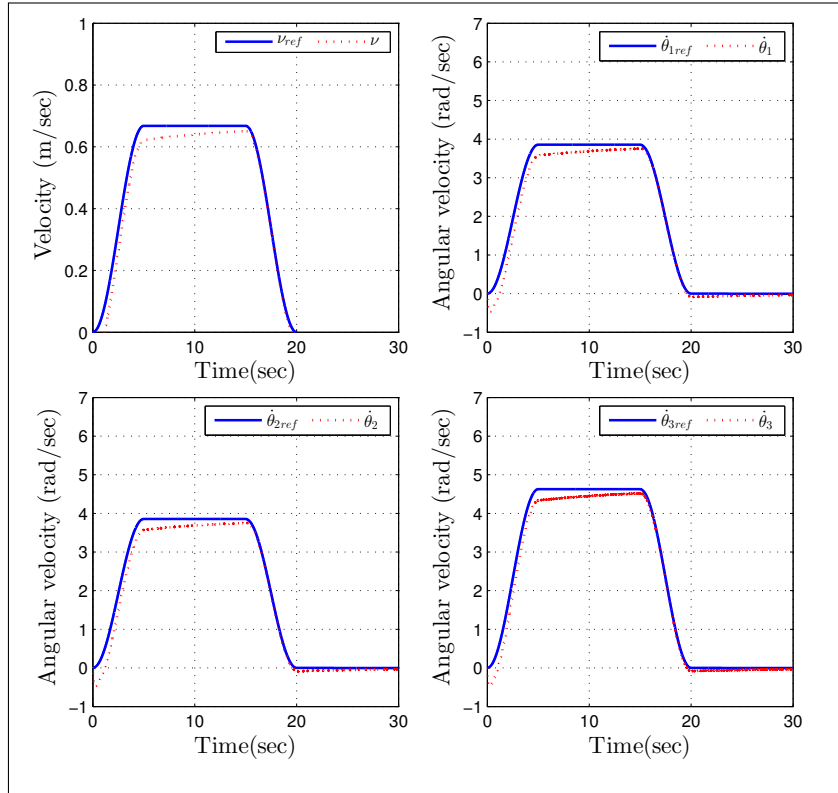FIGURE 3.10: Simulation result for the linear and angular velocity for circular motion in Fig. 3.9

FIGURE 3.11: Simulation result for tracking performance with off-trajectory initial conditions (*d=3.5*)
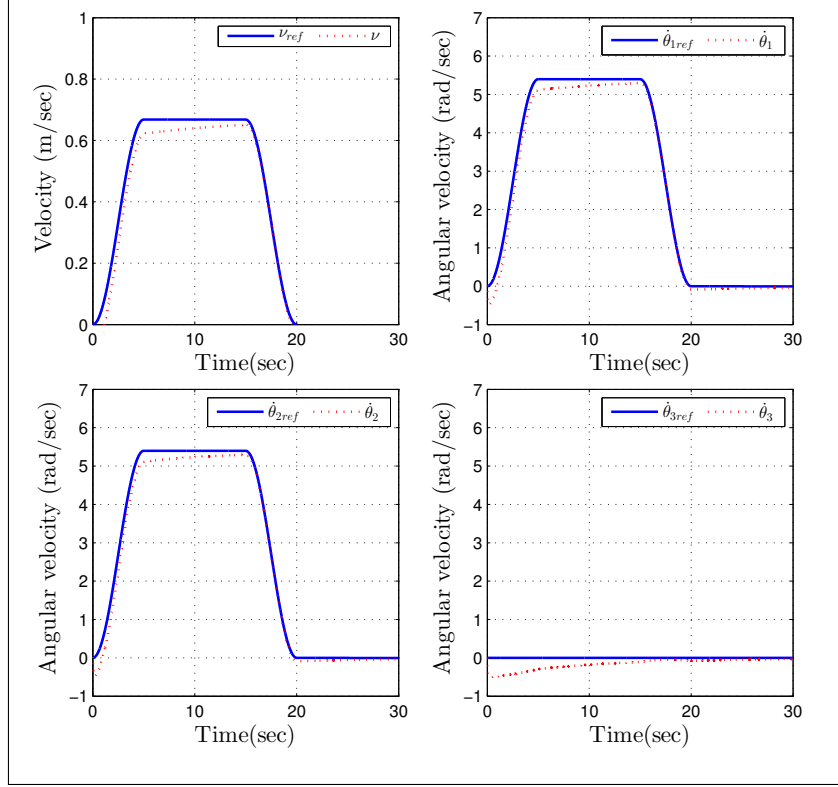
FIGURE 3.12: Simulation result for tracking performance with off-trajectory initial conditions ($d=\infty$)

obtained by the pole placement method (poles are located at -2, -2, -2, -2, -3, -3 [1/s]).

The control law in Eq. (3.15) is implemented using the C# language on a laptop PC (OS: WINDOWS 8.1; CPU: 2.3 GHz) with a sampling interval of 50 ms. In addition, two optical encoders of resolution 0.352 °/count are attached to Motors 1 and 2, and an optical encoder of resolution 0.18 °/count is attached to Motor 3 to measure the angular velocities of the motors. A pulse-counter board with two channels of 24-bit up/down counters and a DA board with 16-bit resolution are used for control. The motor drivers are also used in current-control mode, in which the supplied electrical current depends on the voltage commanded from the laptop PC to each motor.

Figures 3.16, 3.17, and 3.18 show the experimental results of the control input of each motor. Figures 3.19, 3.20, and 3.21 show the experimental results of the translational speed and linear velocity of each motor. In Figure 3.21, for $d = 100$, only Motors 1 and 2 operate, as expected. In Fig. 3.19, for $d = 1$, only Motor 3 operates, as expected, but for any other value of d all three motors will operate, as shown in Fig.

3.20. Circular motion is obtained as shown in Fig. 3.22, and the path has the velocity profile shown in Fig 3.23.

TABLE 3.2: Experimental conditions (controller gains)

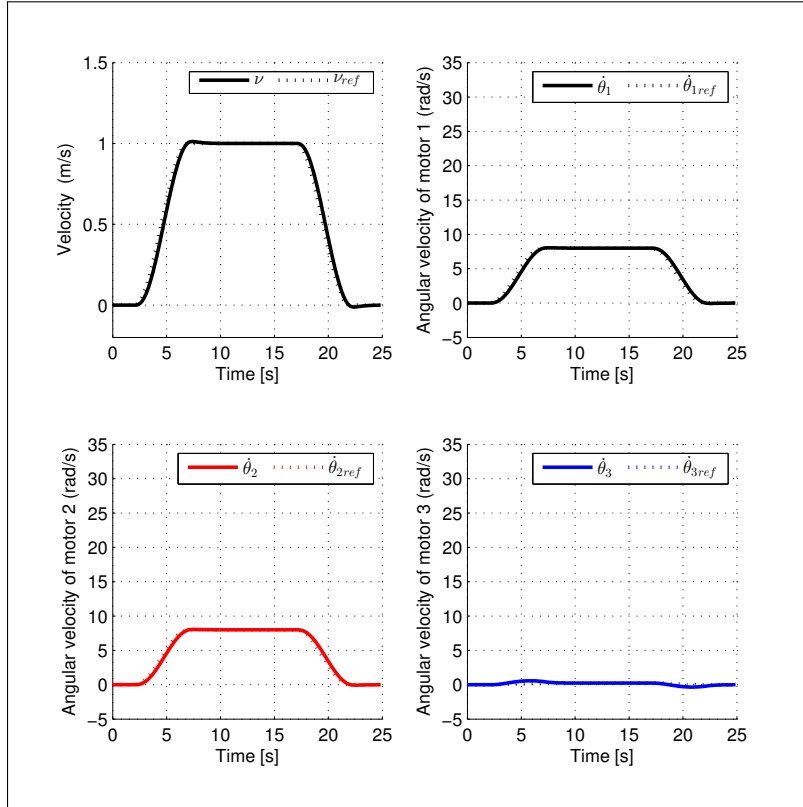| k_{pij}	Value (Nm/rad)	k_{dij}	Value (Nms/rad)
k_{p11}	0.14001	k_{d11}	0.10684
k_{p12}	0.00397	k_{d12}	0.00159
k_{p13}	0.01869	k_{d13}	0.02144
k_{p21}	0.00397	k_{d21}	0.00159
k_{p22}	0.14014	k_{d22}	0.10762
k_{p23}	0.01858	k_{d23}	0.02164
k_{p31}	0.01869	k_{d31}	0.02144
k_{p32}	0.01858	k_{d32}	0.02164
k_{p33}	0.03607	k_{d33}	0.01796

FIGURE 3.13: Simulation result ($d=100$)(robot speed = 1 m/s)
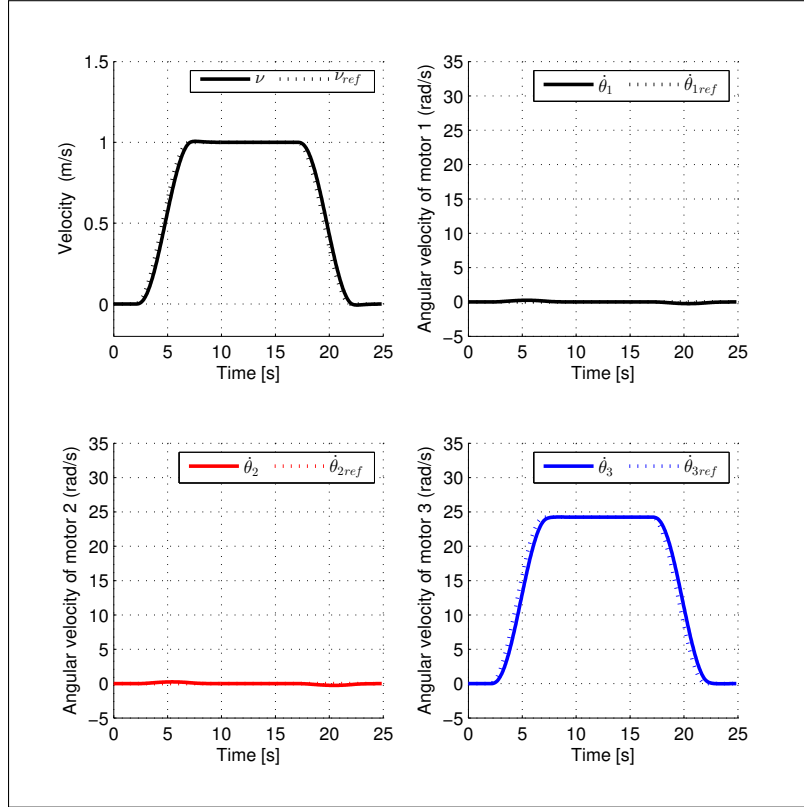
FIGURE 3.14: Simulation result (*d=1*) (robot speed = 1 m/s)
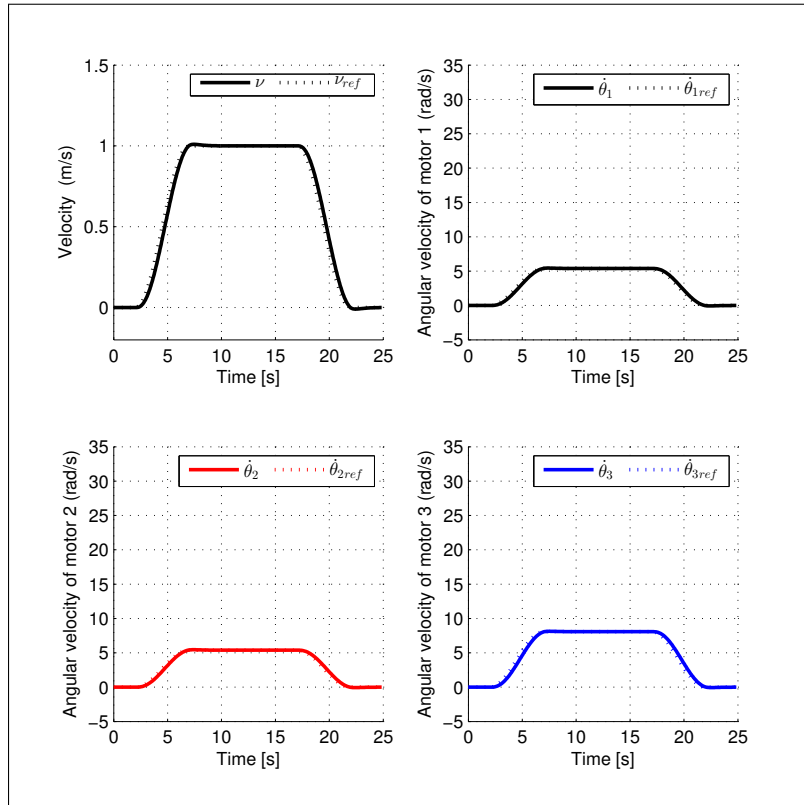
FIGURE 3.15: Simulation result (*d=3.5*) (robot speed = 1 m/s)
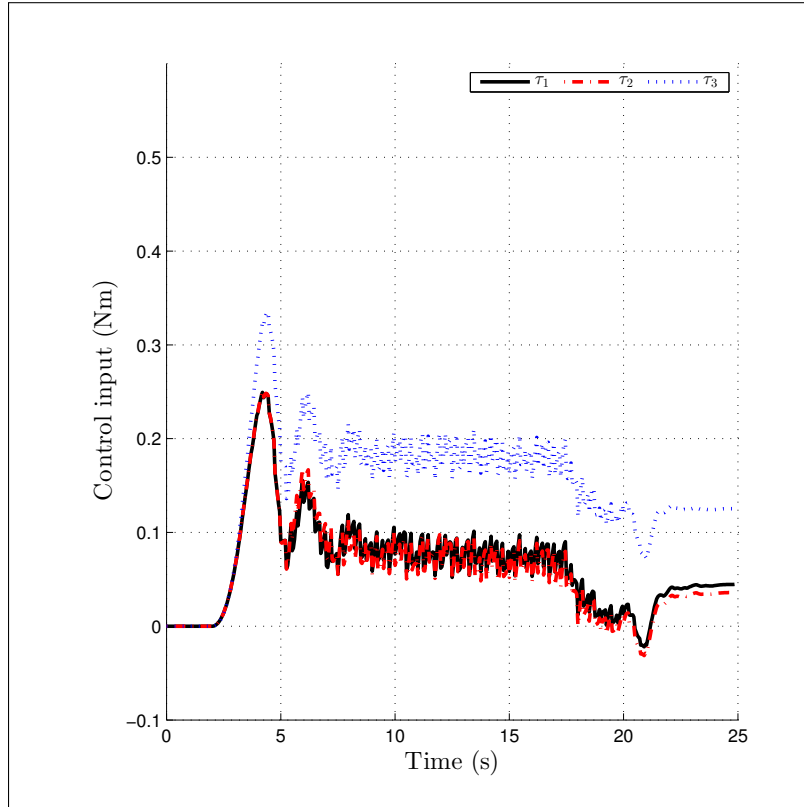
FIGURE 3.16: Control input of all three motors (d=1), the same profile is obtained for τ_1 and τ_2

FIGURE 3.17: Control input of all three motors (d=2)

FIGURE 3.18: Control input of all three motors (*d*=100)

FIGURE 3.19: Experimental results (*d*=1)

FIGURE 3.20: Experimental results (*d*=2)

FIGURE 3.21: Experimental results (*d*=100)

FIGURE 3.22: Experimental result for circular motion (*d*=2)

FIGURE 3.23: Experimental result for the linear and angular velocity for circular motion in Fig. 3.22

3.4   Energy Consumption

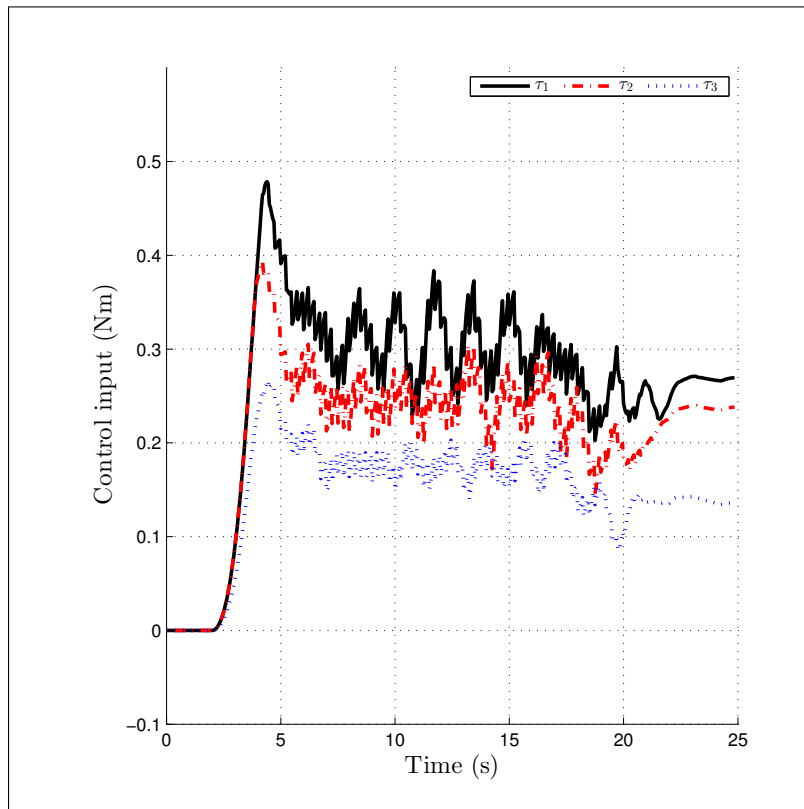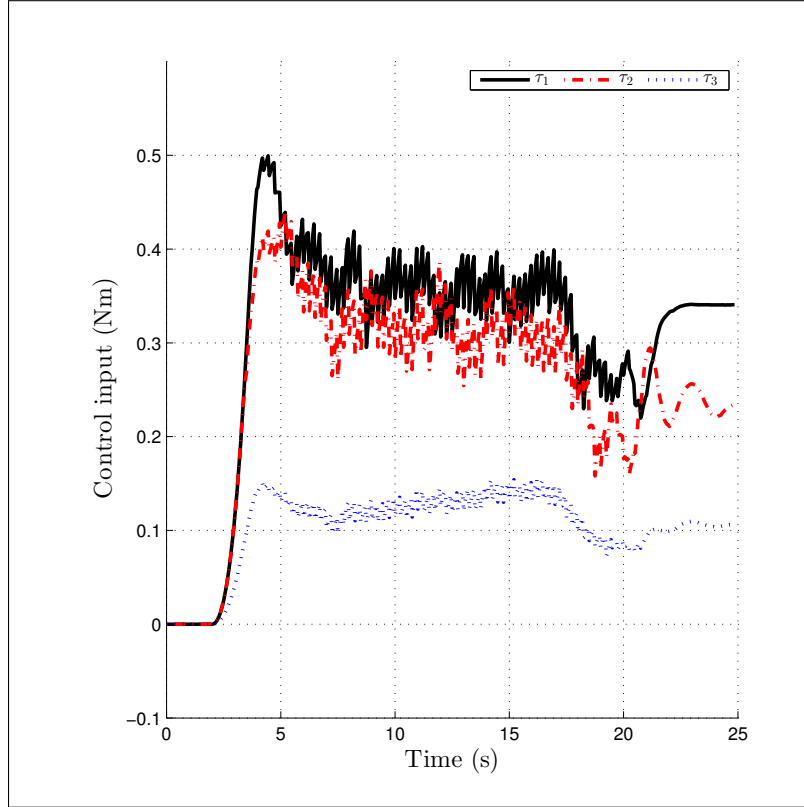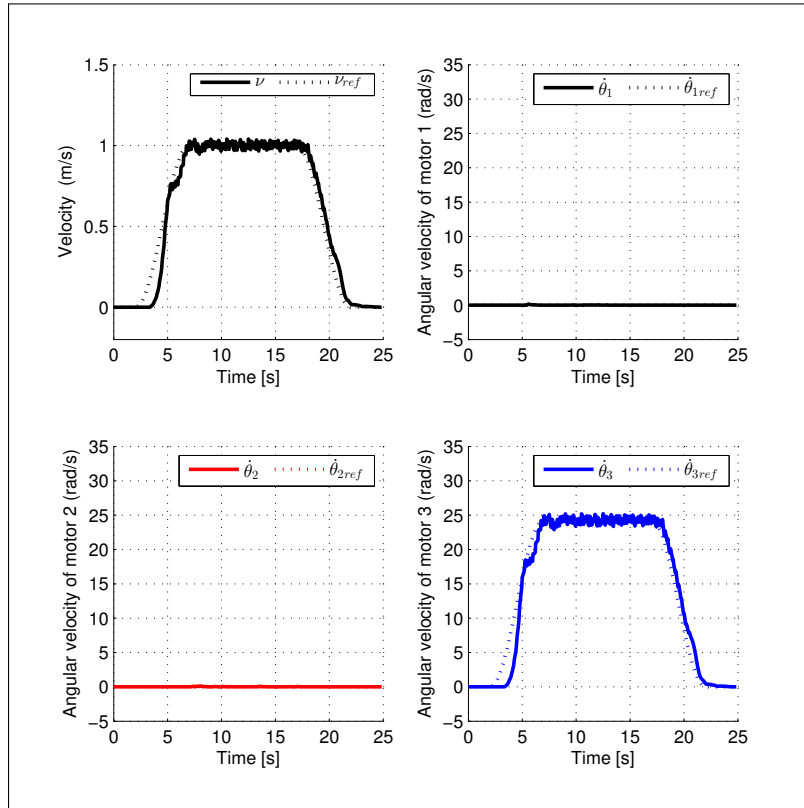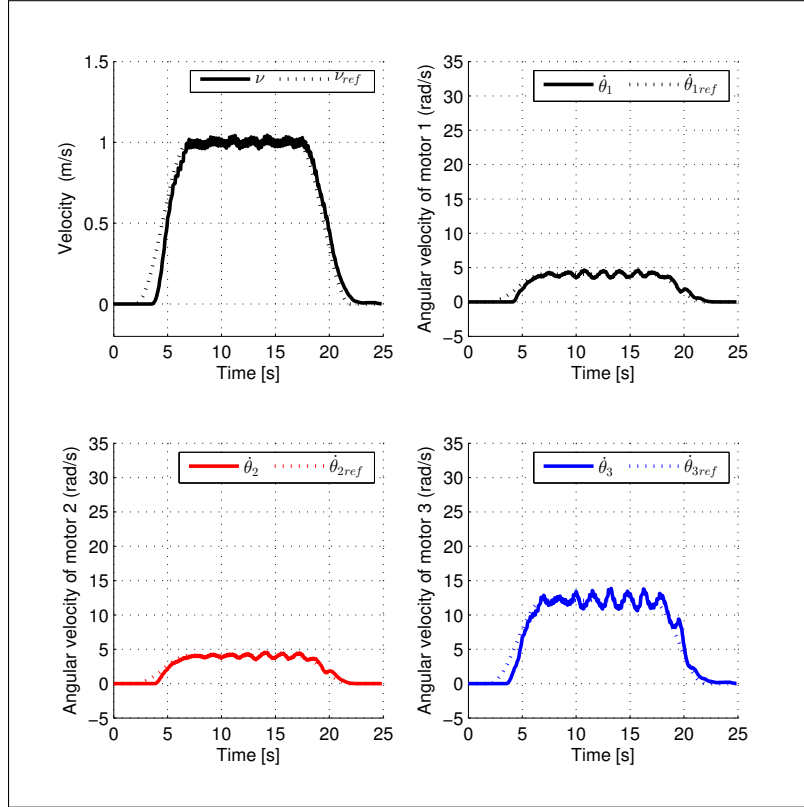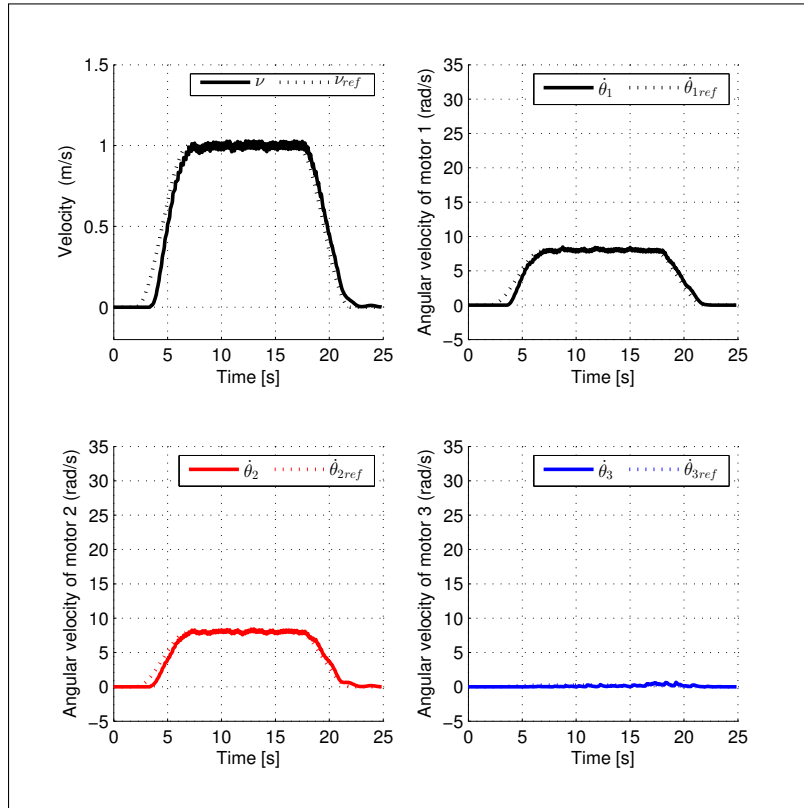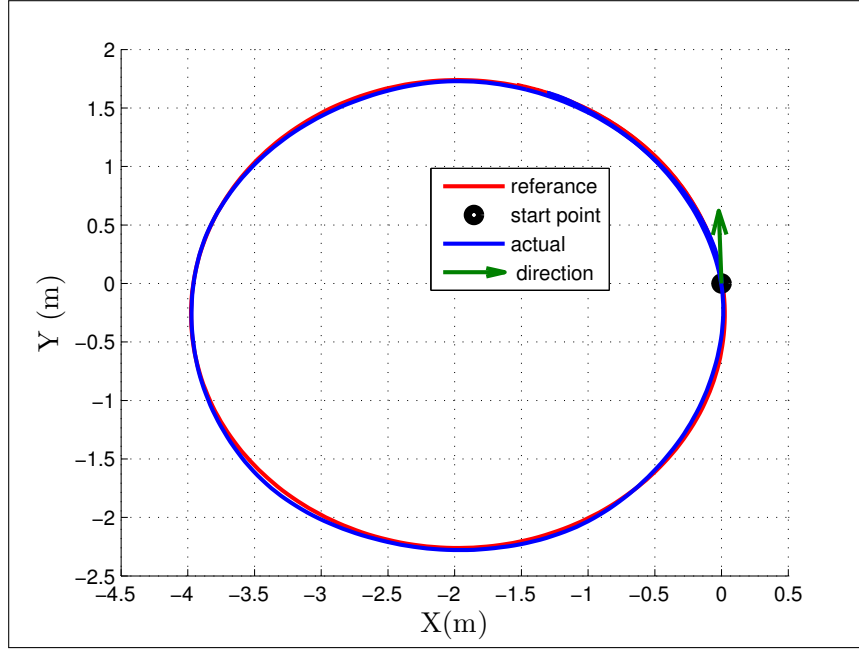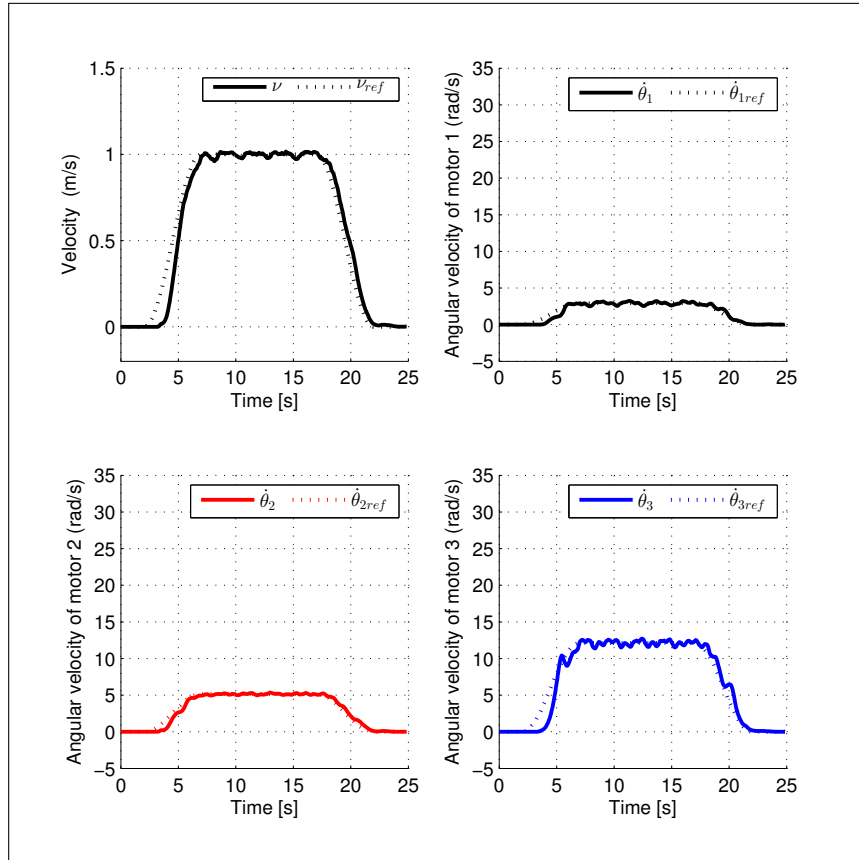A WMR usually carries limited energy sources such as rechargeable batteries, the capacity of which determines the operating time. Electrical property should be considered and it depends on motor, motor driver, and amplifier properties. In this study a simplified energy model is assumed, where the electric power is directly proportional to mechanical power. Therefore, for comparing the energy in simulations and experiments, it is sufficient to use the mechanical energy. Here the effectiveness of the proposed WMR for energy saving is considered. The energy required for the motors is obtained by the following equation[48]:

$$E = \sum_{i=1}^{3} \int_0^t \left| \tau_i \dot{\theta}_i \right| dt, \qquad (3.21)$$

where E is the total energy consumption.

Different robot speeds are assessed in the simulations, as shown in Figs. 3.24-3.27. In all cases, $d = 3.5$ provides the minimum energy consumption. Hence, this value of d is appropriate for the designed system, because the optimum value of d depends on the actuator specifications. At that value of d, the energy was reduced by about 13.99% and 14% for $v_{refmax} = 0.668$ and 1 m/s, respectively, compared to the case of $d = \infty$ for the linear motion, as shown in Figs. 3.24 and 3.25. For circular motion, the energy consumption was reduced by 10.68% and 13.99% for $v_{refmax} = 0.668$ and 1 m/s, respectively, as shown in Figs. 3.26 and 3.27.

The repeatability was verified by conducting multiple experiments with the same conditions. Figures 4.39 and 4.43 show the total energy consumed by all three motors for various values of d for linear and circular motion. The average energy consumption shown in Figs. 4.42 and 4.46 for $d = 2$ provides the minimum energy consumption. At that value of of d, the energy consumption was reduced by about 20.45% and 13.05% compared to the case of $d = 100$ (a typical drive condition for two motors) for linear and circular motion, respectively.
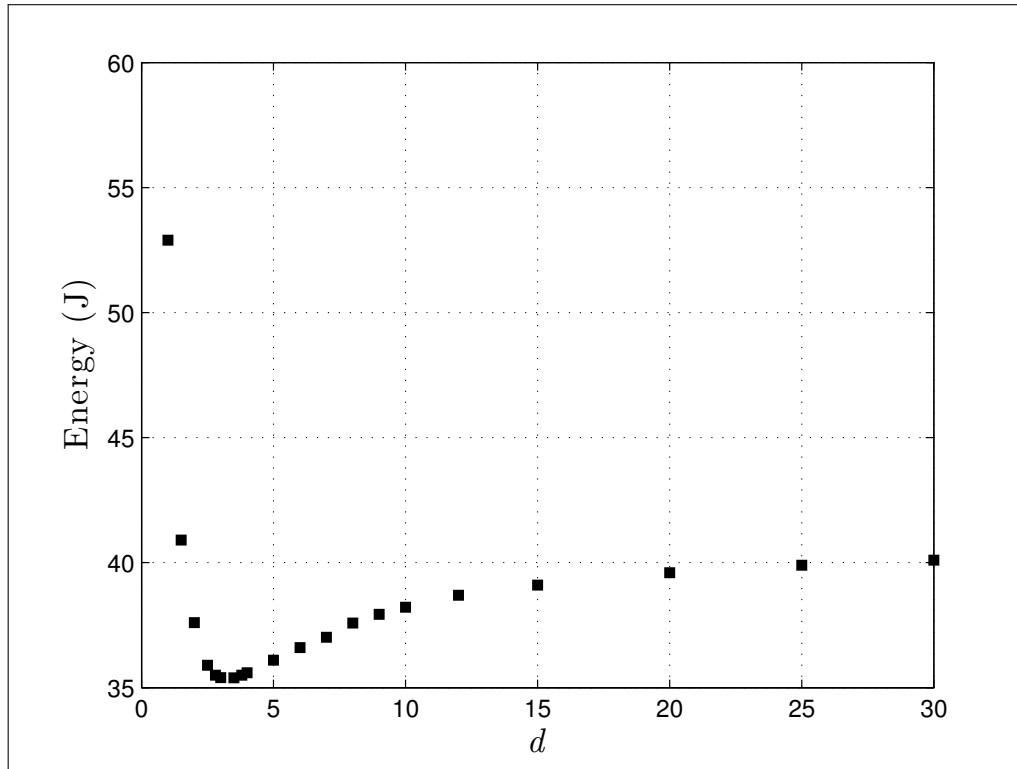
FIGURE 3.24: Total energy consumption for linear motion (robot speed = 0.668 m/s)
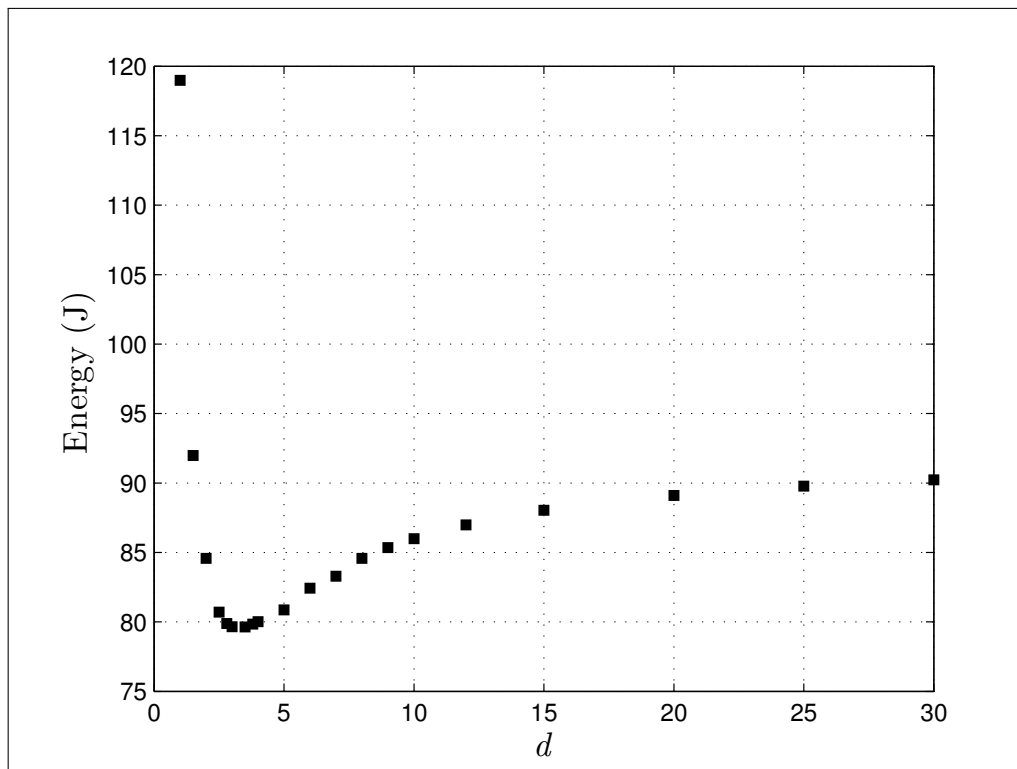
FIGURE 3.25: Total energy consumption for linear motion (robot speed = 1 m/s)
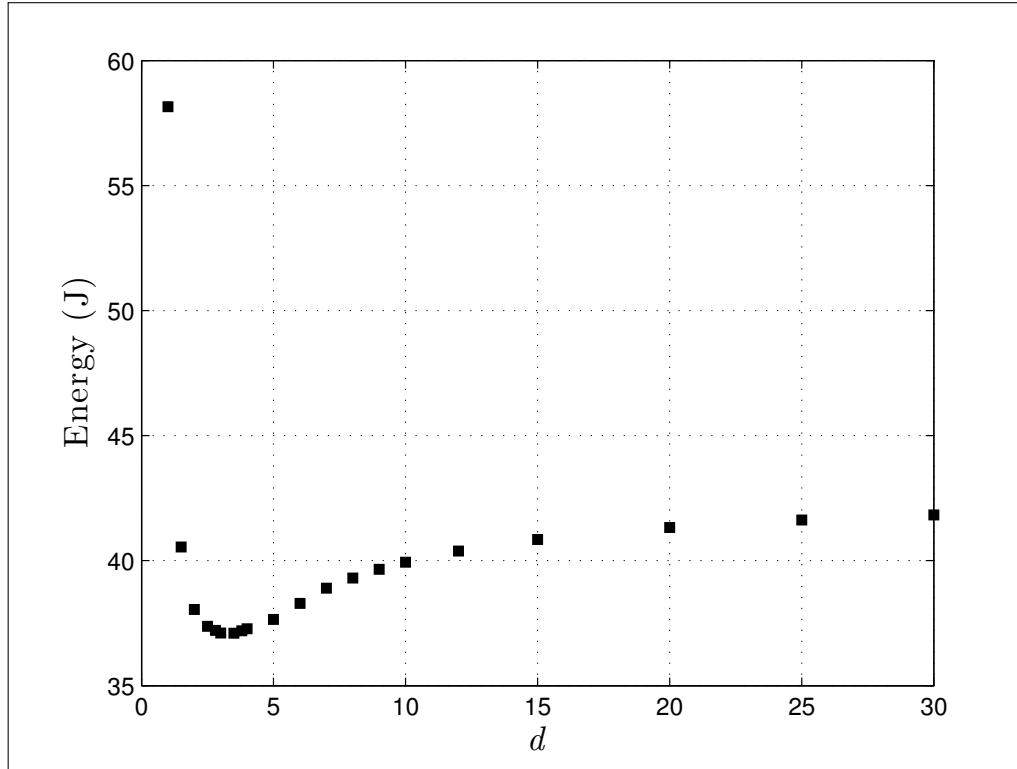
FIGURE 3.26: Total energy consumption for circular motion ($\dot{\phi} = 0.5$ rad/s and robot speed = 0.668 m/s)
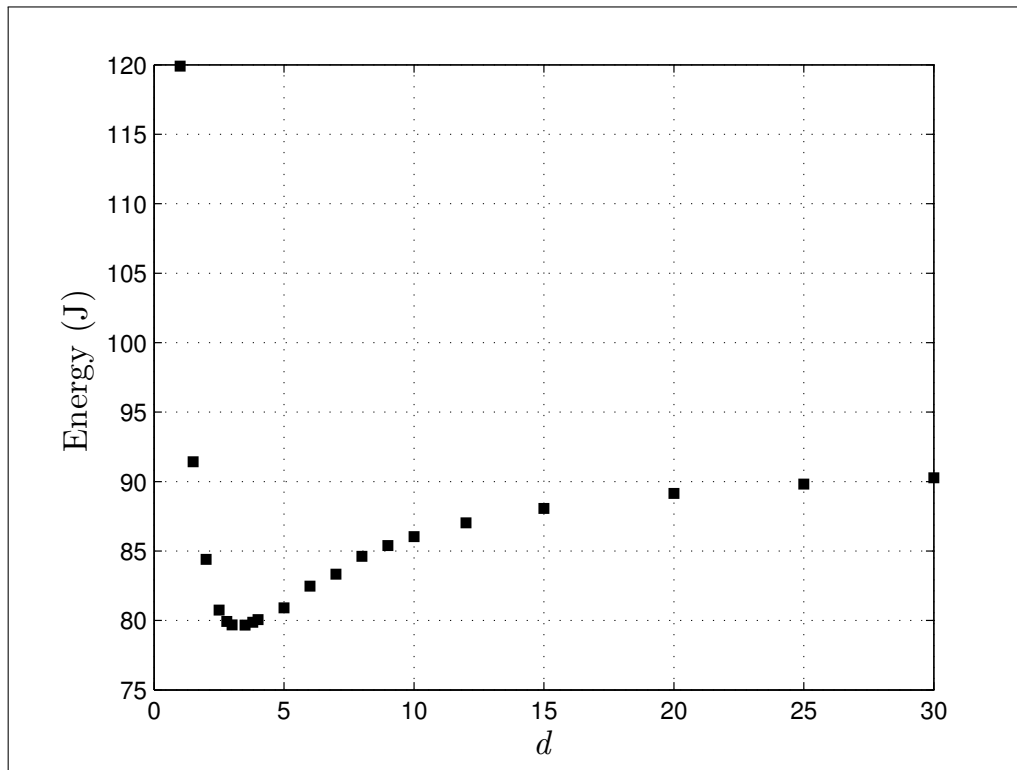
FIGURE 3.27: Total energy consumption for circular motion ($\dot{\phi} = 0.5$ rad/s and robot speed = 1 m/s)

46
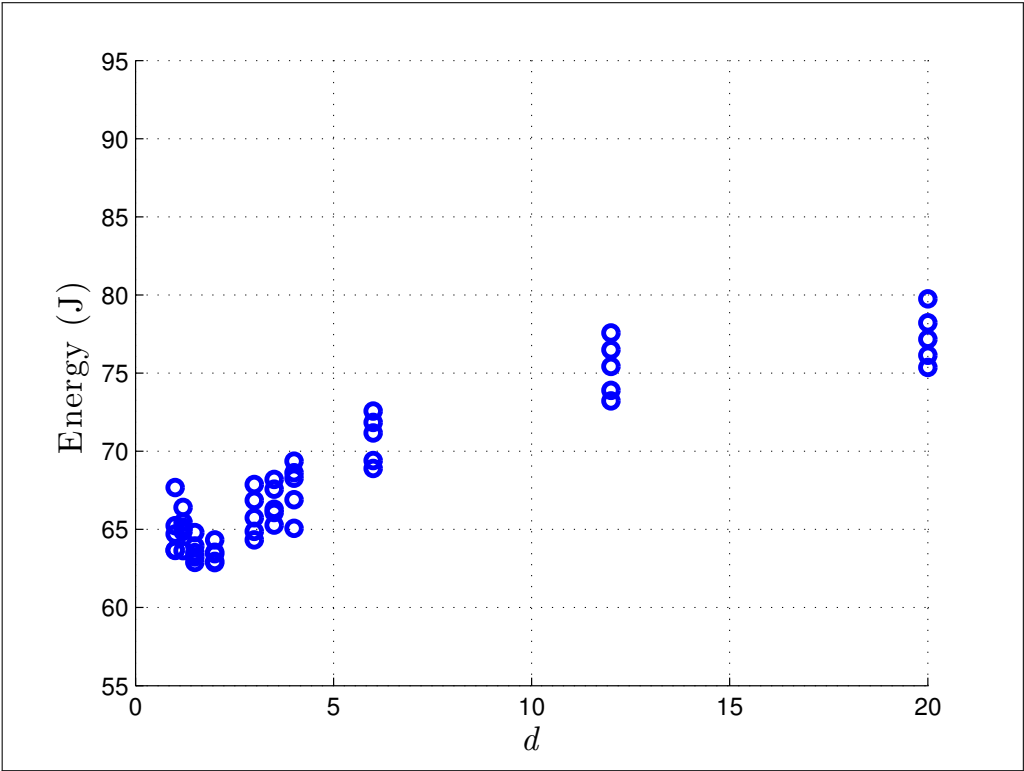
FIGURE 3.28: Total energy consumption for linear motion
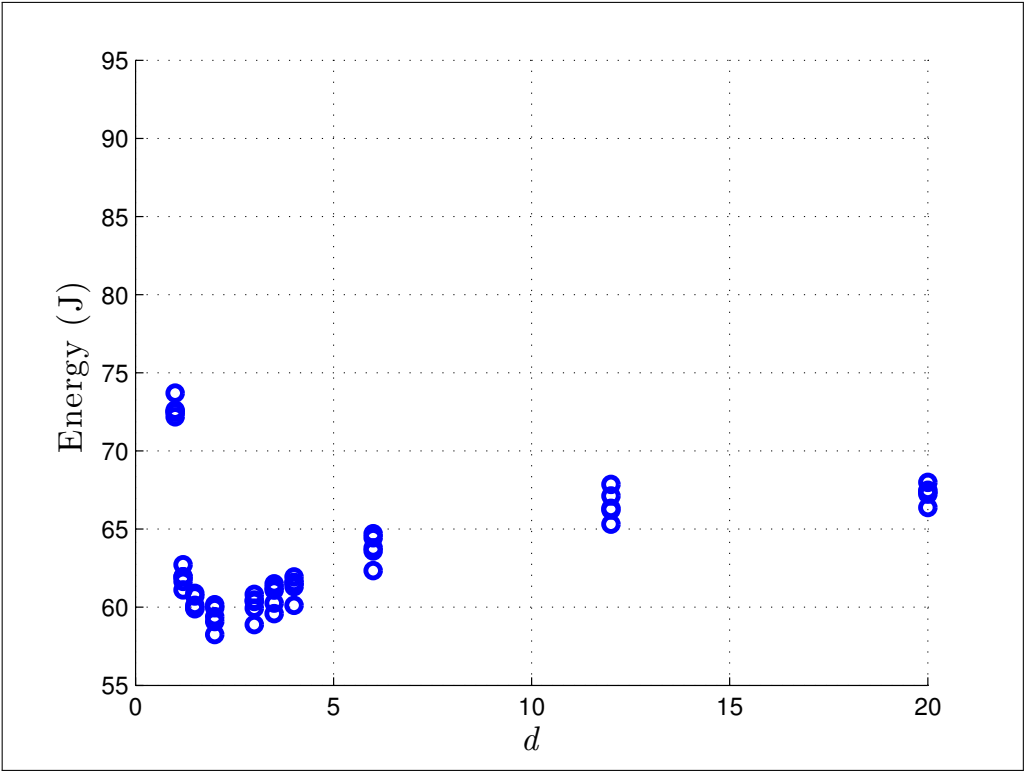
FIGURE 3.29: Total energy consumption for circular motion
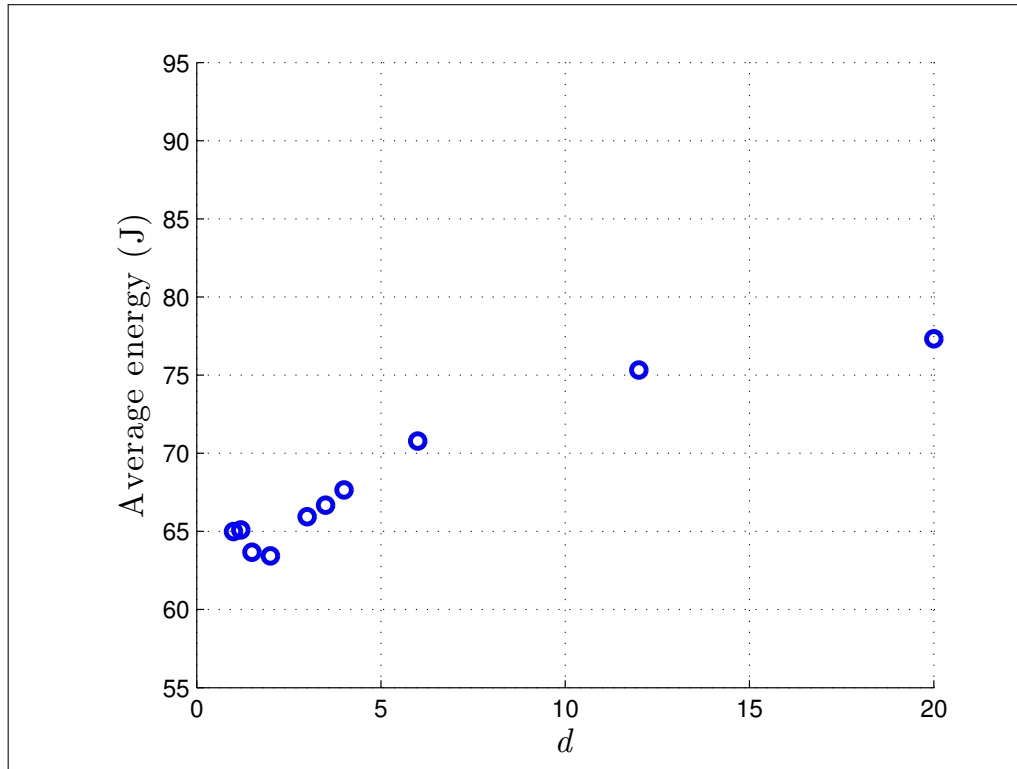
FIGURE 3.30: Average energy consumption for linear motion
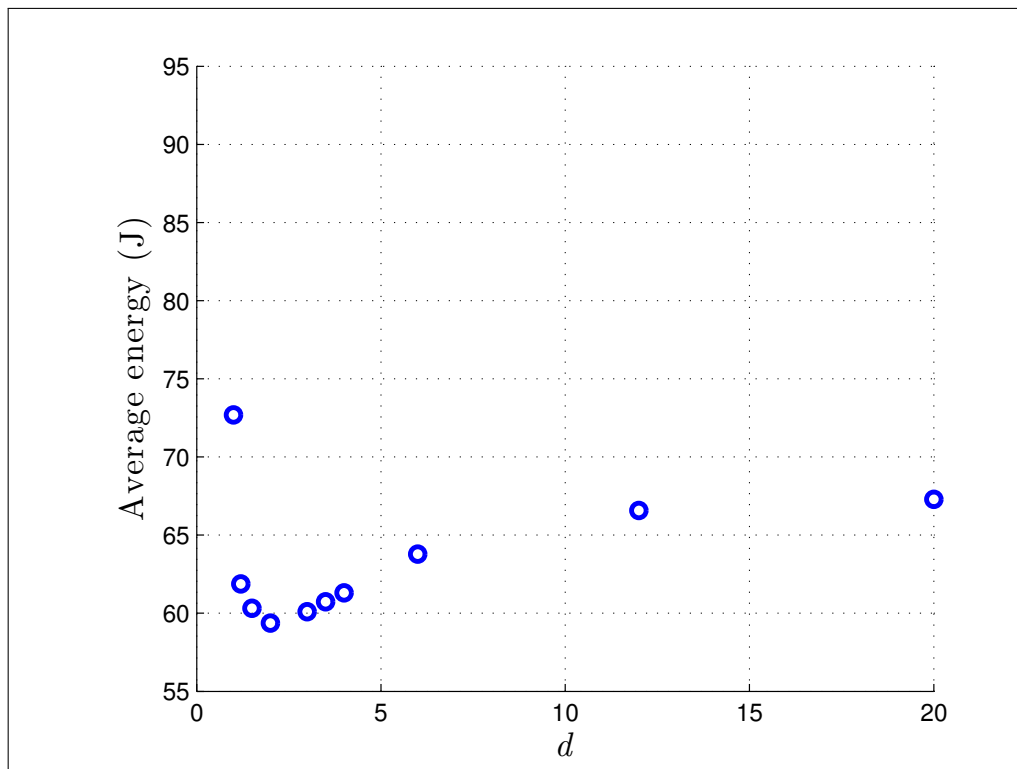
FIGURE 3.31: Average energy consumption for circular motion

3.5   Conclusion

The objective of this chapter was to show the capability of the proposed new drive system for energy saving and fail-safe motion. Distribution and state-feedback controllers are applied for the wheeled drive system. The distribution controller created a reference angular velocity for the motors. Experiments are conducted to verify the effectiveness of the proposed method. A distribution ratio of $d = 2$ provided reduction of 20.45% and 13.05% of in energy consumption during linear and circular motion, respectively, compared to the case in which only two motors are operated.

Chapter 4

Robust Control of a Redundant Wheeled Drive System

4.1 Introduction

WMRs can be used in many different fields for both civil and military applications such as search and rescue, exploration, guidance, hazard detection, surveillance, and transportation [10, 35]. Recently various control strategies have been considered to research the problem of tracking control for WMRs [49–66] . Xin *et al.* proposed robust adaptive tracking control of WMRs [49]. Chen *et al.* proposed adaptive tracking control for a class of nonlinear stochastic system [56]. Yang *et al.* proposed a robust tracking control based on an extended state observer [58]. An adaptive tracking controller for a nonholonomic mobile robot with unknown parameters has been proposed [60]. Many control schemes are potentially useful for tracking control of WMRs, such as dynamic surface control and a disturbance observer based on fuzzy control [61, 67–76]. However, the effectiveness of all these controllers has been shown only by simulation, and their energy saving has been analyzed neither theoretically nor experimentally.

As a robust control approach, SMC of WMRs has begun to receive increasing attention. The advantages of using SMC are a fast response, good transient performance, and robustness against system uncertainty and external disturbance [77–86]. Jorge *et al.* proposed SMC that exploits a property known as differential flatness of the

kinematics of nonholonomic systems [78]. Shim *et al.* proposed SMC in which unicycle-like robots converge to a reference trajectory with bounded errors of position and velocity [79]. Aguilart *et al.* used a path-following feedback controller with SMC for a car-like robot which is robust to localization and curvature estimation errors [80]. Other control approaches such as adaptive control based on a neural network have been proposed for WMRs in recent years [31–34, 50, 87–93], but none considered energy saving.

Furthermore, WMRs are widely used in ports, agriculture, and other different engineering fields because of their loading capability, relative low mechanical complexity, and simple engineering design. In addition, using WMRs is an effective way to enhance the quality of life for people who are elderly and or have disabilities to promote their independence and extend their activities [5, 94]. In fact, energy consumption is considered as one of the important problems currently facing in the field of robotics, in particular WMRs. In the past few decades, much scientific research has been conducted into energy saving in mobile robots [14, 15, 18, 21, 25, 27, 45]. Hardware approaches involve reducing the weights of components and changing actuators to improve the efficiency of the motor power supply. Robust and optimal energy control have become prevailing approaches that are implemented in robot drivers to save consumed energy [15]. A differential-drive steering system with energy saving has been proposed for an omni-directional mobile robot [27], but any improvement in energy consumption was not analyzed neither theoretically nor experimentally. The authors [47] established a new wheeled device with a redundant drive system to continue its motion safely even if one of motors break down for some reason. However, robustness of the control system for practical use was not considered.

This chapter deals with enhancing the tracking performance and conserving energy in the motor drivers of a WMR by using SMC with suitable sliding surfaces. In addition, the focus is on using a new design of WMRs to guarantee secure motion for people who use wheeled mobility to support their self-movement. Using the distribution controller presented in chapter 3, a comparative study is conducted between pole placement control (PPC) and LQR control. Computer simulations are performed to

51

verify the effectiveness of the proposed method; no significant difference is founded between the SMC, LQR and PPC approaches. In the experiments SMC provides a viable and effective method with strong robustness that is better than LQR and PPC. The experimental results show that the SMC approach improves the tracking robustness in a real environment with less energy than for LQR and PPC. This chapter relates to the work presented in Ref. [95].

4.2 Controller Design

4.2.1 SMC and stability analysis

Variable-structure controllers operated in sliding mode were first proposed in the early 1950s. Because of its good robustness to uncertainties, SMC has been accepted as an efficient method for robust control of uncertain systems. Being limited only by practical constraints on the magnitude of the control signals, a sliding-mode controller can in principle treat a variety of uncertainties as well as bounded external disturbances. A key step in the design of the controllers is to introduce a proper transformation of tracking errors to generalized errors so that an nth-order tracking problem can be transformed into an equivalent first-order stabilization problem. Since the equivalent first-order problem is likely to be simpler to handle, a control law may thus be easily developed to achieve the so-called reaching condition.

In order to understand more physically what is happening during SMC, let us consider the following sliding surface for a second-order system [96]:

$$s(x,t) = kx + \dot{x}. \tag{4.1}$$

where x and $\dot{x}$ are the states of the system and k is a positive constant. Figure 4.1 shows the state trajectories in the vicinity of the sliding surface $s(x,t) = 0$. The SMC has two phases as shown in Fig. 4.1: the initial phase when the trajectory is forced towards $s(x,t) = 0$ (known as the *reaching phase*), and the secondary phase when $s(x,t) = 0$ (known as the *sliding phase* or *sliding mode*) . An external disturbance
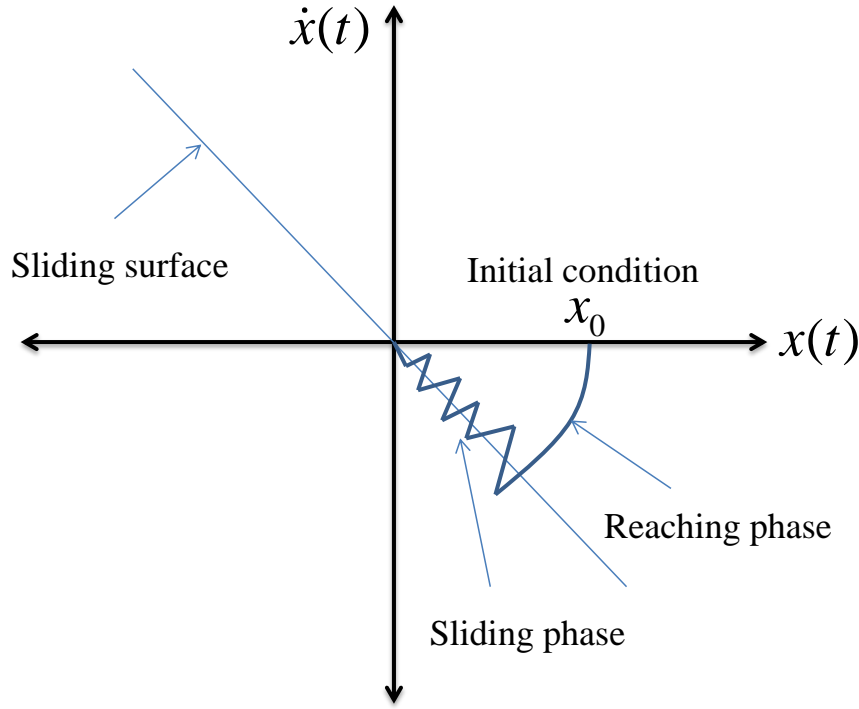
FIGURE 4.1: State trajectory during reaching phase and sliding phase in sliding mode control [96]

can affect the system performance during the reaching phase, whereas during the sliding phase the system motion is insensitive to external disturbances. Because the control law is discontinuous about $s(x,t) = 0$, switching at very high frequency is required to maintain the system on the desired sliding surface consistently.

4.2.2 Application of SMC

In this chapter, the dynamics of the WMR are considered to be the disturbance. Therefore, the dynamics of the WMR in chapter 2 are rewritten as follows:

$$M\ddot{\theta} + C\dot{\theta} = G\tau + h, \tag{4.2}$$

where M is the 3x3 inertia matrix, C is the 3x3 viscous friction matrix, G is the 3x3 control input matrix, and $h = [h_1, h_2, h_3]^T$ is the unknown disturbance vector. Tracking control can be achieved by keeping the system trajectory on the sliding surface. The sliding surface for the *i*th motor is chosen as follows [97]:

$$s_i = \dot{e}_i + \lambda e_i, \quad i = 1, 2, 3 \tag{4.3}$$

$$e_i = \theta_i - \theta_{iref} \tag{4.4}$$

where $e = [e_1, e_2, e_3]^T$ is a vector of tracking errors and λ is a positive constant. Substituting Eq. (4.4) into Eq. (4.3) leads to

$$s_i = \dot{\theta}_i - \dot{\theta}_{ir} \tag{4.5}$$

where $\dot{\theta}_{ir} = \dot{\theta}_{iref} - \lambda(\theta_i - \theta_{iref})$. The following sliding-mode controller is applied.

$$
\begin{aligned}
\tau =& G^{-1}\{M\ddot{\theta}_r + C\dot{\theta}_r - K\text{sign}(s)\}, \\
=& G^{-1}\{(M\ddot{\theta}_{ref} + C\dot{\theta}_{ref}) - M\lambda(\dot{\theta} - \dot{\theta}_{ref}) \\
& - C\lambda(\theta - \theta_{ref}) - K\text{sign}(s)\},
\end{aligned}
\tag{4.6}
$$

where $K = \text{diag}\{k_1, ., k_3\}$, $s = [s_1, s_2, s_3]^T$, and $\text{sign}(s) = [\text{sign}(s_1), ., \text{sign}(s_3)]^T$ is as follows:

$$
\text{sign}(s_i) =
\begin{cases}
1 & if \quad s_i > 0 \\
0 & if \quad s_i = 0 \\
-1 & if \quad s_i < 0
\end{cases}
\tag{4.7}
$$

In Eq. (4.6) sign(.) is a switching function that causes discontinuity in the control signal and produces chattering that should be avoided practically. This chattering can be eliminated by smoothing the control discontinuity in a thin boundary layer neighboring the sliding surface [97]. The sign(.) function is replaced by a saturation function sat(.) as follows:

$$
\text{sat}(s_i) =
\begin{cases}
\text{sign}(s_i) & if \quad |s_i| > \beta_i \\
\frac{s_i}{\beta_i} & if \quad |s_i| \leqslant \beta_i
\end{cases}
\tag{4.8}
$$

where $\beta_i > 0$.

To demonstrate the stability of the proposed system, a Lyapunov function candidate is considered as follows:

$$V(t) = \frac{1}{2}s^T M s \tag{4.9}$$

Differentiating Eq. (4.9) with respect to time, the following equation is obtained as follows:

$$\dot{V}(t) = s^T M \dot{s} \tag{4.10}$$

By applying Eqs. (4.2) and (4.5) to Eq. (4.10), then

$$\dot{V}(t) = s^T (G\tau - C\dot{\theta}_r - M\ddot{\theta}_r + h) - s^T Cs \tag{4.11}$$

Considering the control law in Eq. (4.6), it can be seen that

$$\dot{V}(t) = s^T h - s^T K \text{sign}(s) - s^T Cs \tag{4.12}$$

Thus, with $k_i, \geq |h_i|$ and $C \geq 0$, it is easy to show that.

$$\dot{V} < 0, \tag{4.13}$$

which guarantees the stability.

4.2.3 Linear quadratic control

LQR control is an optimal control method. It requires finding an optimal state-feedback gain that minimizes a certain cost function that reflects the performance of the closed-loop system. The cost function is defined as follows [98]:

$$J = \int_0^\infty (x_e^T Q x_e + \tau^T R \tau) dt \tag{4.14}$$

where x_e is a state vector, Q is an *nxn* symmetric, real, positive (or semi-positive) definite matrix, and R is a positive-definite symmetric matrix. Note that the second term on the right-hand side of Eq. 4.14 accounts for the expenditure of the energy of the control signals. The matrices Q and R are weight matrices that are determine the relative importance of the error and the expenditure of this energy, respectively. The state-feedback control inputs are expressed as follows:

$$\tau = -K x_e, \tag{4.15}$$

where the state-feedback gains are obtained as $K = R^{-1}B^T P$, and P is determined uniquely as a solution of the reduced-matrix Riccati equation as follows [99]:

$$A^T + PA - PBR^{-1}B^T P + Q = 0, \tag{4.16}$$

From this reduced-matrix Riccati equation, the matrix P is determined uniquely and is used to calculate the state-feedback gain K. The quality of the control design using the LQR method depends on the choice of Q and R. Normally, this requires some kind of trial and error. Matrices R and Q are selected via trial and error as follows:

$$Q = \begin{bmatrix} 0.3 & 0 & 0 & 0 & 0 & 0 \\ 0 & 0.3 & 0 & 0 & 0 & 0 \\ 0 & 0 & 0.3 & 0 & 0 & 0 \\ 0 & 0 & 0 & 0.3 & 0 & 0 \\ 0 & 0 & 0 & 0 & 0.3 & 0 \\ 0 & 0 & 0 & 0 & 0 & 0.1 \end{bmatrix}, \tag{4.17}$$

$$R = \begin{bmatrix} 20 & 0 & 0 \\ 0 & 20 & 0 \\ 0 & 0 & 80 \end{bmatrix}, \tag{4.18}$$

For the given A, B, R, and Q matrices, the optimal state-feedback control is determined by solving the Riccati equation as follows:

$$K = \begin{bmatrix} 12.22x10^{-2} & -2.38x10^{-4} & -6.79x10^{-3} & 12.45x10^{-2} & -5.58x10^{-4} & 2.92x10^{-3} \\ -1.36x10^{-4} & 12.28x10^{-2} & -6.74x10^{-3} & -4.27x10^{-4} & 12.51x10^{-2} & 3.13x10^{-3} \\ 3.39x10^{-3} & 3.37x10^{-3} & 6.11x10^{-2} & 7.62x10^{-3} & 7.79x10^{-3} & 3.44x10^{-2} \end{bmatrix},$$

The poles are located at $(-22.6, -3.57, -2.9, -1.81, -1.01, -1.01 \text{ [1/s]})$.

4.3   Simulation Results

To verify the effectiveness of the proposed controller, computer simulations are conducted using SMC to compare between LQR and PPC. This study considers only smooth trajectories: an S-shaped velocity profile is used as the reference translation velocity of the WMR [46]. The parameters of the experimental system are as follows: M_w = 46.0 kg, I = 0.625 kg.m ^{2}, R_w = 0.165 m, L = 0.275 m, $J_1 = J_2 = 0.149$ x 10^{-1} kg.m ^{2}, $J_3 = 0.181$ x 10^{-2} kg.m ^{2}, $J_L = J_R = 0.034$ kg.m ^{2}, $C_1 = C_2 = 0.268$ x 10^{-1} N.m.s/rad, $C_3 = 0.102$ x 10^{-1} N.m.s/rad, $C_L = 0.713$ x 10^{-2} N.m.s/rad, $C_R = 0.584$ x 10^{-2} N.m.s/rad, and $R = 3$.

The PPC feedback gains used in the simulation, as listed in Table 4.1, are obtained by poles at $-2, -2, -2, -2, -3, -3$ [1/s]. The SMC parameters are tuned to achieve the best results and are obtained as follows (units are omitted): K = diag {0.05, 0.05, 0.05}, λ = diag {12, 12, 12}, and $\beta = 0.2$. Figures 4.2, 4.3, and 4.4 show the simulation results for the translational velocity of the WMR and the velocity of each motor by SMC, LQR, and PPC, respectively. Figures 4.5, 4.6, and 4.7 show the simulation results for the control input for each motor corresponding to Figs. 4.2, 4.3, and 4.4, respectively. The tracking errors in the simulations resulting from all control approaches are shown in Figs. 4.8, 4.9, and 4.10. It can be seen that all approaches achieve similar tracking errors and display good tracking performance. The mean tracking errors are given in Table 4.2.

TABLE 4.1: Feedback gains of PPC

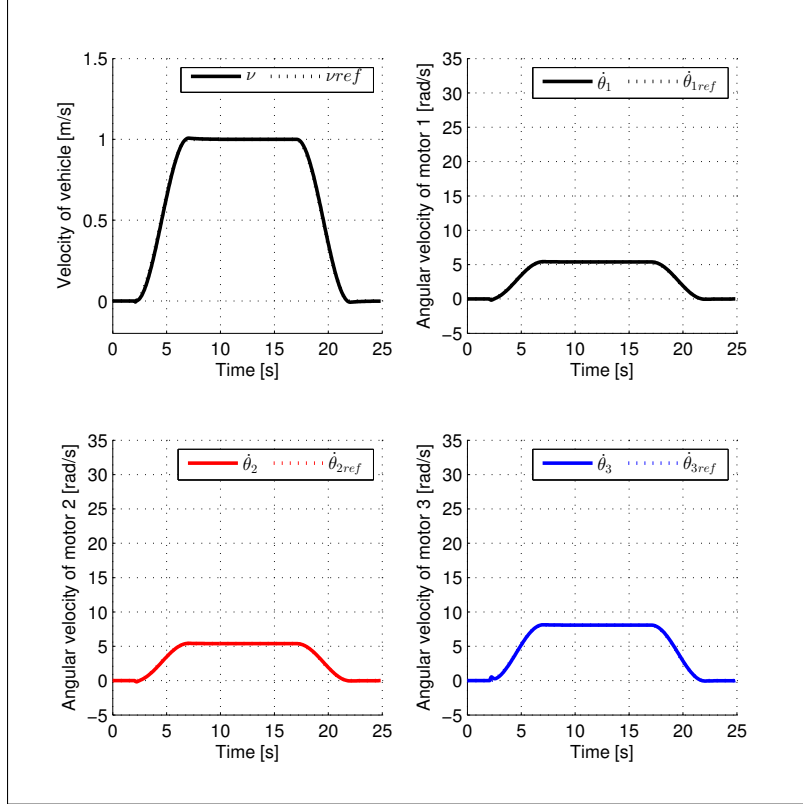| k_{pij}	Value (Nm/rad)	k_{dij}	Value (Nms/rad)
k_{p11}	1.40 x 10^{-1}	k_{d11}	1.07 x 10^{-1}
k_{p12}	3.97 x 10^{-3}	k_{d12}	1.6 x 10^{-3}
k_{p13}	1.87 x 10^{-2}	k_{d13}	2.14 x 10^{-2}
k_{p21}	3.97 x 10^{-3}	k_{d21}	1.6 x 10^{-3}
k_{p22}	1.40 x 10^{-1}	k_{d22}	1.08 x 10^{-1}
k_{p23}	1.86 x 10^{-2}	k_{d23}	2.16 x 10^{-2}
k_{p31}	1.87 x 10^{-2}	k_{d31}	2.14 x 10^{-2}
k_{p32}	1.86 x 10^{-2}	k_{d32}	2.16 x 10^{-2}
k_{p33}	3.61 x 10^{-2}	k_{d33}	1.80 x 10^{-2}

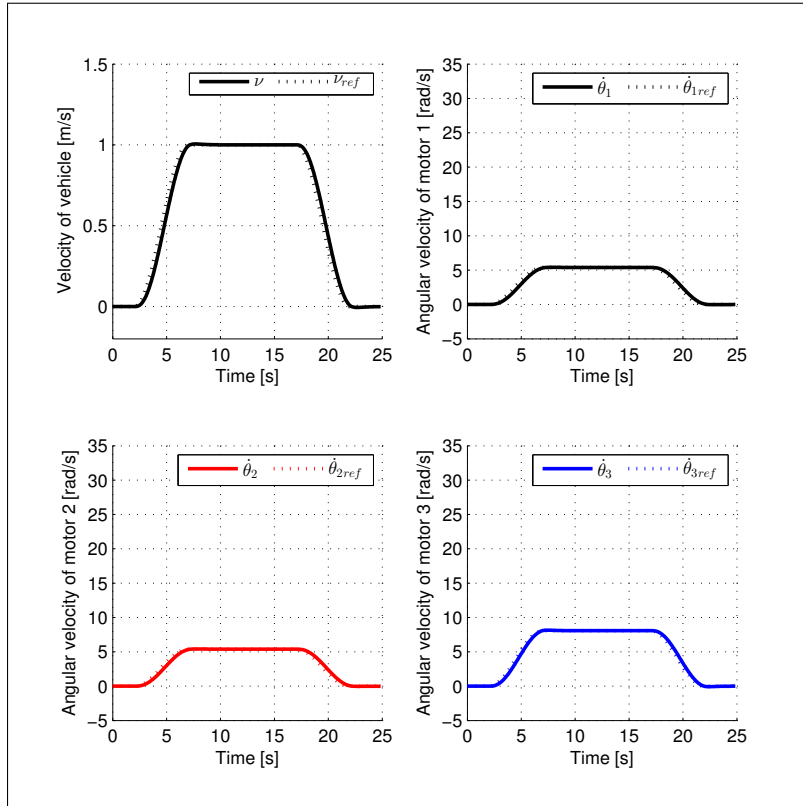FIGURE 4.2: Simulation results with SMC (*d=3*)

FIGURE 4.3: Simulation results with LQR (*d=3*)
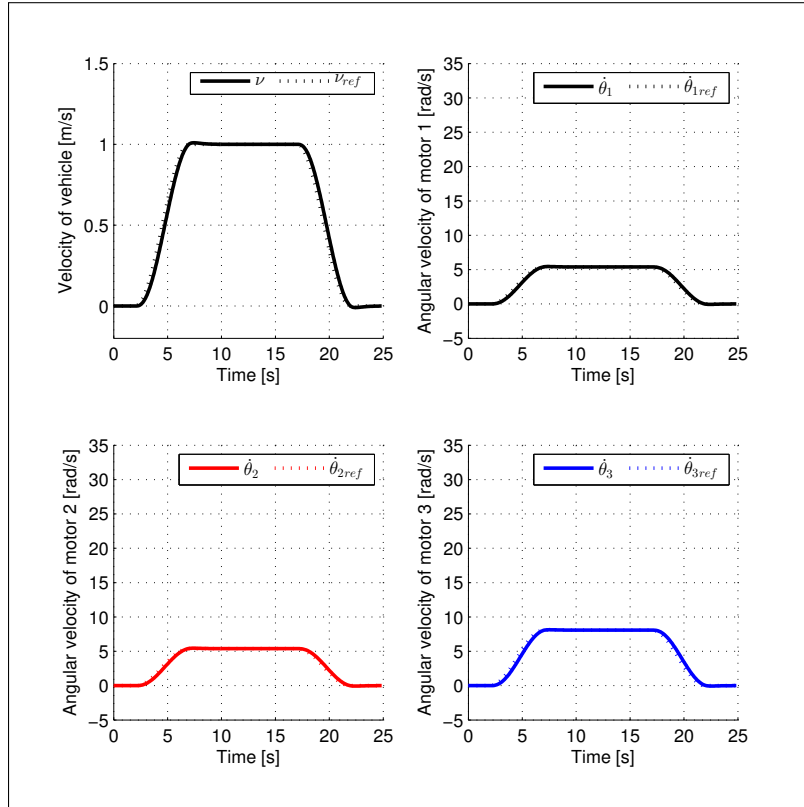
FIGURE 4.4: Simulation results with PPC (*d=3*)

FIGURE 4.5: Simulation results with SMC (*d=3*); control input of all three motors. Same profile is obtained for τ_1 and τ_2

FIGURE 4.6: Simulation results with LQR (*d=3*); control input of all three motors. Same profile is obtained for τ_1 and τ_2
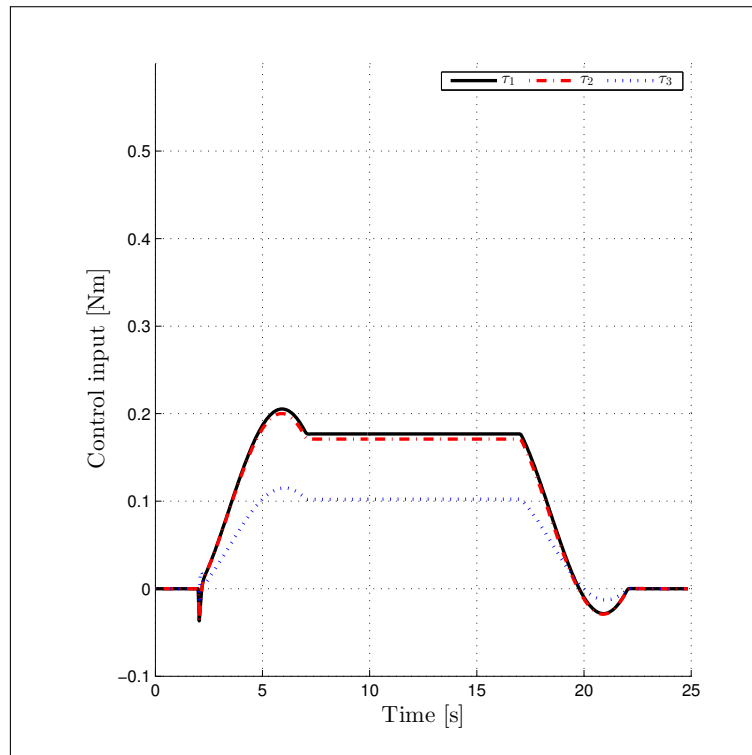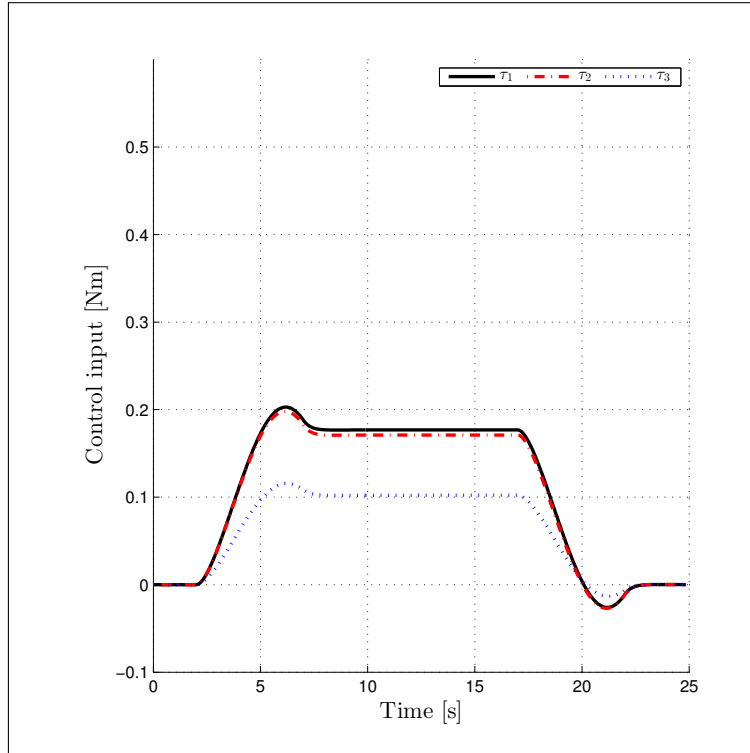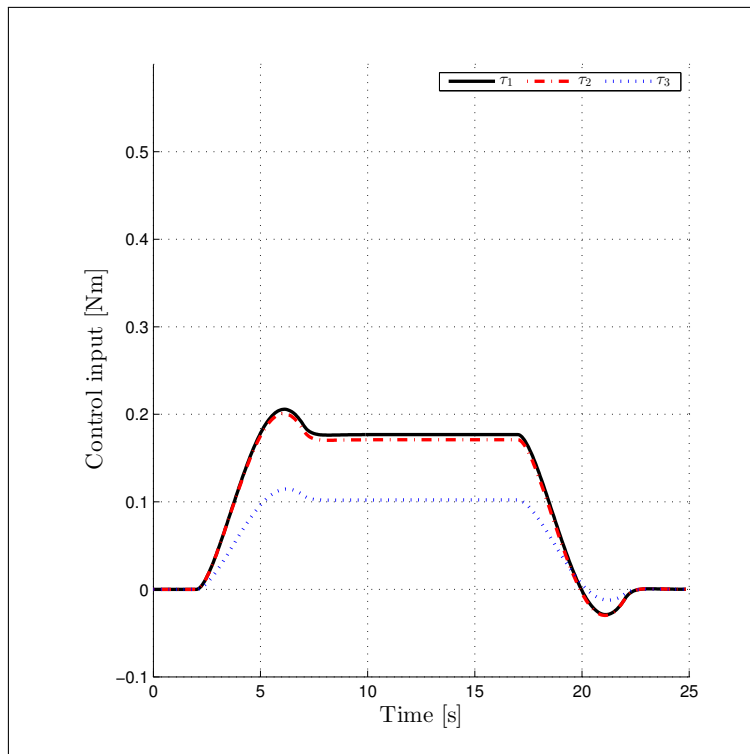

FIGURE 4.7: Simulation results with PPC (*d=3*); control input of all three motors. Same profile is obtained for τ_1 and τ_2
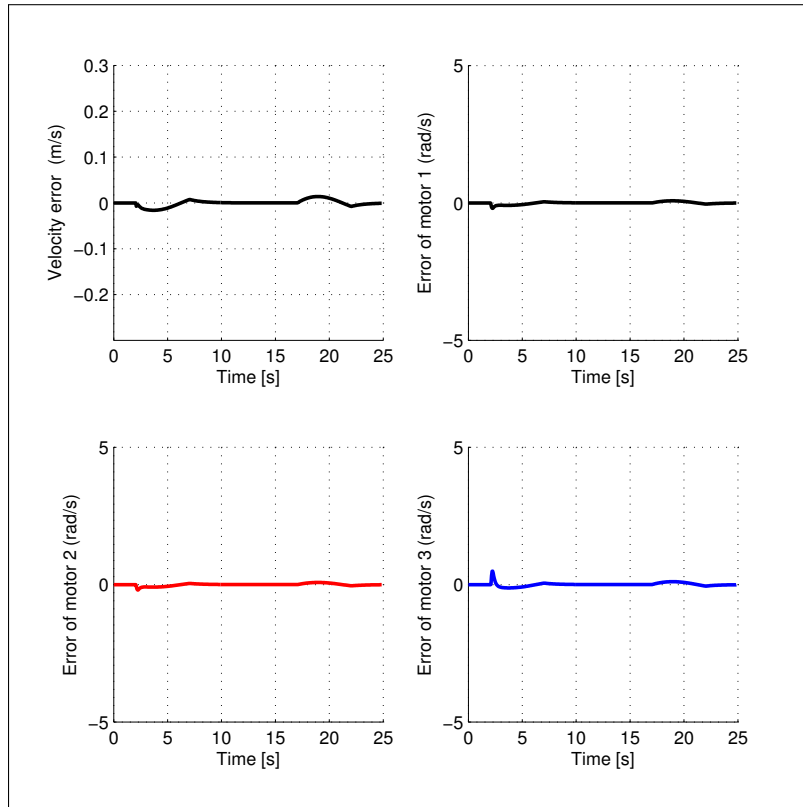
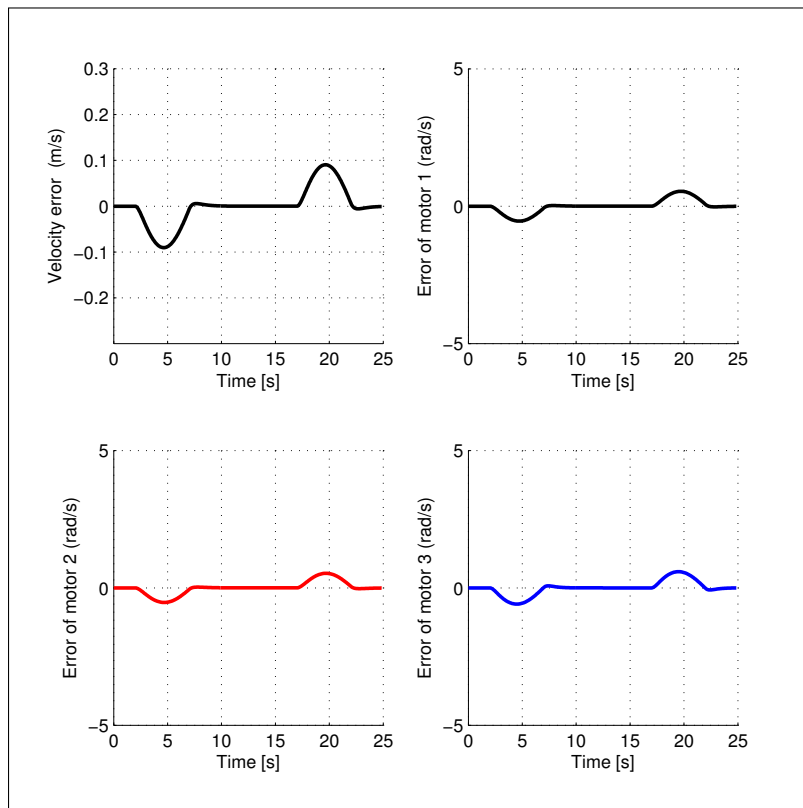FIGURE 4.8: Simulation result with SMC depicted in Fig. 4.2

FIGURE 4.9: Simulation result with LQR depicted in Fig. 4.3
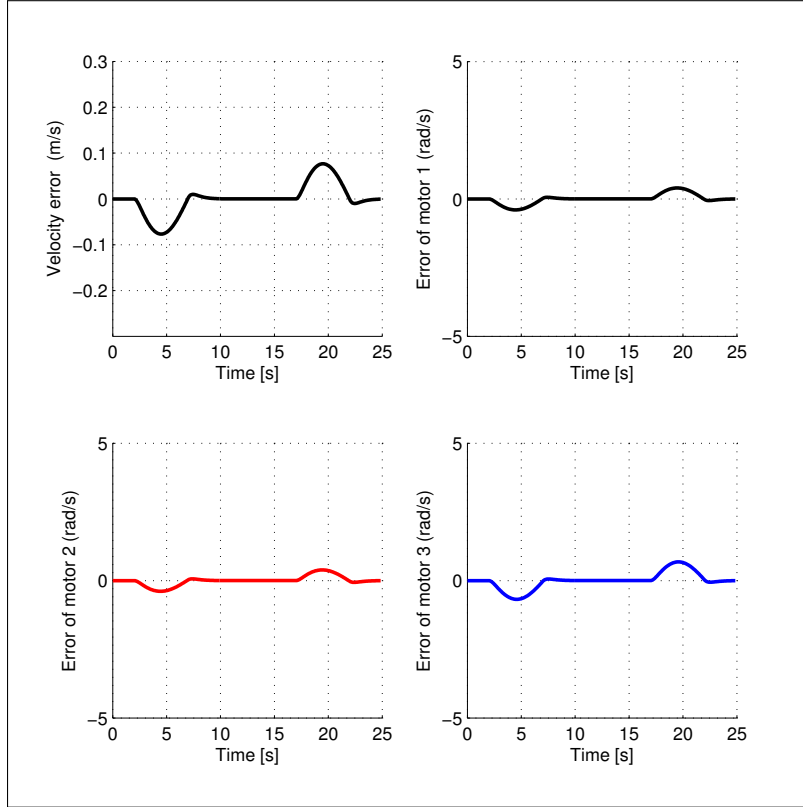
FIGURE 4.10: Simulation result with PPC depicted in Fig. 4.4

TABLE 4.2: Average of root mean square error (RMSE)

RMSE	SMC	LQR	PPC	Unit
Velocity of WMR	6.7×10^{-3}	4.02×10^{-3}	3.4×10^{-2}	m/s
Velocity of Motor 1	4.3×10^{-2}	2.4×10^{-1}	1.7×10^{-1}	rad/s
Velocity of Motor 2	4.32×10^{-2}	2.36×10^{-1}	1.7×10^{-1}	rad/s
Velocity of Motor 3	6.5×10^{-2}	2.6×10^{-1}	3.01×10^{-1}	rad/s

Figures 4.14, 4.15, and 4.16 show the simulation results for the control input under disturbance for each motor by SMC, LQR, and PPC, respectively, corresponding to Figs. 4.11, 4.12, and 4.13, respectively, by applying the disturbance term $h = \text{rand}(-1, 1)$ N.m in Eq. (4.2). The tracking errors in the simulations resulting from all control approaches with disturbance are shown in Figs. 4.17, 4.18, and 4.19. It can be seen that SMC approach achieves smaller tracking errors than do LQR and PPC. The mean tracking errors with disturbance are given in Table 4.3.
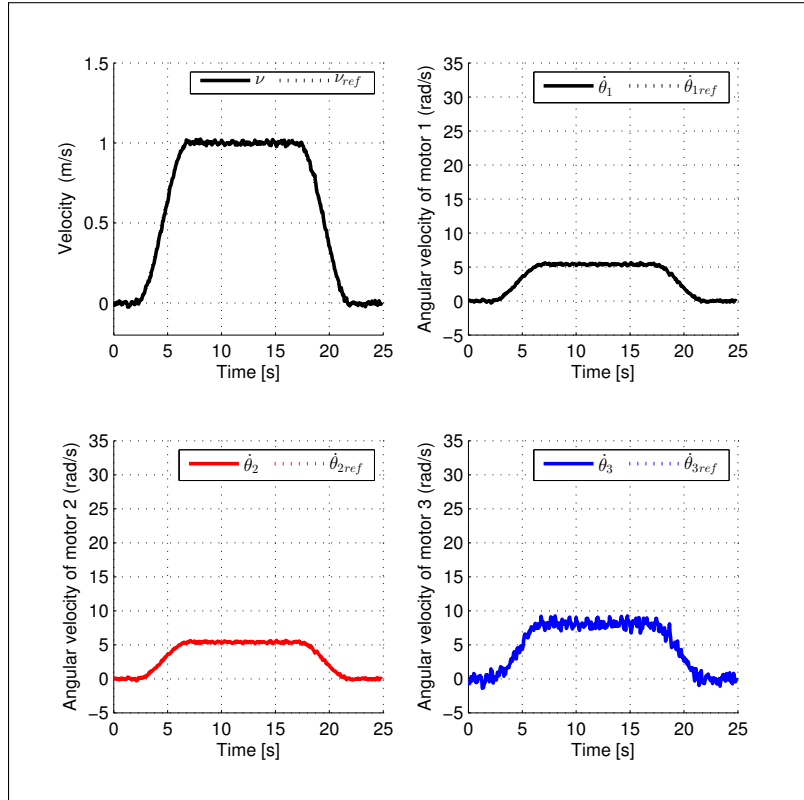
FIGURE 4.11: Simulation results with SMC under disturbance (*d=3*)
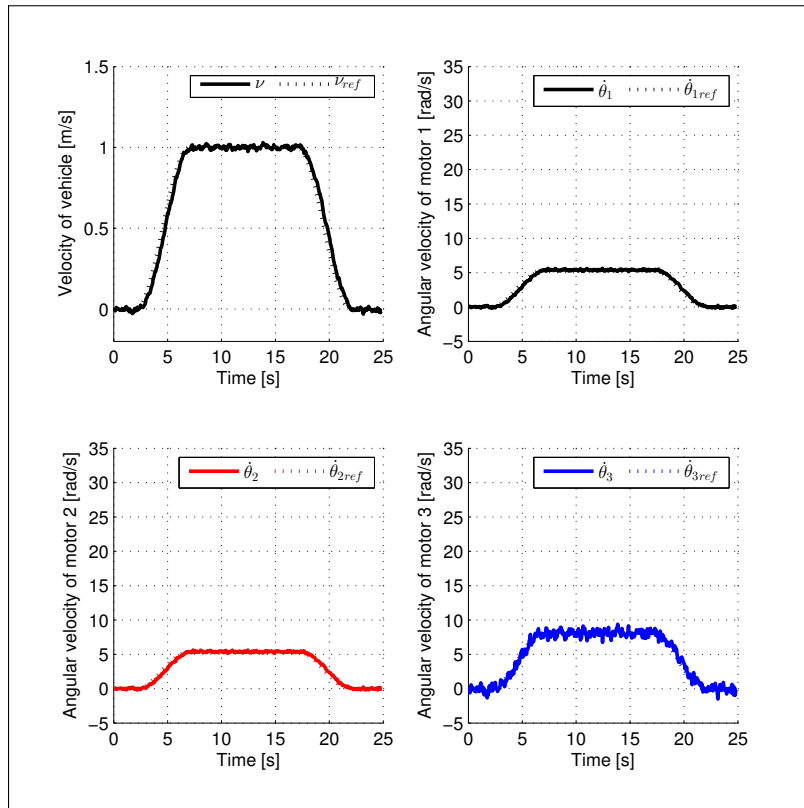
FIGURE 4.12: Simulation results with LQR under disturbance (*d=3*)
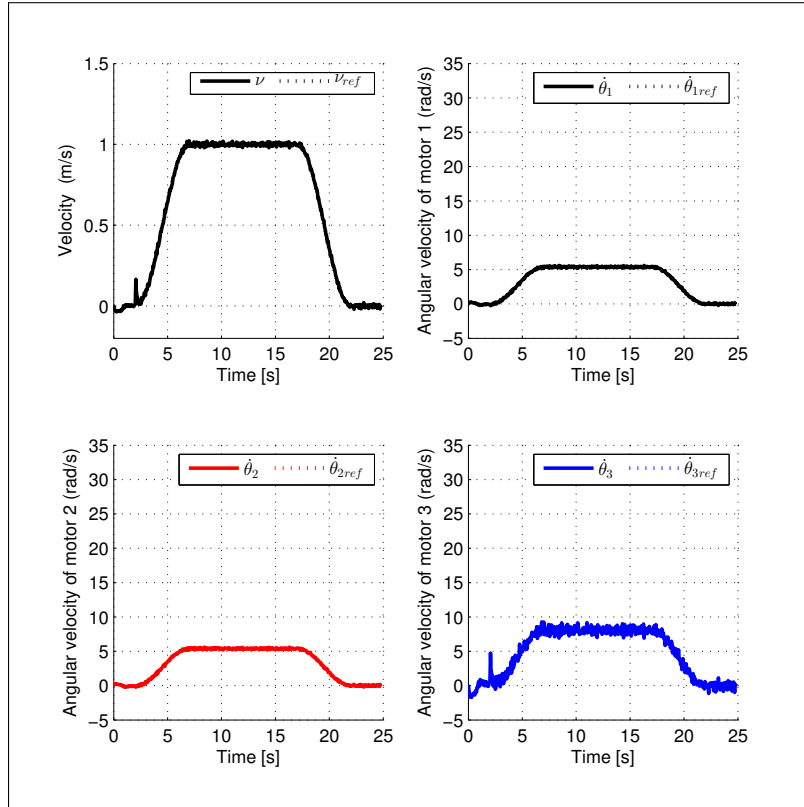
FIGURE 4.13: Simulation results with PPC under disturbance (*d=3*)

FIGURE 4.14: Simulation results with SMC under disturbance (*d=3*); control input of all three motors

FIGURE 4.15: Simulation results with LQR under disturbance (*d=3*); control input of all three motors
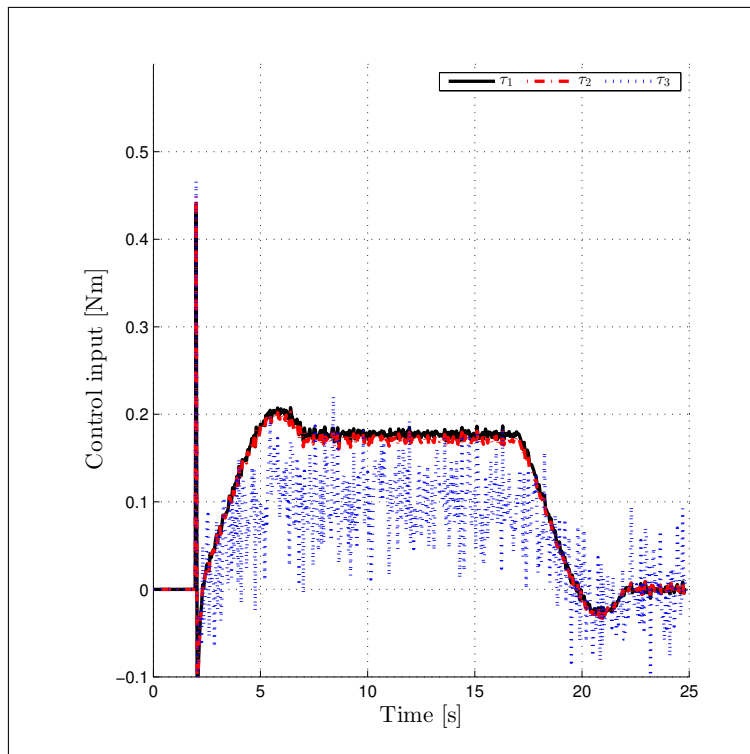
FIGURE 4.16: Simulation results with PPC under disturbance (*d=3*); control input of all three motors
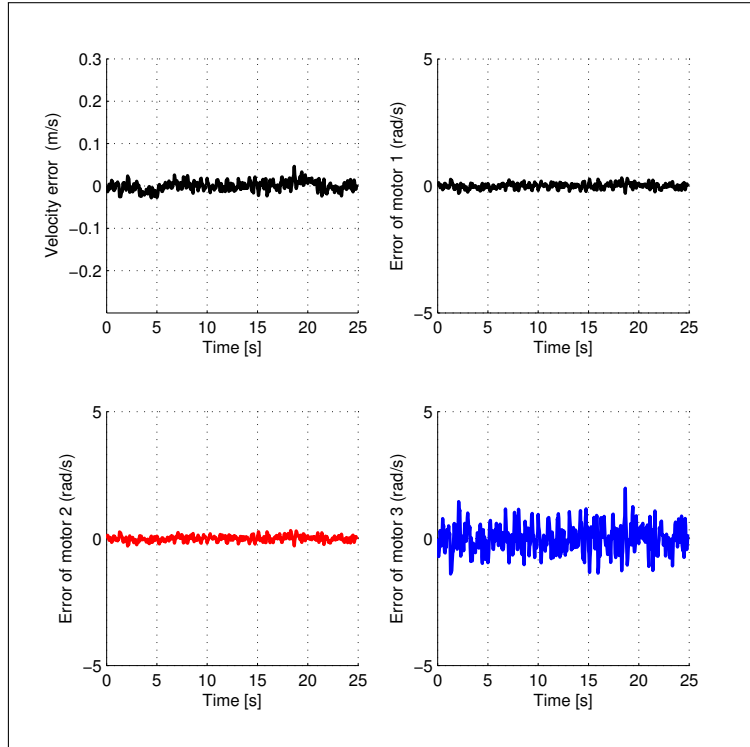
FIGURE 4.17: Simulation result with SMC under disturbance depicted in Fig. 4.11

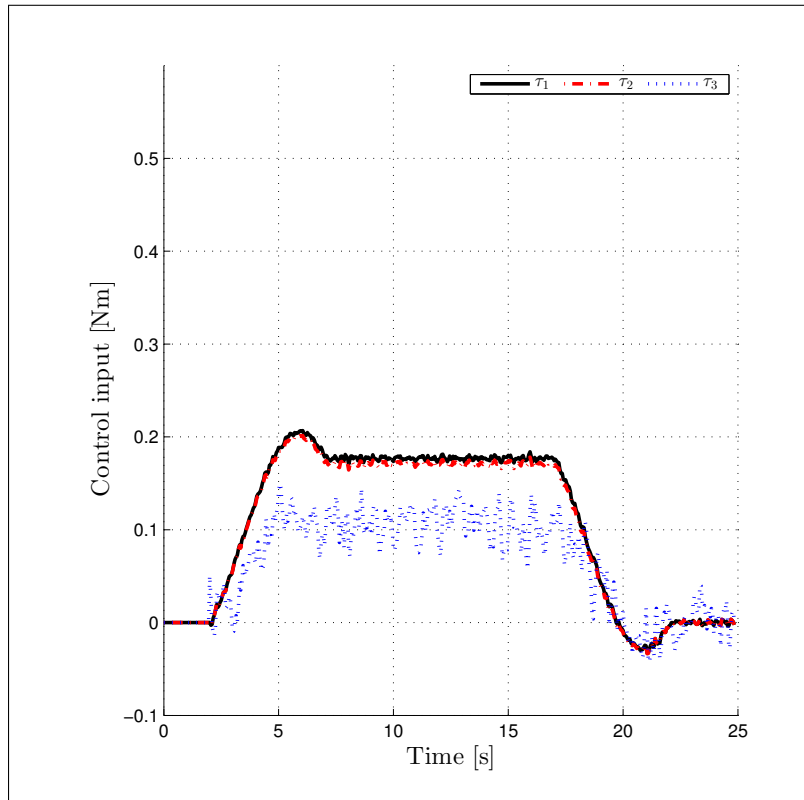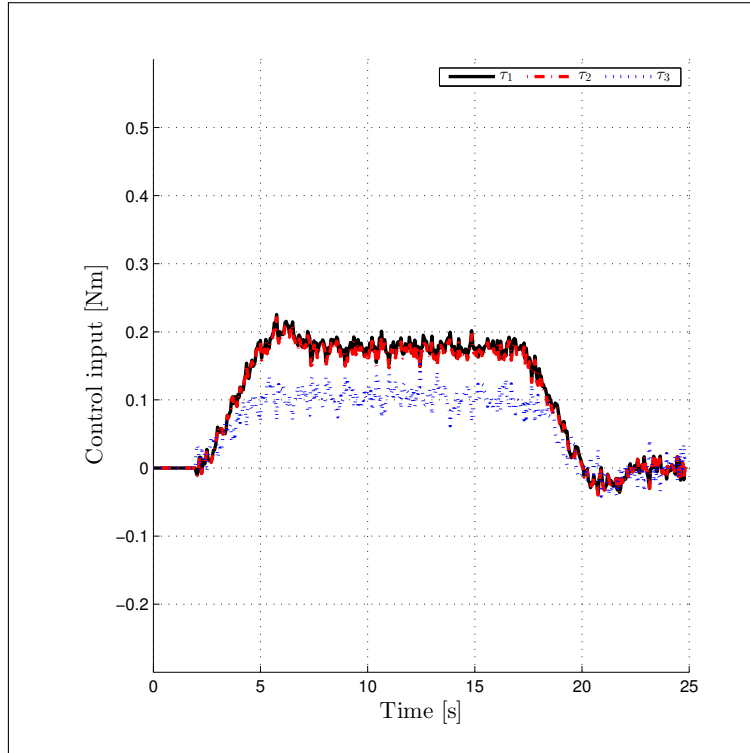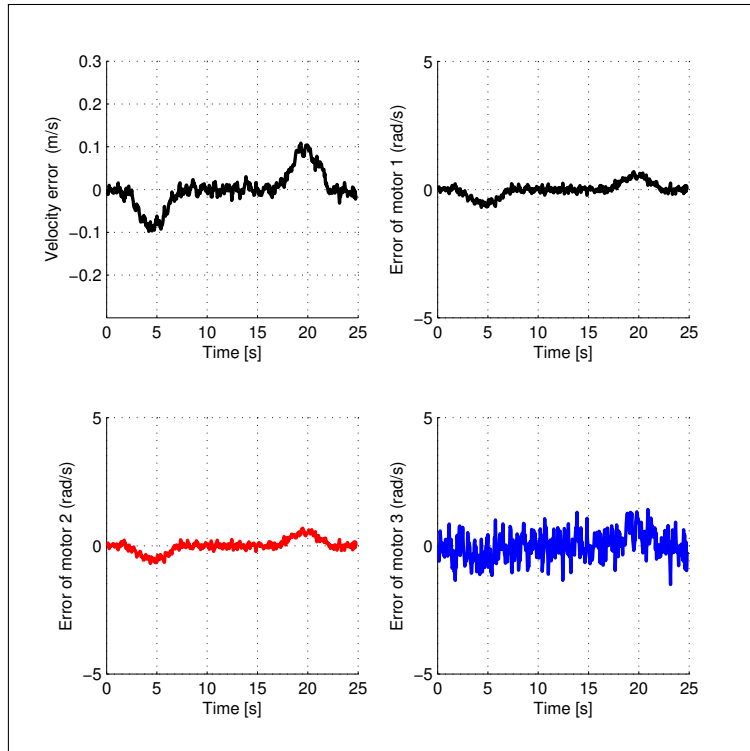FIGURE 4.18: Simulation result with LQR under disturbance depicted in Fig. 4.12
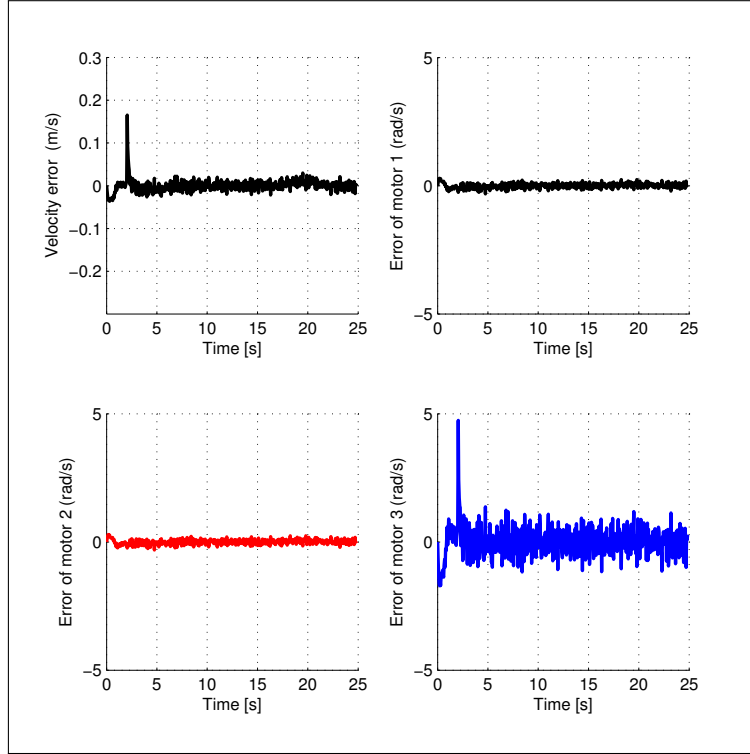
FIGURE 4.19: Simulation result with PPC under disturbance depicted in Fig. 4.13

TABLE 4.3: Average of root mean square error (RMSE) with disturbance

RMSE	SMC	LQR	PPC	Unit
Velocity of WMR	10×10^{-3}	40×10^{-3}	13×10^{-3}	m/s
Velocity of Motor 1	10.1×10^{-2}	25.7×10^{-2}	10.7×10^{-2}	rad/s
Velocity of Motor 2	10.2×10^{-2}	25.2×10^{-2}	10.6×10^{-2}	rad/s
Velocity of Motor 3	50.8×10^{-2}	51.4×10^{-2}	59.5×10^{-2}	rad/s

4.4 Experiments

In this work, the proposed controller was verified experimentally and compared with LQR and PPC. The control law in Eq. (4.6) is implemented using the C# language on a laptop PC (OS: WINDOWS 8.1, CPU: 2.3 GHz) with a sampling interval of 50 ms. In addition, two optical encoders of resolution $0.352°$/count are attached to Motors 1 and 2, and an optical encoder of resolution $0.18°$/count is attached to Motor 3 to measure the angular velocities of the motors. A pulse-counter board with two channels of 24-bit up/down counters and a DA board with 16-bit resolution are used. The motor drivers are also used in current-control mode, in which electrical

current supplied is proportional to the voltage commanded from the laptop PC to each motor. The control parameters of PPC, LQR, and SMC used in the experiments are the same as those in the simulations. Figures 4.20, 4.21, 4.22, and 4.23 show the experimental results of the translational velocity of the WMR and velocity of each motor with SMC, SMC with sat(.), LQR, and PPC, respectively.

The tracking performance of the redundant wheeled drive system is improved by using SMC, as shown in Figs. 4.20, 4.21, 4.22, and 4.23. Figures 4.24, 4.25, 4.26, and 4.27 show the experimental results for the control input of each motor corresponding to Figs. 4.20, 4.21, 4.22, and 4.23, respectively. The chattering in the control input as shown in Fig. 4.24 can be eliminated by replacing the sign(.) function by sat(.) function, as shown in Fig.4.25.
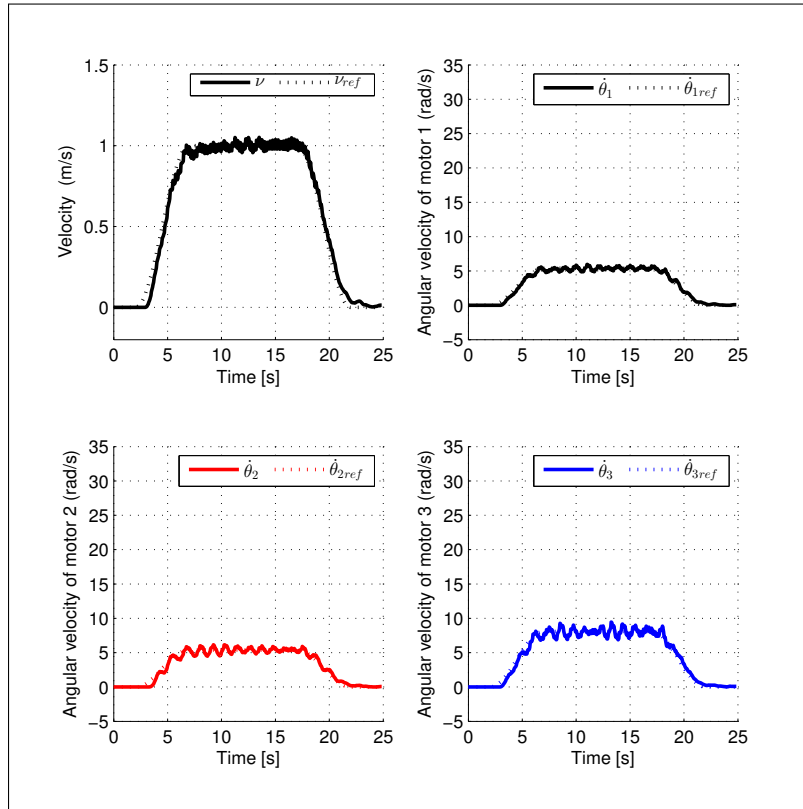
FIGURE 4.20: Experimental result with SMC

The tracking errors resulting from all control approaches in the experiment are shown in Figs. 4.28, 4.29, 4.30, and 4.31. It can be seen that the SMC approach achieves smaller tracking errors than do LQR and PPC.
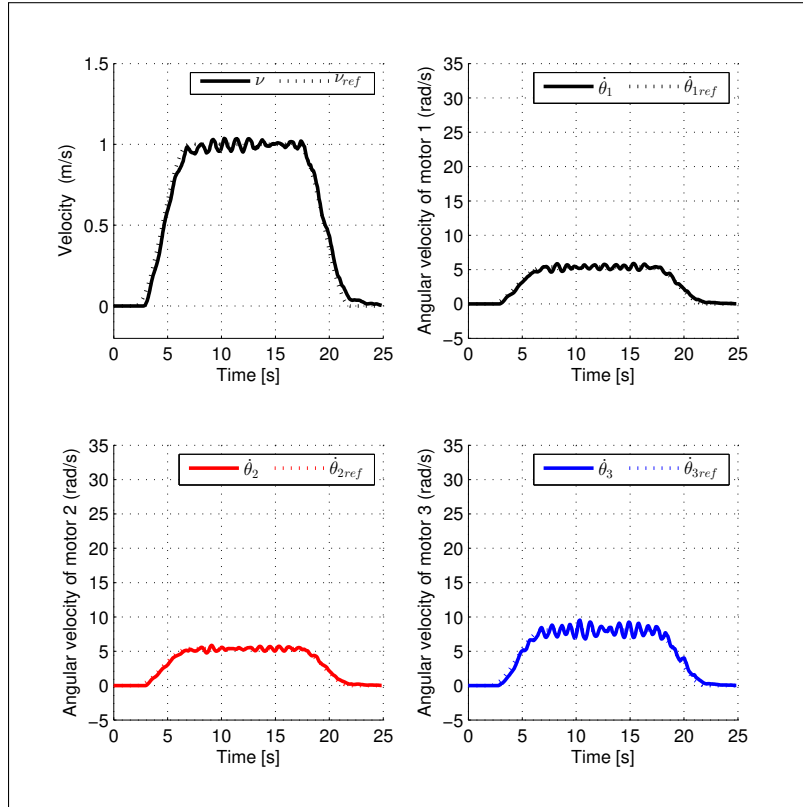
FIGURE 4.21: Experimental result with SMC (sat(.))
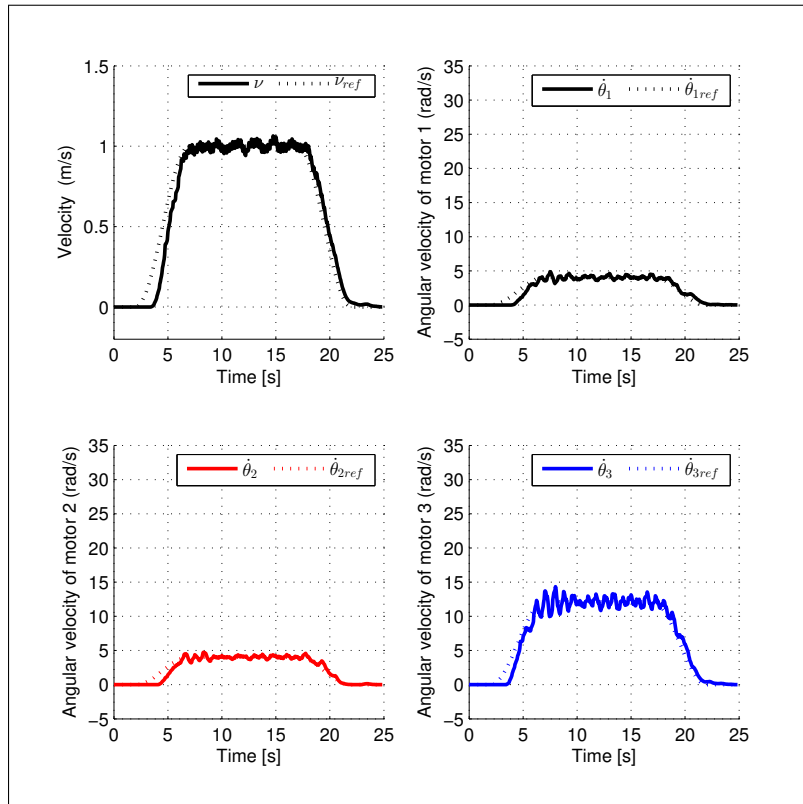
FIGURE 4.22: Experimental result with LQR
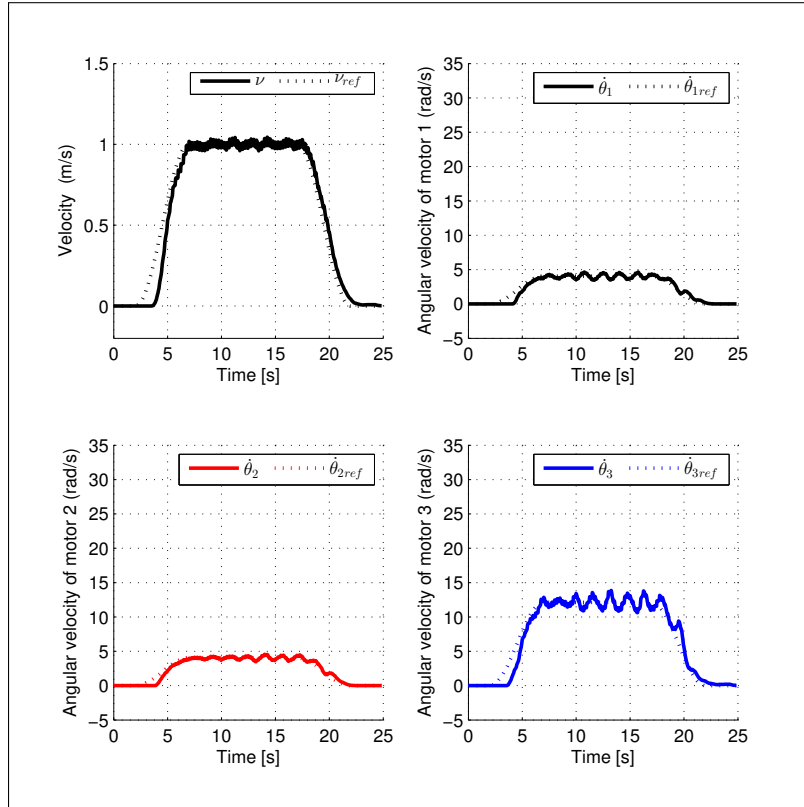
FIGURE 4.23: Experimental result with PPC
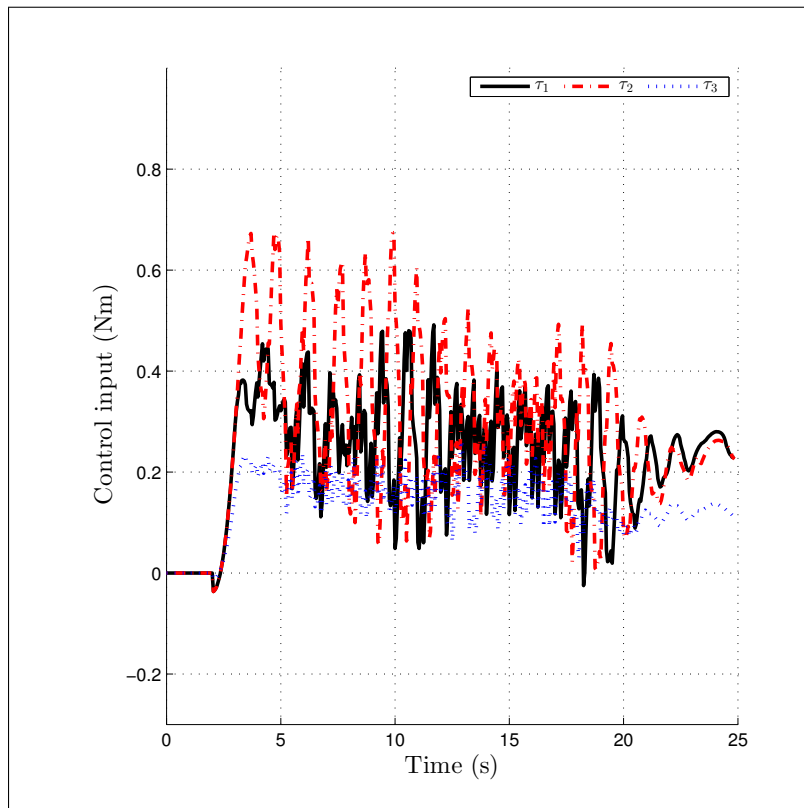
FIGURE 4.24: Experimental result with SMC; control input of all three motors
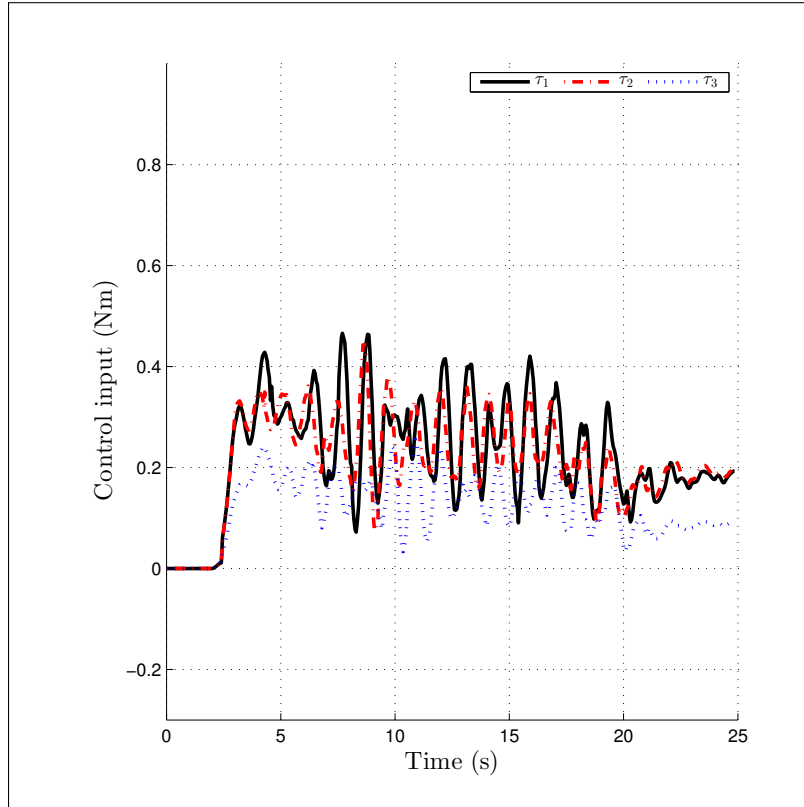
FIGURE 4.25: Experimental result with SMC (sat(.)); control input of all three motors
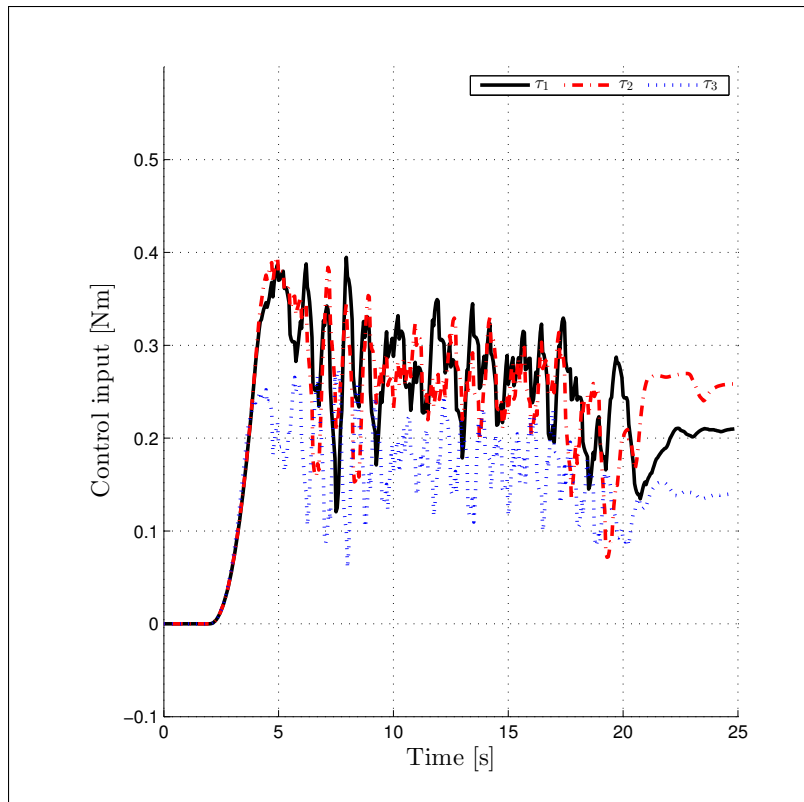
FIGURE 4.26: Experimental result with LQR; control input of all three motors
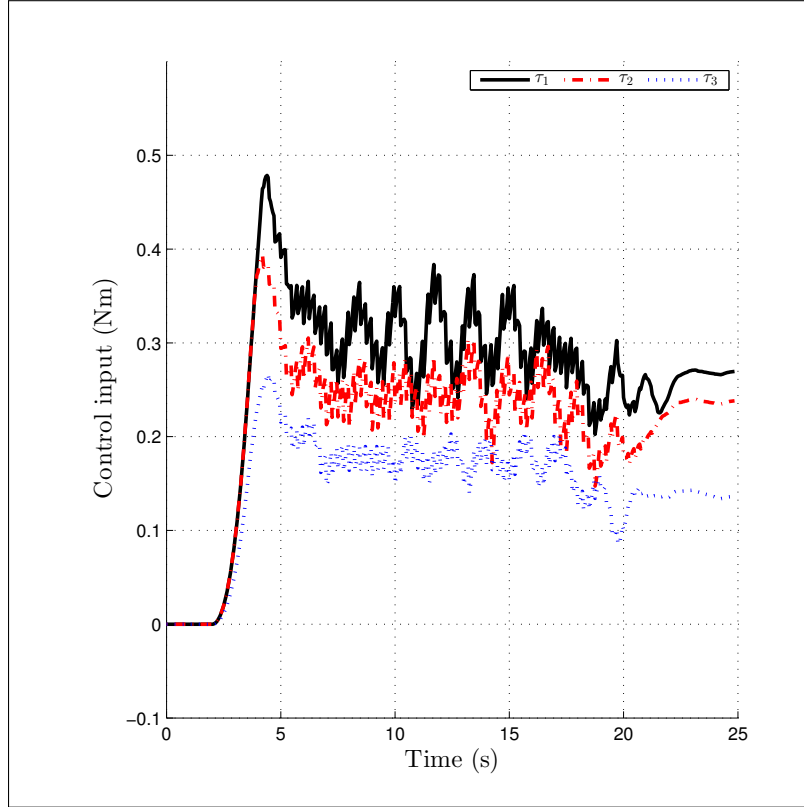
FIGURE 4.27: Experimental result with PPC; control input of all three motors

To verify the repeatability of all approaches, the same experiments that were performed in Figs. 4.20, 4.21, 4.22, 4.23, 4.24, 4.25, 4.26, and 4.27 were repeated five times, and the mean magnitude of the tracking error were compared for the SMC, SMC with sat(.), LQR, and PPC approaches, as shown in Figs. 4.32 and 4.33. It can be seen that the SMC with sat(.) approach reduces the mean value of the tracking-error magnitude and provides robust tracking control in a real environment.

Using SMC, the WMR executed circular motion on a circle with 2-m radius and with the same S-curve velocity profile as for linear motion but now for the tangential velocity [46], as shown in Figs. 4.34 and 4.35. This trajectory is considered for energy comparison in the next section. Figure 4.36 shows video captures for the circular motion that was executed by SMC.
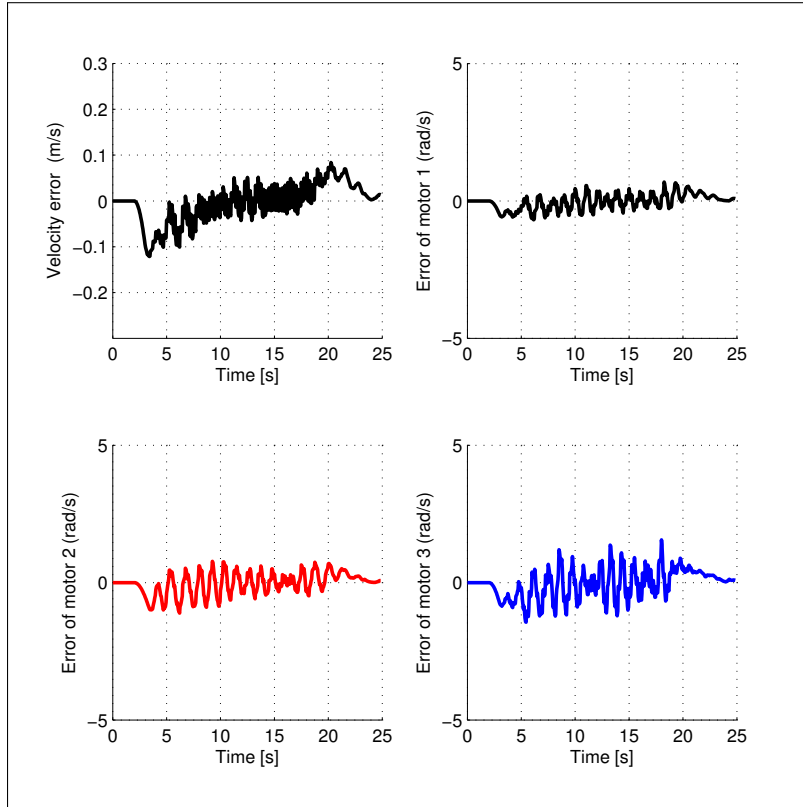
FIGURE 4.28: Experimental result with SMC depicted in Fig. 4.20
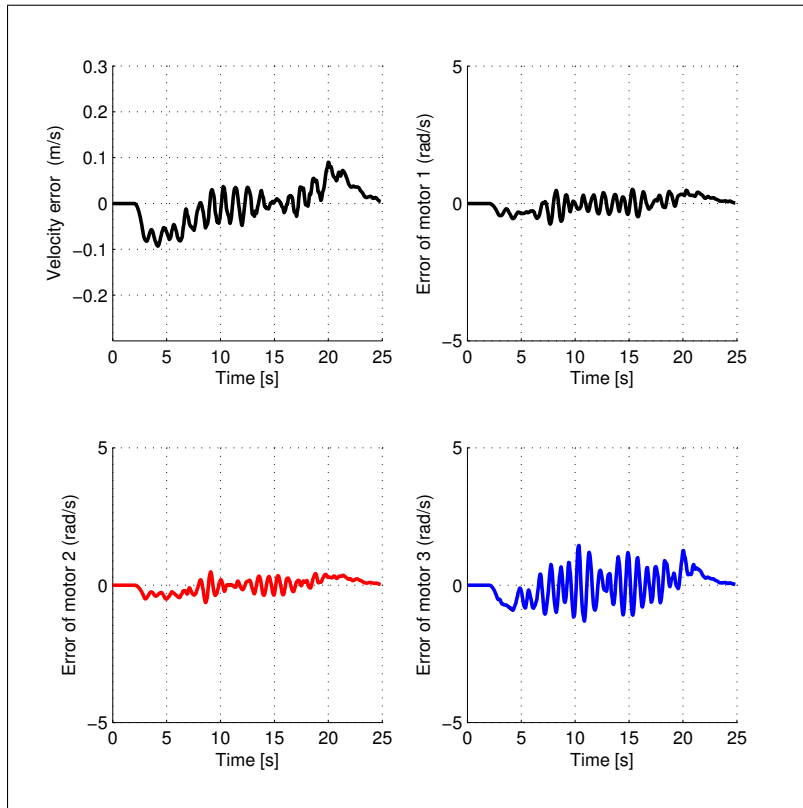
FIGURE 4.29: Experimental result with SMC (sat(.)) depicted in Fig. 4.21
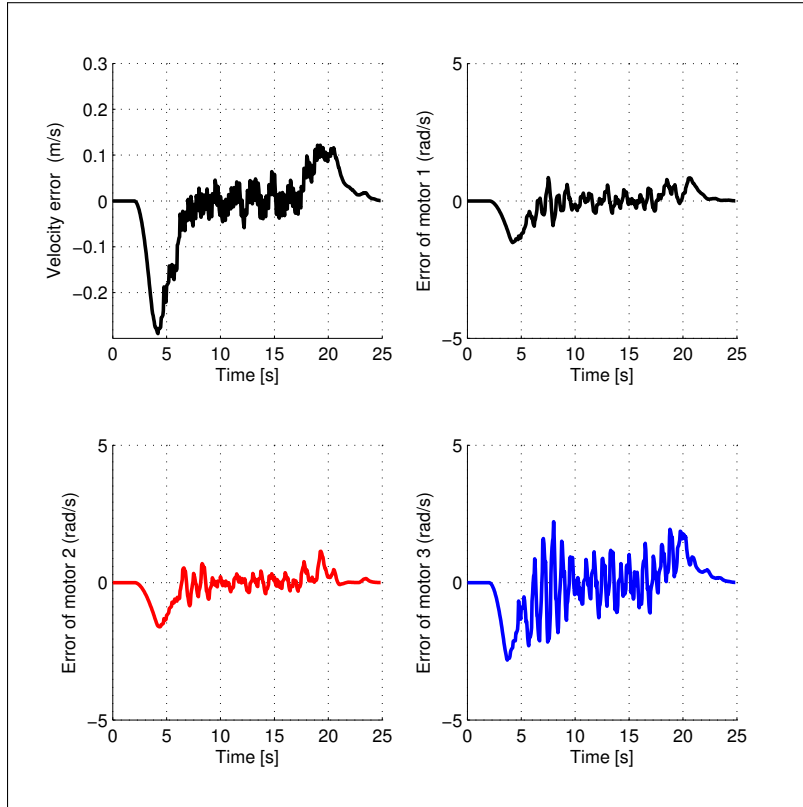
FIGURE 4.30: Experimental result with LQR depicted in Fig. 4.22
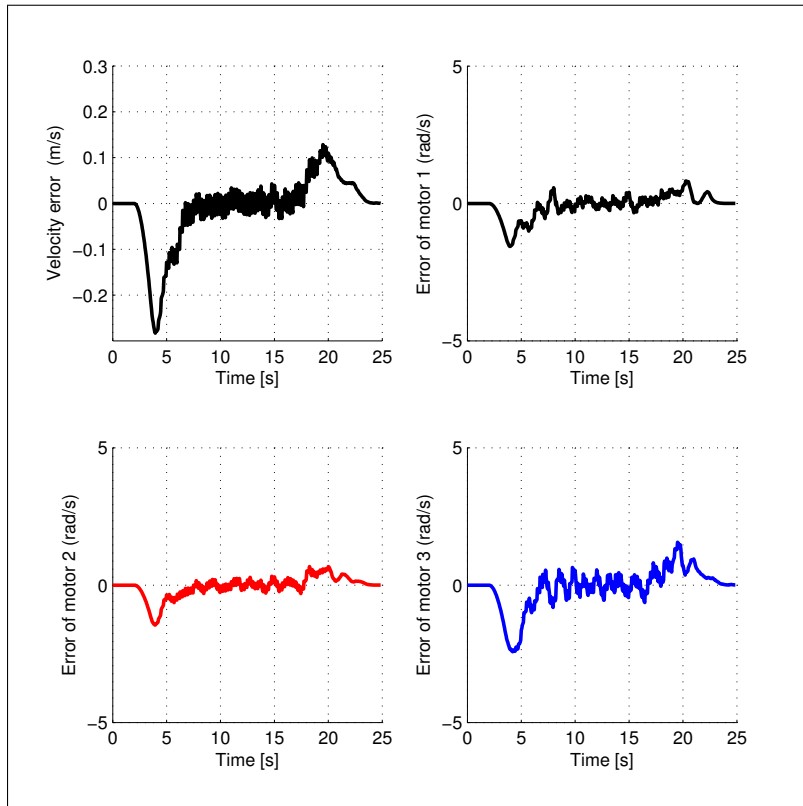
FIGURE 4.31: Experimental result with PPC depicted in Fig. 4.23
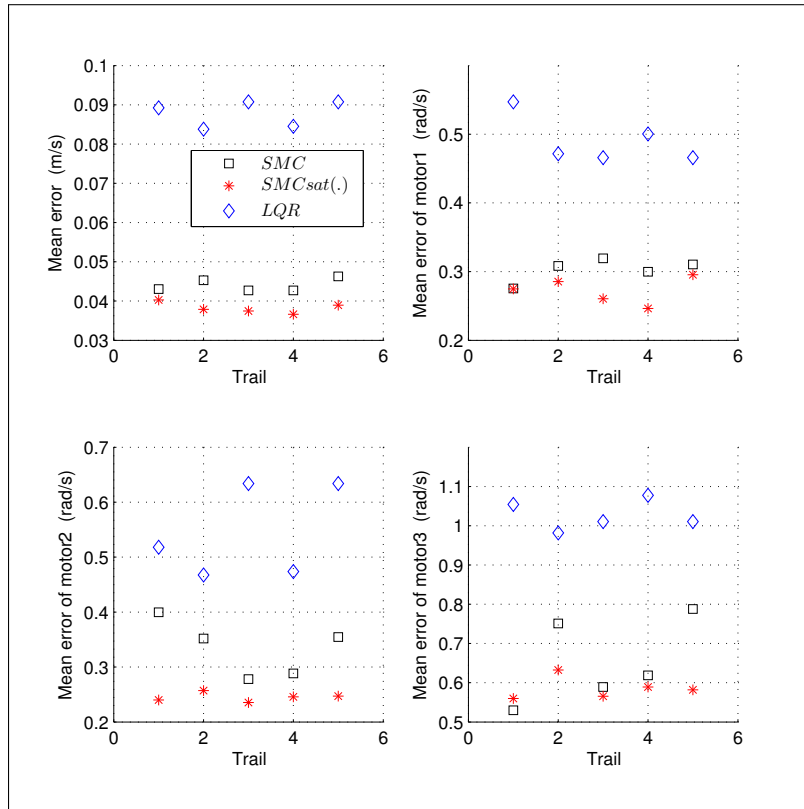
FIGURE 4.32: Experimental result. Mean tracking error magnitude
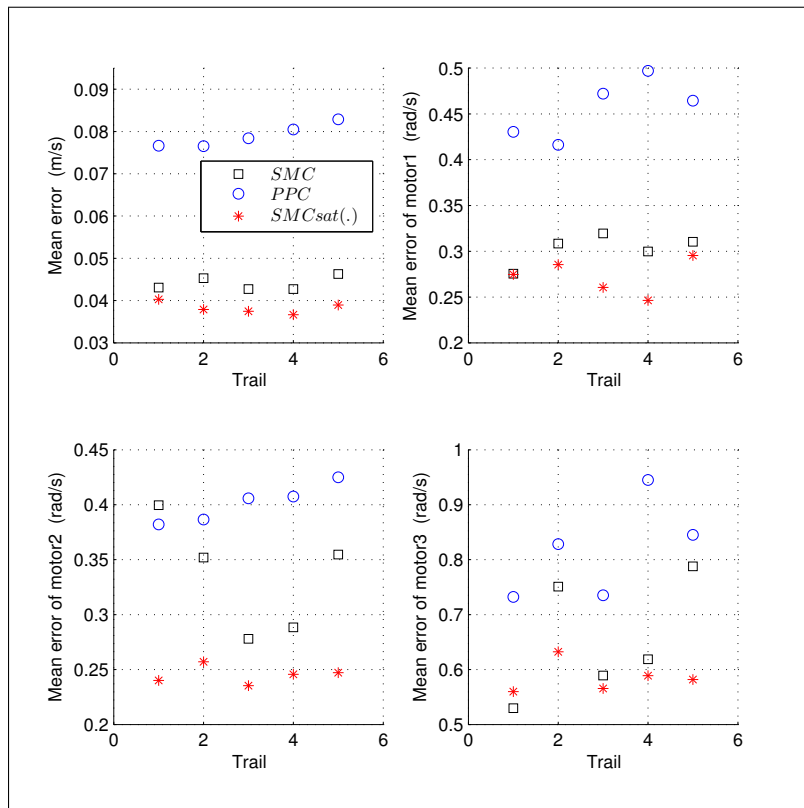
FIGURE 4.33: Experimental result. Mean tracking error magnitude
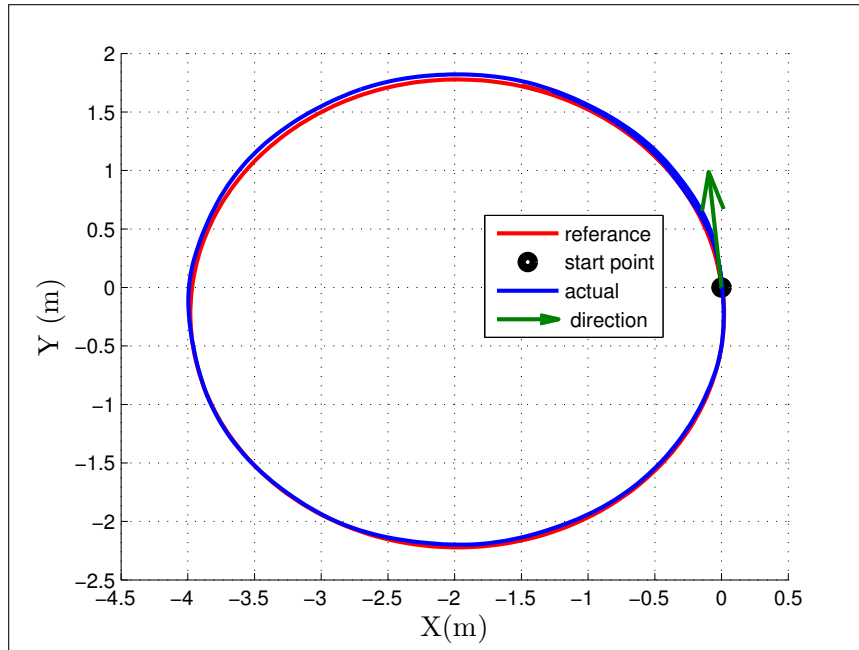
FIGURE 4.34: Experimental result for circular motion with SMC
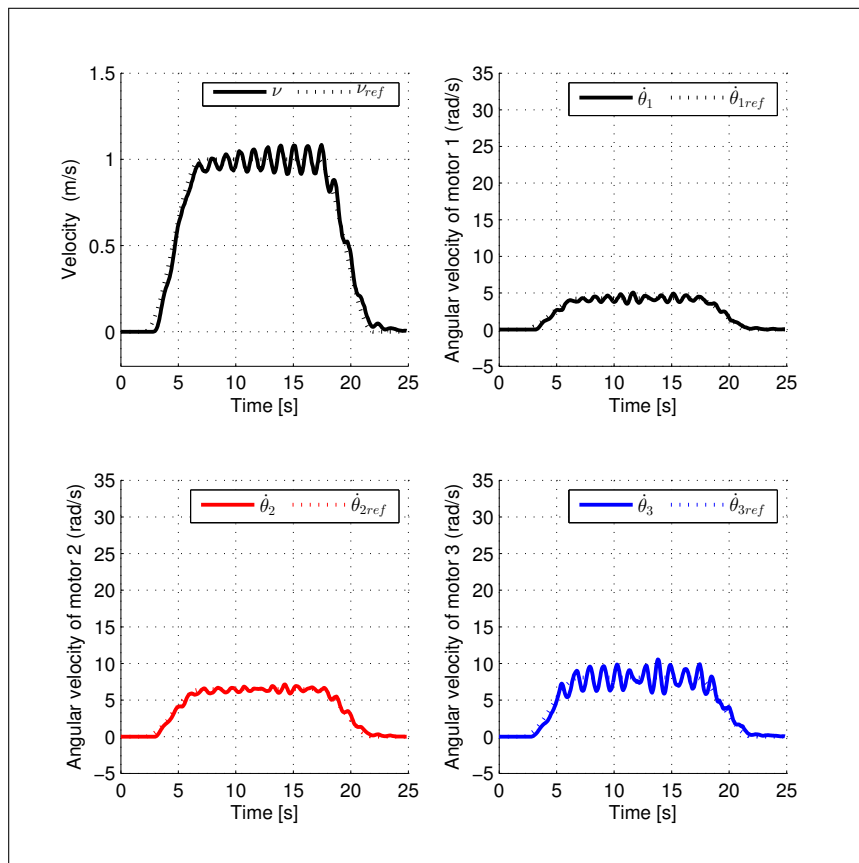
FIGURE 4.35: Experimental result for the linear and angular velocity for circular motion depicted in Fig. 4.34

(A) Time = 0 s

(B) Time = 2 s
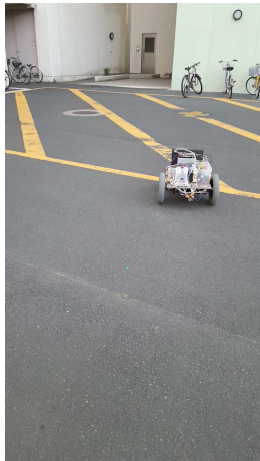
(C) Time = 5 s
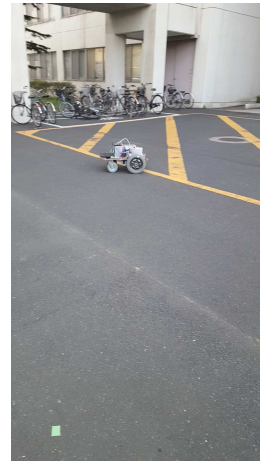
(D) Time = 9 s

(E) Time = 12 s

(F) Time = 15 s

FIGURE 4.36: Video captures from result in Figure 4.34

4.5 Energy Evaluation

Mobile robots are operated using embedded batteries, and hence, energy saving is studied to increase the operation time. For evaluating the energy consumption there are two approaches in literature, electrical energy [16, 20, 21, 100] and mechanical energy consumption [48]. Electrical energy consumption is more accurate and considers the motor, motor driver and amplifier properties. In many cases these properties are described by work load depending efficiencies [101, 102]. These are constant for all times, a linear relation between mechanical and electrical energy holds and mechanical energy can be used for energy consumption evaluation. In this work a constant efficiency is assumed and therefore, for comparing the energy in simulations and experiments, it is sufficient to use the mechanical energy. The energy required for the motors is obtained by the following equation [47, 48]:

$$E = \sum_{i=1}^{3} \int_0^t \left| \tau_i \dot{\theta}_i \right| dt, \tag{4.19}$$

where E is the total energy consumption. Figures 4.37 and 4.38 show the simulation results for the total energy consumed by all the motors for various values of d using SMC, LQR, and PPC for linear and circular motion, respectively. In the simulation, it can be seen that the SMC, LQR, and PPC approaches have almost the same energy consumption. In addition, in all cases, $d = 3$ provides the best efficiency; compared to $d = 20$ (similar to a general two-wheel-drive case), around 20% energy reduction is achieved .

The practicability was verified by conducting five experiments under the same conditions. Figures 4.39, 4.40, 4.41, and 4.42 show the total energy consumed by all the motors for various values of d for linear motion using SMC, SMC with sat(.), LQR, and PPC, respectively. The minimum mean energy required was 50.08 J when using SMC ($d = 1.5$ in Fig. 4.39), 38 J for SMC with sat(.) ($d = 2$ in Fig. 4.40), 59.89 J for LQR ($d = 2$ in Fig. 4.41), and 63.43 J for PPC ($d = 2$ in Fig. 4.42). The total energy consumption for circular motion is shown in Figs. 4.43, 4.44, 4.45, and 4.46 using SMC, SMC with sat(.), LQR, and PPC, respectively. The minimum mean energy required was 50.92 J when using SMC ($d = 1.5$ in Fig. 4.43), 41.32 J for SMC

with sat(.) ($d = 2$ in Fig. 4.44), 57.3 J for LQR ($d = 1.5$ in Fig. 4.45), and 59.37 J for PPC ($d = 2$ in Fig. 4.46). The SMC with sat(.) approach requires less energy in a real environment while achieving better tracking performance, as shown in Figs. 4.32 and 4.33.
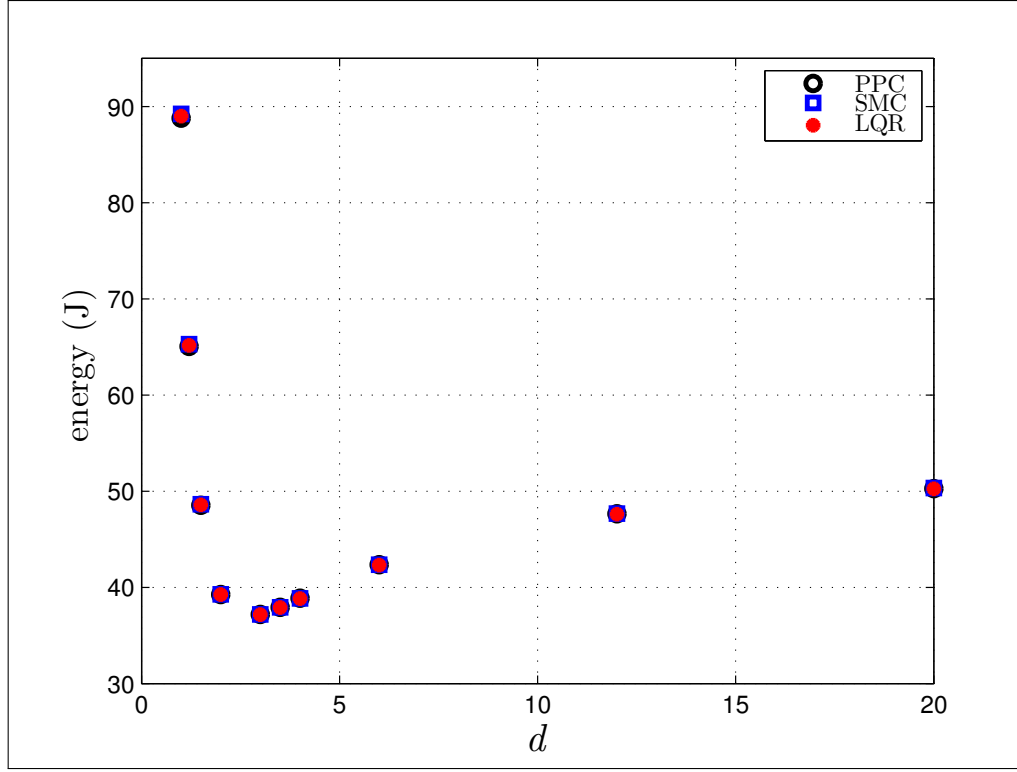
FIGURE 4.37: Simulation result total energy consumption for linear motion

From the viewpoint of the tracking performance and consumed energy in the simulations and experiments, the SMC with sat(.) approach is more effective only in a real case as shown in Figs 4.32 and 4.33. Equation (4.6) consists of three parts: the first is for feed-forward control, which gives better tracking, the second is for position and velocity feedback control, which is similar to LQR or PPC, and the third guarantees robustness. These control terms have a positive effect on the tracking performance with less energy as shown in Fig. 4.40, the minimum mean energy required was 38 J for SMC with sat(.).

The difference of the optimal value of the fixed ratio d in experiment and simulation follows from the simplified simulation model, where nonlinearities especially from the planetary-gear system are neglected. The gearbox has higher friction than modeled and the control input of motors in the experiment are higher than the control
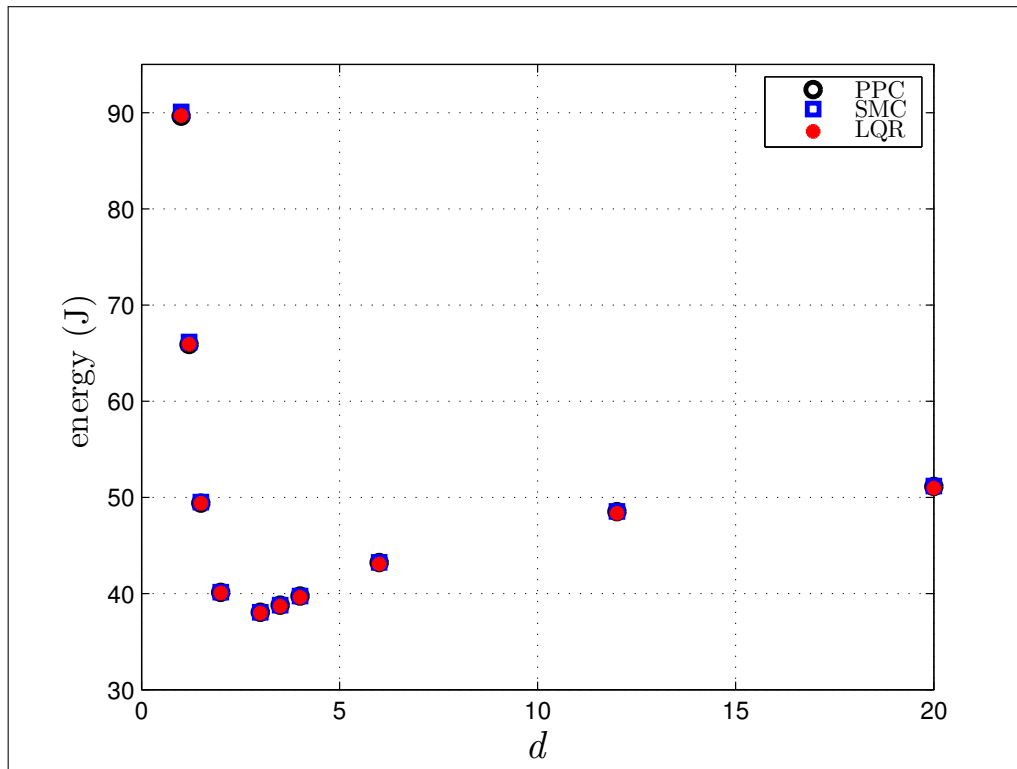
FIGURE 4.38: Simulation result total energy consumption for circular motion
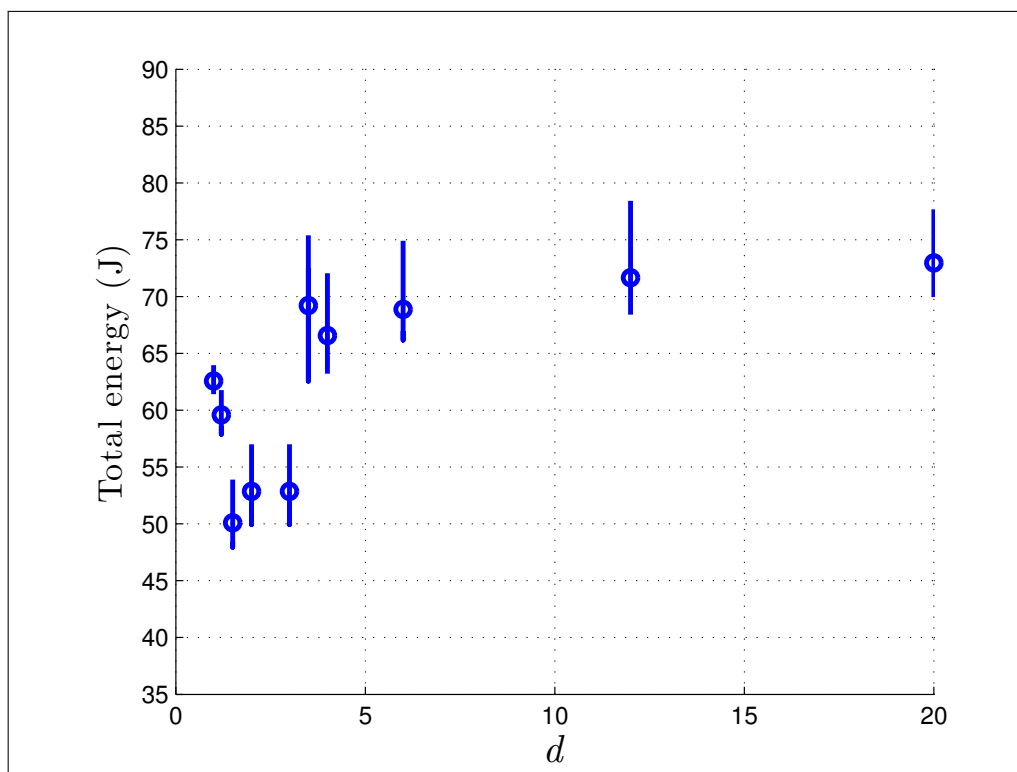
FIGURE 4.39: Experimental result with SMC; total energy consumption for linear motion
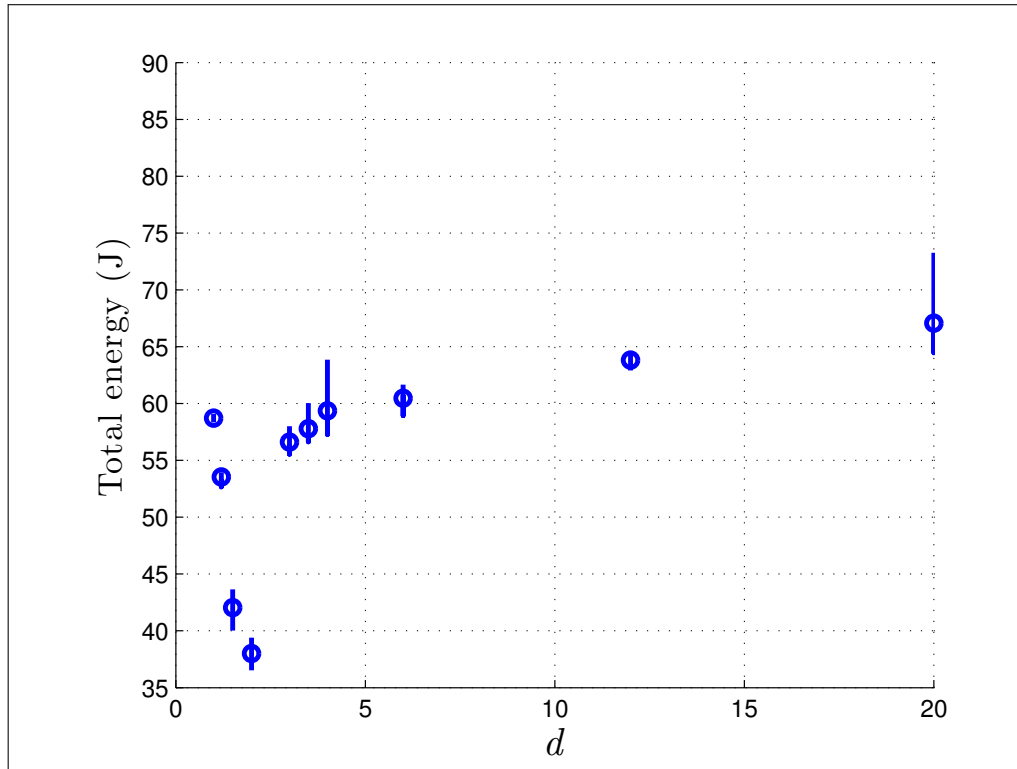
FIGURE 4.40: Experimental result with SMC (sat(.)); total energy consumption for linear motion
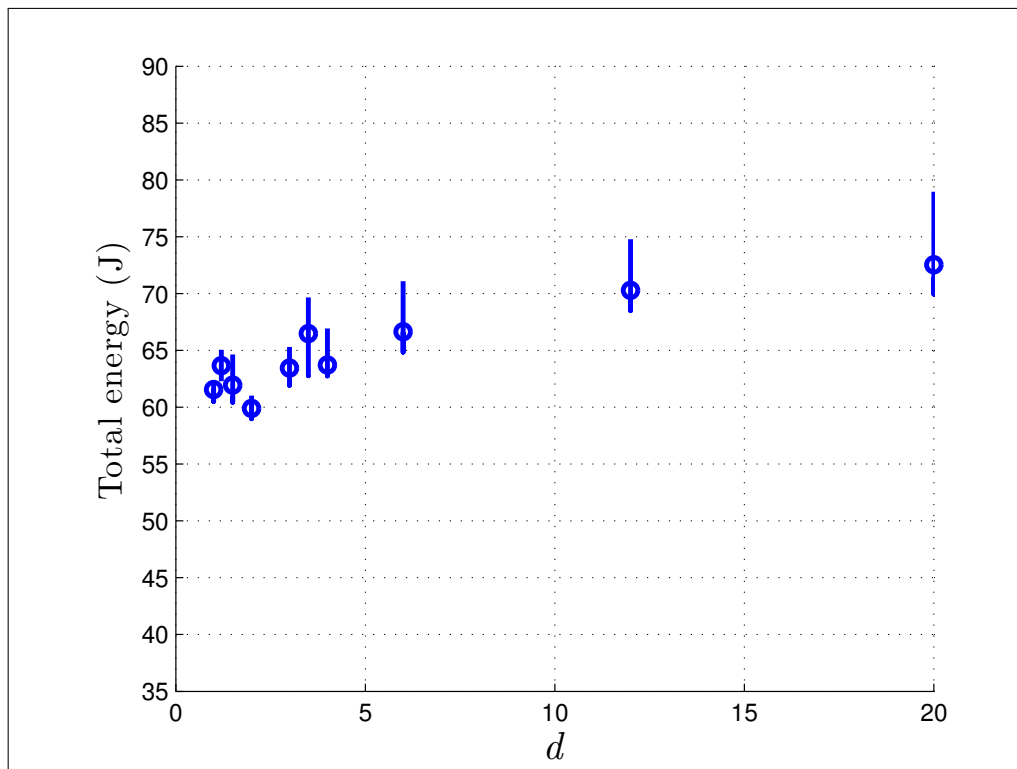
FIGURE 4.41: Experimental result with LQR; total energy consumption for linear motion
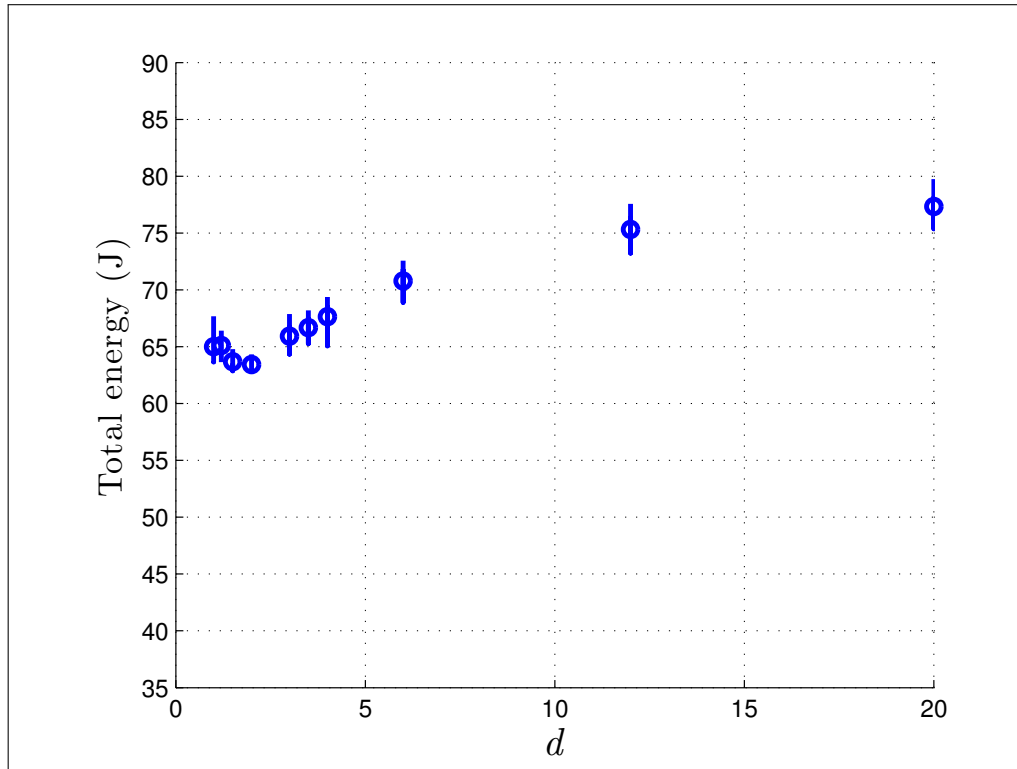
FIGURE 4.42: Experimental result with PPC; total energy consumption for linear motion
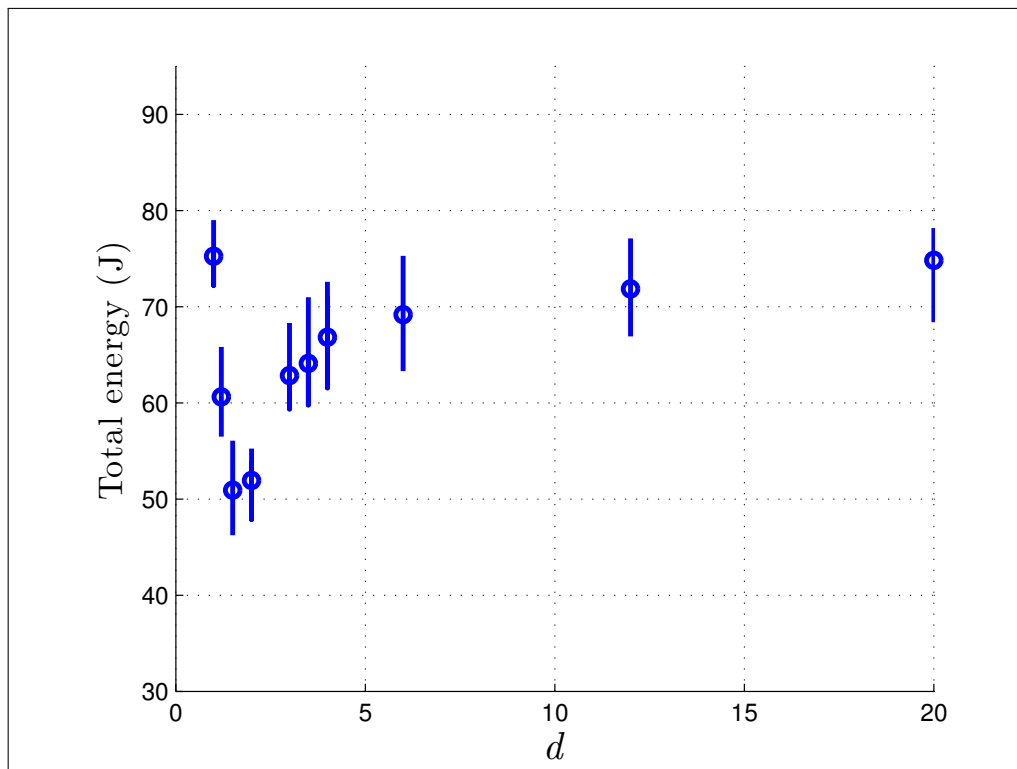
FIGURE 4.43: Experimental result with SMC; total energy consumption for circular motion
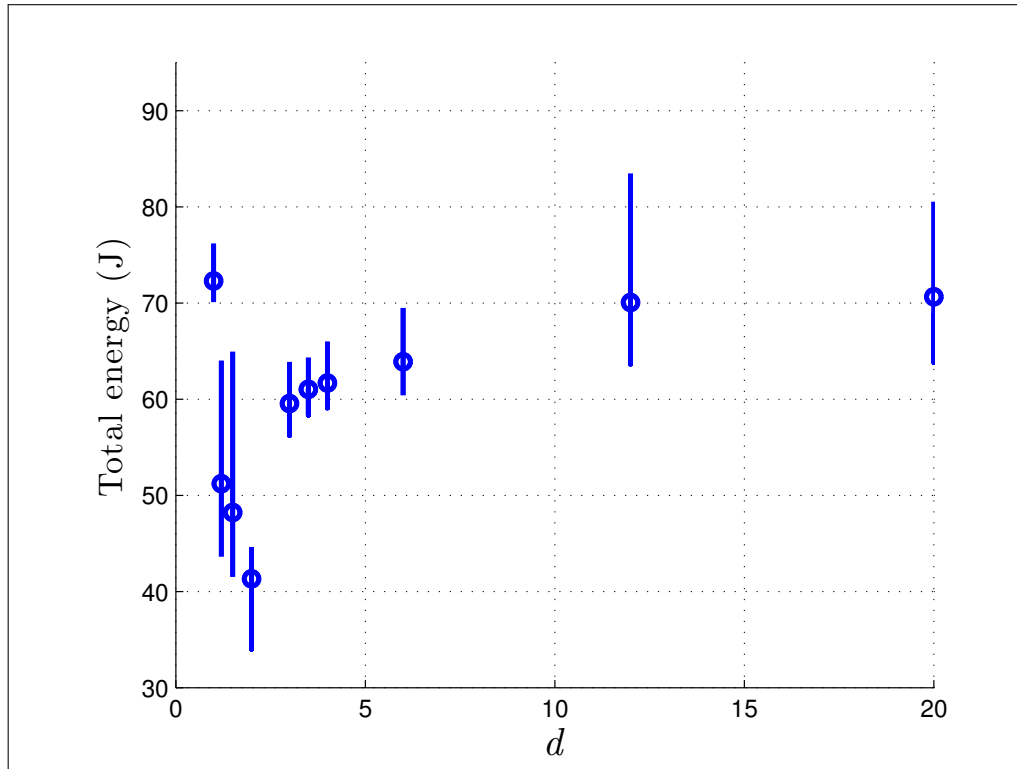
FIGURE 4.44: Experimental result with SMC (sat(.)); total energy consumption for circular motion
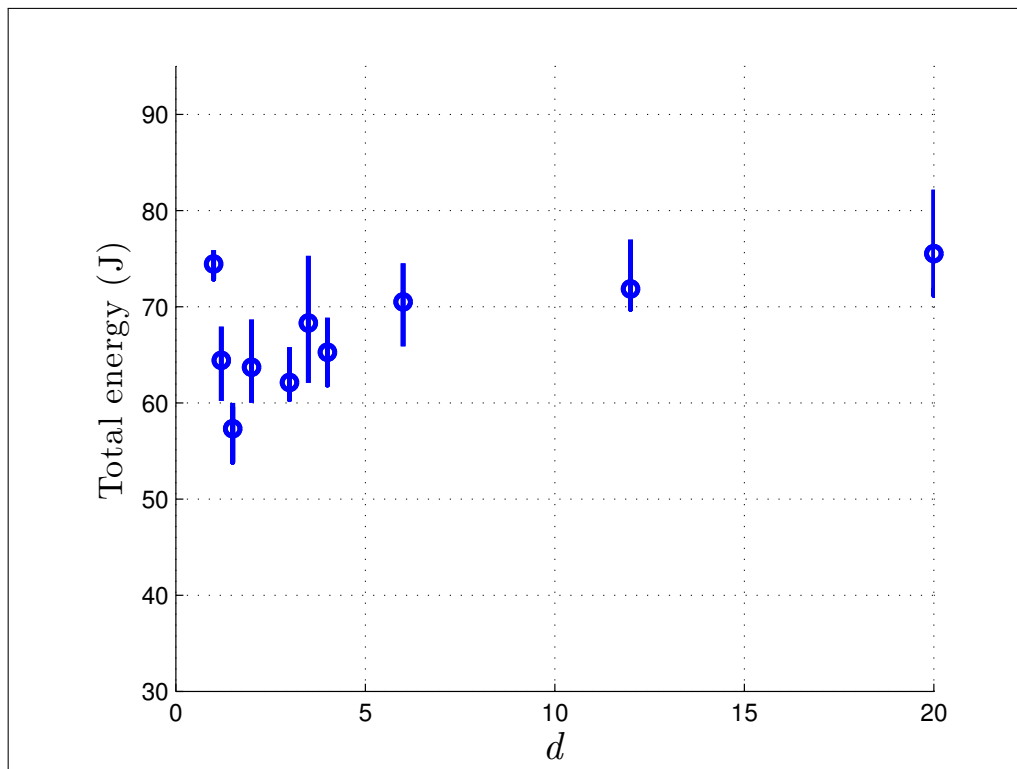
FIGURE 4.45: Experimental result with LQR; total energy consumption for circular motion
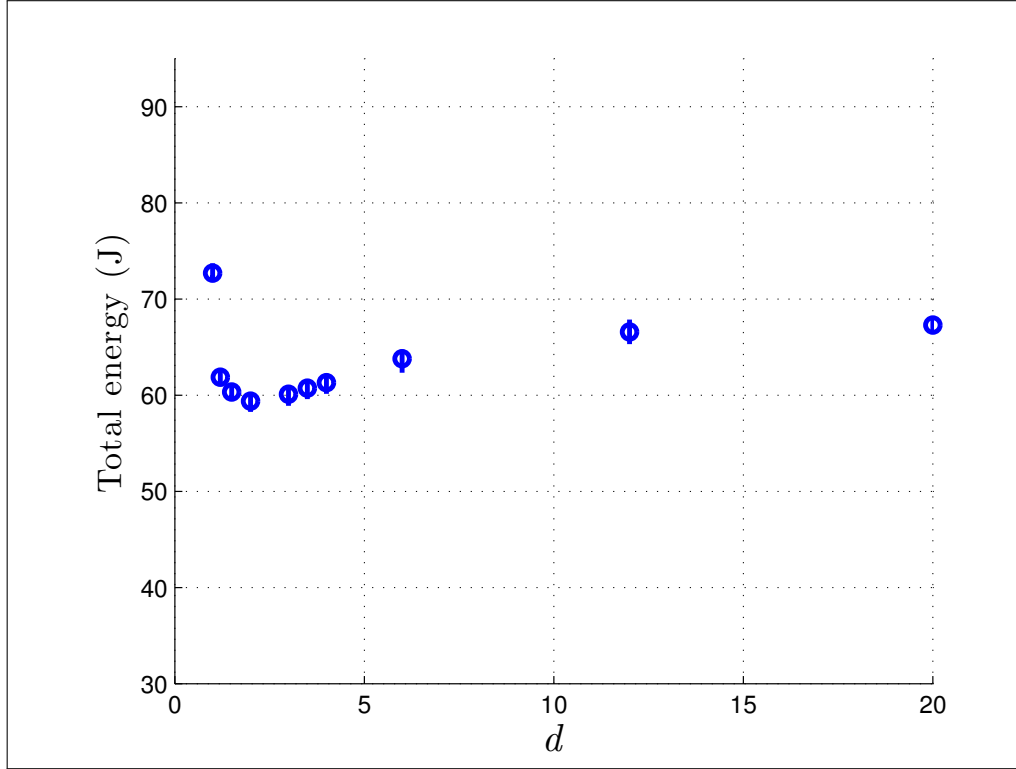
FIGURE 4.46: Experimental result with PPC; total energy consumption for circular motion

input of motors in the simulation especially from Motor 2 as shown in Figs 4.5 and 4.24. Therefore more power in experiment than simulation is required which lead to lower fixed ratio d.

4.6 Conclusion

In this chapter, robust tracking and energy-saving control was considered for a redundant wheeled drive system using SMC. Using to the distribution controller presented in chapter 3, a comparative study was conducted between LQR and PPC. Computer simulations were performed to verify the effectiveness of the proposed method, and there was no significant difference between the SMC, LQR, and PPC approaches. The effectiveness and reliability of the proposed method in a real environment with disturbances were evaluated by performing several repeated experiments. The results showed that SMC with sat(.) provides robust tracking performance with less energy.

Chapter 5

Conclusions and Future Work

5.1 Conclusions

Mobile robots are expected to be applied not only to transportation work in factories but also to living support in an aging society. With ever more people who are elderly and disabilities, there is growing demand for mobility support devices and care equipment to improve quality of life. Although many drive mechanisms have been proposed to date for mobile robots, from the viewpoint of practicality, differential wheeled mobile robots such as electric wheelchairs are still widely used. With a differential wheeled mobile robot, by controlling the speed of both each wheel independently, the operator's body can be translated and rotated. However, this movement cannot be continued if one wheel fails. For this reason, it is important to increase the number of drive wheels and add redundancy. In addition, mobile robots are powered mainly by rechargeable batteries, but these generally take time to charge. Therefore, saving energy is studied to increase the operating time. To this end, this thesis proposed a new system consisting of a redundant drive system to continue the motion safely should one of the motors break down for some reason, and also that is able to operate for longer by saving energy.

This dissertation considered of three parts.
The first part considered the dynamic modeling of a redundant wheeled drive system with nonholonomic constraints. In addition, it was assumed that, as with a personal mobility vehicle such as an electric wheelchair, the operator of the vehicle specifies

its desired linear and angular velocities. These velocities are typically transformed into desired velocities of the left and right wheels, whereupon these wheel velocities are transformed into motor velocities of the three motors by using a distribution controller. In addition, by introducing a fixed ratio d of angular velocities of a wheels to the velocity of Motor 3. The optimum value of d depends on the actuator specifications and the driving situation, and must be found by simulation/experiment for different WMR systems.

The second part of the research showed the possibility of the proposed new drive system for energy saving and fail safety by applying two controllers. Distribution and state-feedback controllers were applied to the wheeled drive system. The distribution controller created a reference angular velocity for the motors. In addition, by assuming that the commercial motor controllers were based on PD control, and the state-feedback controller was applied to the proposed WMR as a feedback controller. The feedback gains of that controller were obtained by the pole placement method. Experiments were conducted to verify the effectiveness of the proposed method. A distribution ratio of $d = 2$ provided 20.45 % and 13.05 % reductions (for linear and circular motion, respectively) in the consumed energy compared to the case in which only two motors operated.

The third part of the research considered robust tracking and energy-saving control for a redundant wheeled drive system using SMC. Using to the distribution controller presented in the second part of dissertation , a comparative study was conducted between LQR and PPC . Computer simulations were performed to verify the effectiveness of the proposed method, and there was no significant difference between the SMC, LQR, and PPC approaches. The effectiveness and reliability of the proposed method in a real environment with disturbances were evaluated by performing several repeated experiments. The results showed that SMC with sat(.) provided robust tracking performance with less energy.

5.2   Future Work

- The effectiveness and performance of all the control strategies discussed in this thesis were evaluated using an experimental testbed for redundant wheeled drive systems . In the future, this work will be extended by applying the proposed method on rough terrain and public roads over large distances.

- Consideration will be given to finding an optimal value of the fixed ratio d depending on the driving situation.

- Collaboration will be undertaken with companies to develop highly practical equipment, including a collision-avoidance function using a distance sensor.

- The proposed new method will be applied to other systems such as the cleaning robots which used in recycling centers.

- Detection of motor failure and control of the system with defective motors.

- The proposed system will be compared with a non-redundant system.

- The energy saving from the electrical systems due to the electrical characteristics of motors, amplifier resistance in motor drivers and viscous friction will be considered.

Bibliography

[1] Alex Mihailidis, Pantelis Elinas, Jennifer Boger, and Jesse Hoey. "An intelligent powered wheelchair to enable mobility of cognitively impaired older adults: An anticollision system". *IEEE Transactions on Neural Systems and Rehabilitation Engineering* 15.1 (2007), pp. 136–143.

[2] E. Prassler, J. Scholz, and P. Fiorini. "A robotics wheelchair for crowded public environment". *IEEE Robotics & Automation Magazine* 8.1 (2001), pp. 38–45.

[3] David P. Miller and Marc G. Slack. "Design and testing of a low-cost robotic wheelchair prototype". *Autonomous Robots* 2.1 (1995), pp. 77–88.

[4] M Babel, F Pasteau, B Fraudet, S Achille, A Colin, B Nicolas, A Durufle, L Le Pape, and P Gallien. "Assessment of a navigation assistance system for power wheelchair". *Annals of Physical and Rehabilitation Medicine* 58 (2015), e99.

[5] Yutaka Satoh and Katsuhiko Sakaue. "An omnidirectional stereo vision-based smart wheelchair". *EURASIP Journal on Image and Video Processing* 1 (2007), pp. 1–11.

[6] Takashi Gomi and Ann Griffith. "Developing intelligent wheelchairs for the handicapped". *Assistive Technology and Artificial Intelligence* (1998), pp. 150–178.

[7] Eun Yi Kim. "Wheelchair navigation system for disabled and elderly people". *Sensors* 16.11 (2016), p. 1806.

[8] Holly Yanco. "Wheelesley: A robotic wheelchair system: Indoor navigation and user interface". *Assistive Technology and Artificial Intelligence* (1998), pp. 256–268.

[9]   Vinod Sharma, Richard C Simpson, Edmund F LoPresti, and Mark Schmeler. "Clinical evaluation of semiautonomous smart wheelchair architecture (DriveSafe System) with visually impaired individuals". *Journal of Rehabilitation Research & Development* 49.1 (2012), pp. 35–50.

[10]   Spyros G Tzafestas. *Introduction to mobile robot control*. Elsevier, (2013).

[11]   Ronald P Gaal, Nancy Rebholtz, Ralf D Hotchkiss, and Peter F Pfaelzer. "Wheelchair rider injuries: causes and consequences for wheelchair design and selection". *Journal of Rehabilitation Research and Development* 34.1 (1997), pp. 58–71.

[12]   Huiyun Xiang, AM Chany, and Gary A Smith. "Wheelchair related injuries treated in US emergency departments". *Injury Prevention* 12.1 (2006), pp. 8–11.

[13]   Lynn Worobey, Michelle Oyster, Gregory Nemunaitis, Rory Cooper, and Michael L Boninger. "Increases in wheelchair breakdowns, repairs, and adverse consequences for people with traumatic spinal cord injury". *American Journal of Physical Medicine & Rehabilitation/Association of Academic Physiatrists* 91.6 (2012), pp. 463–469.

[14]   Sedat Dogru and Lino Marques. "Energy Efficient Coverage Path Planning for Autonomous Mobile Robots on 3D Terrain". *IEEE International Conference on Autonomous Robot Systems and Competitions* (2015), pp. 118–123.

[15]   A. Barili, M. Ceresa, and C. Parisi. "Energy-saving motion control for an autonomous mobile robot". *IEEE International Symposium on Industrial Electronics* 2 (1995), pp. 674–676.

[16]   Chong Hui Kim and Byung Kook Kim. "Minimum-Energy Translational Trajectory Generation for Differential-Driven Wheeled Mobile Robots". *Journal of Intelligent and Robotic Systems* 49.4 (2007), pp. 367–383.

[17]   P. E. Rybski, N. P. Papanikolopoulos, S. A. Stoeter, D. G. Krantz, K. B. Yesin, M. Gini, R. Voyles, D. F. Hougen, B. Nelson, and M. D. Erickson. "Enlisting rangers and scouts for reconnaissance and surveillance". *IEEE Robotics & Automation Magazine* 7.4 (2000), pp. 14–24.

[18] Yongguo Mei, Yung-Hsiang Lu, Y Charlie Hu, and CS George Lee. "A case study of mobile robot's energy consumption and conservation techniques". *International Conference on Advanced Robotics*. (2005), pp. 492–497.

[19] AM Trzynadlowski. "Energy optimization of a certain class of incremental motion dc drives". *IEEE Transactions on Industrial Electronics* 35.1 (1988), pp. 60–66.

[20] Chong Hui Kim and Byung Kook Kim. "Energy-saving 3-step velocity control algorithm for battery-powered wheeled mobile robots". *IEEE International Conference on Robotics and Automation* (2005), pp. 2375–2380.

[21] Yongguo Mei, Yung-Hsiang Lu, Y Charlie Hu, and CS George Lee. "Energy-efficient motion planning for mobile robots". *IEEE International Conference on Robotics and Automation* 5 (2004), pp. 4344–4349.

[22] Wu Weiguo, Chen Huitang, and Woo Peng-Yung. "Optimal motion planning for a wheeled mobile robot". *IEEE International Conference on Robotics and Automation* 1 (1999), pp. 41–46.

[23] Shuang Liu and Dong Sun. "Optimal motion planning of a mobile robot with minimum energy consumption". *IEEE/ASME International Conference on Advanced Intelligent Mechatronics*. (2011), pp. 43–48.

[24] Tsugio Makimoto and Yoshio Sakai. "Evolution of low power electronics and its future applications". *International Symposium on Low Power Electronics and Design*. (2003), pp. 2–5.

[25] Yongguo Mei, Yung-Hsiang Lu, Yu Charlie Hu, and CS George Lee. "Deployment of mobile robots with energy and timing constraints". *IEEE Transactions on Robotics* 22.3 (2006), pp. 507–522.

[26] Inge Spangelo and Inge Spangelo. "Trajectory Optimization for Vehicles Using Control Vector Parametrization and Nonlinear Programming". PhD thesis. The Norwegian Institute of Technology, Trondheim, Norway, (1994).

[27] Yuki Ueno, Takashi Ohno, Kazuhiko Terashima, Hideo Kitagawa, Kazuhiro Funato, and Kiyoaki Kakihara. "Novel differential drive steering system with energy saving and normal tire using spur gear for an omni-directional mobile robot". *IEEE International Conference on Robotics and Automation*. (2010), pp. 3763–3768.

[28] Guixiang Zhang, A Schmidhofer, and A Schmid. "Efficiency optimisation at DC drives for small electrical vehicles". *International Conference on Industrial Technology* 2 (2003), pp. 1150–1155.

[29] Amol Deshmukh, Patricia A Vargas, Ruth Aylett, and Keith Brown. "Towards socially constrained power management for long-term operation of mobile robots". *11th Conference Towards Autonomous Robotic Systems*. (2010).

[30] Ignacy Duleba and Jurek Z Sasiadek. "Nonholonomic motion planning based on Newton algorithm with energy optimization". *IEEE Transactions on Control Systems Technology* 11.3 (2003), pp. 355–363.

[31] Francisco G Rossomando, Carlos Soria, and Ricardo Carelli. "Autonomous mobile robots navigation using RBF neural compensator". *Control Engineering Practice* 19.3 (2011), pp. 215–222.

[32] Yung Hsiang Chen, Tzuu Hseng S Li, and Yung Yue Chen. "A practical trajectory tracking approach for autonomous mobile robots: Nonlinear adaptive H2 design". *Transactions of the Canadian Society for Mechanical Engineering* 37.3 (2013), pp. 385–394.

[33] Tamoghna Das, IN Kar, and S Chaudhury. "Simple neuron-based adaptive controller for a nonholonomic mobile robot including actuator dynamics". *Neurocomputing* 69.16 (2006), pp. 2140–2151.

[34] Jun Ye. "Adaptive control of nonlinear PID-based analog neural networks for a nonholonomic mobile robot". *Neurocomputing* 71.7 (2008), pp. 1561–1565.

[35] Ronald Ping Man Chan, Karl A Stol, and C Roger Halkyard. "Review of modelling and control of two-wheeled robots". *Annual Reviews in Control* 37.1 (2013), pp. 89–103.

[36] Tresna Dewi, Naoki Uchiyama, and Shigenori Sano. "Simple obstacle avoidance for a mobile robot moving through via points". *IEEE/SICE International Symposium on System Integration*. (2013), pp. 111–114.

[37] Tresna Dewi. "Collision Avoidance and Object Following Control for a Mobile Robot in Human Living Environment". PhD thesis. Toyohashi University of Technology, Japan, (2016).

[38]   Roland Siegwart, Illah Reza Nourbakhsh, and Davide Scaramuzza. *Introduction to autonomous mobile robots*. MIT press, (2011).

[39]   Charles Nutakor, Adam Kłodowski, Jussi Sopanen, Aki Mikkola, and José I. Pedrero. "Planetary gear sets power loss modeling: Application to wind turbines". *Tribology International* 105 (2017), pp. 42–54.

[40]   Jing Wei, Aiqiang Zhang, Datong Qin, Teik C. Lim, Ruizhi Shu, Xiaoyan Lin, and Fanming Meng. "A coupling dynamics analysis method for a multistage planetary gear system". *Mechanism and Machine Theory* 110 (2017), pp. 27–49.

[41]   Akinori Yamada. "Optimal speed distribution method and control for wheel moving devices with redundancy". Master's Thesis. Toyohashi University of Technology, Japan, (2017), (In Japanese).

[42]   Yongguo Mei, Yung-Hsiang Lu, C. S. G. Lee, and Y. C. Hu. "Energy-efficient mobile robot exploration". *IEEE International Conference on Robotics and Automation*. (2006), pp. 505–511.

[43]   D. Kurabayashi, J. Ota, T. Arai, and E. Yoshida. "Cooperative sweeping by multiple mobile robots". *IEEE International Conference on Robotics and Automation* 2 (1996), pp. 1744–1749.

[44]   R. M. DeSantis. "Modeling and path-tracking control of a mobile wheeled robot with a differential drive". *Robotica* 13.4 (1995), pp. 401–410.

[45]   T. Kato, Shigenori Sano, and Naoki Uchiyama. "Design and Control of a Redundant Wheeled Drive System". *IEEE/SICE Annual Conferance*. (2013), pp. 2004–2006.

[46]   Shuaiby Mohamed, Akinori Yamada, Shigenori Sano, and Naoki Uchiyama. "Simulation study on velocity distribution for energy saving of a redundant wheeled drive system". *IEEE/SICE International Symposium on System Integration*. (2015), pp. 116–120.

[47]   Shuaiby Mohamed, Akinori Yamada, Shigenori Sano, and Naoki Uchiyama. "Design of a redundant wheeled drive system for energy saving and fail safe motion". *Advances in Mechanical Engineering* 8.11 (2016), pp. 1–15.

[48]   Kenneth J Waldron, Mohammad O Tokhi, and Gurvinder S Virk. *Nature-inspired mobile robotics*. World Scientific, (2013).

[49] Linjie Xin, Qinglin Wang, Jinhua She, and Yuan Li. "Robust adaptive tracking control of wheeled mobile robot". *Robotics and Autonomous Systems* 78 (2016), pp. 36–48.

[50] Tairen Sun, Hailong Pei, Yongping Pan, and Caihong Zhang. "Robust wavelet network control for a class of autonomous vehicles to track environmental contour line". *Neurocomputing* 74.17 (2011), pp. 2886–2892.

[51] Warren E Dixon, Darren M Dawson, Erkan Zergeroglu, and Aman Behal. "Adaptive tracking control of a wheeled mobile robot via an uncalibrated camera system". *IEEE Transactions on Systems, Man, and Cybernetics, Part B (Cybernetics)* 31.3 (2001), pp. 341–352.

[52] Răzvan Şolea and Daniela Cristina Cernega. "Obstacle Avoidance for Trajectory Tracking Control of Wheeled Mobile Robots". *Service Orientation in Holonic and Multi Agent Manufacturing and Robotics*. Springer, (2013), pp. 279–290.

[53] Alessandro De Luca, Giuseppe Oriolo, and Marilena Vendittelli. "Control of wheeled mobile robots: An experimental overview". *Ramsete: Articulated and Mobile Robotics for Services and Technologies*. Springer, (2001), pp. 181–226.

[54] H. Chen, M. M. Ma, H. Wang, Z. Y. Liu, and Z. X. Cai. "Moving Horizon H_∞ Tracking Control of Wheeled Mobile Robots With Actuator Saturation". *IEEE Transactions on Control Systems Technology* 17.2 (2009), pp. 449–457.

[55] C. L. Philip Chen, Guo-Xing Wen, Yan-Jun Liu, and Zhi Liu. "Observer-Based Adaptive Backstepping Consensus Tracking Control for High-Order Nonlinear Semi-Strict-Feedback Multiagent Systems". *IEEE Transactions on Cybernetics* 46.7 (2016), pp. 1591–1601.

[56] C. L. Philip Chen, Yan-Jun Liu, and Guo-Xing Wen. "Fuzzy Neural Network-Based Adaptive Control for a Class of Uncertain Nonlinear Stochastic Systems". *IEEE Transactions on Cybernetics* 44.5 (2014), pp. 583–593.

[57] Bin Xu, Zhongke Shi, Chenguang Yang, and Fuchun Sun. "Composite Neural Dynamic Surface Control of a Class of Uncertain Nonlinear Systems in Strict-Feedback Form". *IEEE Transactions on Cybernetics* 44.12 (2014), pp. 2626–2634.

[58]   Hongjiu Yang, Xiaozhao Fan, Yuanqing Xia, and Changchun Hua. "Robust tracking control for wheeled mobile robot based on extended state observer". *Advanced Robotics* 30.1 (2015), pp. 68–78.

[59]   Guo-Xing Wen, Yan-Jun Liu, C.L. Philip Chen, and Zhi Liu. "Neural-network-based adaptive leader-following consensus control for second-order non-linear multi-agent systems". *IET Control Theory & Applications* 9.13 (2015), pp. 1927–1934.

[60]   T. Fukao, H. Nakagawa, and N. Adachi. "Adaptive tracking control of a non-holonomic mobile robot". *IEEE Transactions on Robotics and Automation* 16.5 (2000), pp. 609–615.

[61]   J Taheri-Kalani and MJ Khosrowjerdi. "Adaptive trajectory tracking control of wheeled mobile robots with disturbance observer". *International Journal of Adaptive Control and Signal Processing* 28.1 (2014), pp. 14–27.

[62]   Chih-Yang Chen, Tzuu-Hseng S Li, and Ying-Chieh Yeh. "EP-based kinematic control and adaptive fuzzy sliding-mode dynamic control for wheeled mobile robots". *Information Sciences* 179.1 (2009), pp. 180–195.

[63]   Zhen-yu Liu, Rui-huan Jing, Xiang-qian Ding, and Jian-hua Li. "Trajectory tracking control of wheeled mobile robots based on the artificial potential field". *International Conference on Natural Computation* 7 (2008), pp. 382–387.

[64]   Dongbing Gu and Huosheng Hu. "Receding horizon tracking control of wheeled mobile robots". *IEEE Transactions on Control Systems Technology* 14.4 (2006), pp. 743–749.

[65]   Danwei Wang and Guangyan Xu. "Full-state tracking and internal dynamics of nonholonomic wheeled mobile robots". *IEEE/ASME Transactions on Mechatronics* 8.2 (2003), pp. 203–214.

[66]   Kyoung Chul Koh and Hyung Suck Cho. "A smooth path tracking algorithm for wheeled mobile robots with dynamic constraints". *Journal of Intelligent & Robotic Systems* 24.4 (1999), pp. 367–385.

[67]   Yongping Pan and Haoyong Yu. "Dynamic surface control via singular perturbation analysis". *Automatica* 57 (2015), pp. 29–33.

[68] Bin Xu. "Disturbance Observer-Based Dynamic Surface Control of Transport Aircraft With Continuous Heavy Cargo Airdrop". *IEEE Transactions on Systems, Man, and Cybernetics: Systems* 47.1 (2017), pp. 161–170.

[69] Yongping Pan and Haoyong Yu. "Composite Learning From Adaptive Dynamic Surface Control". *IEEE Transactions on Automatic Control* 61.9 (2016), pp. 2603–2609.

[70] Bin Xu, Fuchun Sun, Yongping Pan, and Badong Chen. "Disturbance Observer Based Composite Learning Fuzzy Control of Nonlinear Systems with Unknown Dead Zone". *IEEE Transactions on Systems, Man, and Cybernetics: Systems* (2016), pp. 1–9.

[71] Shaohua Luo, Songli Wu, Zhaoqin Liu, and Hao Guan. "Wheeled mobile robot RBFNN dynamic surface control based on disturbance observer". *ISRN Applied Mathematics* (2014), pp. 1–9.

[72] Sung-Hoon Yu, Chang-Ho Hyun, and Hyo Seok Kang. "Robust dynamic surface tracking control for uncertain wheeled mobile robot with skidding and slipping". *IEEE International Conference on Control and Robotics Engineering*. (2016), pp. 1–4.

[73] Dawei Huang, Junyong Zhai, Weiqing Ai, and Shumin Fei. "Disturbance Observer-based Robust Control for Trajectory Tracking of Wheeled Mobile Robots". *Neurocomputing* 198 (2016), pp. 74–79.

[74] Chih-Yang Chen, Tzuu-Hseng S Li, Ying-Chieh Yeh, and Cha-Cheng Chang. "Design and implementation of an adaptive sliding-mode dynamic controller for wheeled mobile robots". *Mechatronics* 19.2 (2009), pp. 156–166.

[75] Dongkyoung Chwa. "Fuzzy adaptive tracking control of wheeled mobile robots with state-dependent kinematic and dynamic disturbances". *IEEE Transactions on Fuzzy Systems* 20.3 (2012), pp. 587–593.

[76] H Sira-Ramírez, C López-Uribe, and M Velasco-Villa. "Linear Observer-Based Active Disturbance Rejection Control of the Omnidirectional Mobile Robot". *Asian Journal of Control* 15.1 (2013), pp. 51–63.

[77]   Jafar Keighobadi, Mohammad Shahidi Sadeghi, and K Alioghli Fazeli. "Dynamic sliding mode controller for trajectory tracking of nonholonomic mobile robots". *International Federation of Automatic Control* 44.1 (2011), pp. 962–967.

[78]   A Jorge, B Chacal, and H Sira-Ramirez. "On the sliding mode control of wheeled mobile robots". *IEEE International Conference on Systems, Man and Cybernetics* (1994), pp. 1938–1943.

[79]   Hyun-Sik Shim, Jong-Hwan Kim, and Kwangill Koh. "Variable structure control of nonholonomic wheeled mobile robot". *IEEE International Conference on Robotics and Automation* 2 (1995), pp. 1694–1699.

[80]   Luis E Aguilar, Tarek Hamel, and Philippe Soueres. "Robust path following control for wheeled robots via sliding mode techniques". *Intelligent Robots and Systems* 3 (1997), pp. 1389–1395.

[81]   Jong-Min Yang and Jong-Hwan Kim. "Sliding mode control for trajectory tracking of nonholonomic wheeled mobile robots". *IEEE Transactions on Robotics and Automation* 15.3 (1999), pp. 578–587.

[82]   Adrian Filipescu, AL Stancu, Silviu Filipescu, and Grigore Stamatescu. "Real-time Sliding-mode Adaptive Control of a Mobile Platform Wheeled Mobile Robot". *International Federation of Automatic Control* 41.2 (2008), pp. 4393–4399.

[83]   Tai-Yu Wang and Ching-Chih Tsai. "Adaptive Robust Control of Nonholonomic Wheeled Mobile Robots". *International Federation of Automatic Control* 38.1 (2005), pp. 475–480.

[84]   T Hamel and D Meizel. "Robust control laws for wheeled mobile robots". *International Journal of Systems Science* 27.8 (1996), pp. 695–704.

[85]   ML Corradini and G Orlando. "Control of mobile robots with uncertainties in the dynamical model: a discrete time sliding mode approach with experimental results". *Control Engineering Practice* 10.1 (2002), pp. 23–34.

[86]   Da Lingrong and Tian Zhixiang. "First order dynamic sliding mode control for wheeled mobile robots". *Innovative Computing and Information* (2011), pp. 373–381.

[87] Tairen Sun, Hailong Pei, Yongping Pan, and Caihong Zhang. "Robust adaptive neural network control for environmental boundary tracking by mobile robots". *International Journal of Robust and Nonlinear Control* 23.2 (2013), pp. 123–136.

[88] Caihong Zhang, Tairen Sun, and Yongping Pan. "Neural Network Observer-Based Finite-Time Formation Control of Mobile Robots". *Mathematical Problems in Engineering* (2014), pp. 1–9.

[89] Mohamed Boukens, Abdelkrim Boukabou, and Mohammed Chadli. "Robust adaptive neural network-based trajectory tracking control approach for nonholonomic electrically driven mobile robots". *Robotics and Autonomous Systems* 92 (2017), pp. 30–40.

[90] Ngoc-Bach Hoang and Hee-Jun Kang. "Neural network-based adaptive tracking control of mobile robots in the presence of wheel slip and external disturbance force". *Neurocomputing* 188 (2016), pp. 12–22.

[91] ZP Wang, SS Ge, and TH Lee. "Adaptive neural network control of a wheeled mobile robot violating the pure nonholonomic constraint". 5 (2004), pp. 5198–5203.

[92] Warren E Dixon, WE Galluzo, Guoqiang Hu, and Carl Crane. "Adaptive velocity field control of a wheeled mobile robot". *Robot Motion and Control*. (2005), pp. 145–150.

[93] Jasmin Velagic, Nedim Osmic, and Bakir Lacevic. "Neural network controller for mobile robot motion control". *World Academy of Science, Engineering and Technology* 47 (2008), pp. 193–198.

[94] Masahiro Horiuchi, Satoshi Muraki, Yukari Horiuchi, Naofumi Inada, and Daijiro Abe. "Energy cost of pushing a wheelchair on various gradients in young men". *International Journal of Industrial Ergonomics* 44.3 (2014), pp. 442–447.

[95] Shuaiby Mohamed, Tobias Rainer Schäfle, and Naoki Uchiyama. "Robust control of a redundant wheeled drive system for energy saving and fail safe motion". *Advances in Mechanical Engineering* 9.5 (2017), pp. 1–16.

[96] Abd El Khalick Mohammad. "Nonlinear Control for High Precision Motion and Energy Saving in Multi-Axis Industrial". PhD thesis. Toyohashi University of Technology, Japan, (2013).

[97] Jean-Jacques E Slotine, Weiping Li, et al. *Applied nonlinear control*. Vol. 199. 1. prentice-Hall Englewood Cliffs, NJ, (1991).

[98] Katsuhiko Ogata. *Modern Control Engineering (Fifth Edition)*. Prentice-Hall Englewood Cliffs, NJ, (2010).

[99] Seong I Han and Jang M Lee. "Balancing and velocity control of a unicycle robot based on the dynamic model". *IEEE Transactions on Industrial Electronics* 62.1 (2015), pp. 405–413.

[100] Mostafa I Yacoub, Dan S Necsulescu, and Jurek Z Sasiadek. "Energy Consumption Optimization for Mobile Robots Motion Using Predictive Control". *Journal of Intelligent & Robotic Systems* 83.3-4 (2016), pp. 585–602.

[101] Anton Rassõlkin, Hardi Hõimoja, and Raivo Teemets. "Energy saving possibilities in the industrial robot IRB 1600 control". *International Conference-Workshop on Compatibility and Power Electronics*. (2011), pp. 226–229.

[102] Matthias Brossog, Johannes Kohl, Jochen Merhof, Simon Spreng, Jörg Franke, et al. "Energy consumption and dynamic behavior analysis of a six-axis industrial robot in an assembly system". *Procedia CIRP* 23 (2014), pp. 131–136.

——-

Publications

Much of the work presented in this thesis has been published as journal or conference papers. Following is a list of these papers.

International Journal Papers

(1) S. Mohamed, A. Yamada, S. Sano, and and N. Uchiyama, "Design of a redundant wheeled drive system for energy saving and fail safe motion", Advances in Mechanical Engineering, vol. 8, no. 11 , (2016), pp. 1-15. (*Impact Factor: 0.827*)

(2) S. Mohamed, A. Yamada, S. Sano, and and N. Uchiyama, "Robust control of a redundant wheeled drive system for energy saving and fail safe motion", Advances in Mechanical Engineering, vol. 9, no. 5 , (2017), pp. 1-16. (*Impact Factor: 0.827*)

International Conferences Papers

(1) S. Mohamed, A. Yamada, S. Sano, and and N. Uchiyama, "Simulation study on velocity distribution for energy saving of a redundant wheeled drive system", IEEE/SICE International Symposium on System Integration, (2015), pp. 116–120.

(2) TR Schäfle, S. Mohamed, N. Uchiyama and O. Sawodny, "Coverage path planning for mobile robots using genetic algorithm with energy optimization, International Electronics Symposium, IEEE , (2016), pp. 99-104.

Shuaiby Mohamed Shuaiby Ragab

Toyohashi University of Technology

July 2017